The Influence of Elemental Partitioning on Hardness in a 12% Chromium Dual-Phase Steel.

by

Ann E. Philcox

A thesis submitted to the Faculty of Engineering, University of Cape Town in fulfilment of the degree of Master of Science in Applied Science.

Department of Materials Engineering,
University of Cape Town,
March 1989

ACKNOWLEDGEMENTS

I would like to thank the following people who assisted me in the research work.

Dr Martin Shaw for his help and advice.

Robert Knutsen for his always friendly assistance.

Mr N Dreze and Mr G Newins for their technical assistance.

Mr J Peterson and Mr B Greeves for the photographic work.

Mrs H Bohm and Ms S Betz for their assistance in the preparation of the manuscript.

Middelburg Steel and Alloys (Pty) Ltd for financial support.

ABSTRACT

During the annealing treatment in the production of dual phase steels, partitioning of alloying elements can occur depending on competitive solubility in the ferrite and austenite for the specific partitioning species. An investigation of the partitioning of substitutional elements was considered paramount in understanding certain anomalies that had been identified by previous researchers in various studies of a dual-phase 12% Chromium steel, designated 3CR12. These anomalies concerned observed increases in bulk hardness that could not be attributed to changes in the volume fraction of martensite produced after exposure to a range of temperatures within the dual phase field. Subsequent experiments revealed an unexpected increase in the microhardness of the martensite phase produced by heat treatment in the temperature range of interest.

In this thesis conventional analytical measurements using Energy dispersive X-ray analysis facilities attached to a Scanning Electron microscope have been utilised to determine the compositions of the two phases in the alloy. A range of temperatures in the dual phase region have been investigated at holding durations of 1, 4 and 20 hours.

It was found that partitioning of substitutional elements was occurring, however no changes were observed as a function of holding time. Further empirical data was obtained using dilatometric methods. This strongly suggested that interstitial concentrations were increasing as a function of annealing time and clarified the anomalies observed during previous studies on 3CR12.

Further study includes that of substitutional element partitioning in the prior states of the commercially produced hot-rolled and annealed 3CR12 alloy. These include the as cast slab and the hot-rolled slab, as well as the final hot-rolled and annealed slab.

Segregation was found to occur in the as cast slab. Subsequent investigation showed the presence of δ-ferrite in the final processing stages of the hot-rolled and annealed product.

CONTENT

CHAPTER 1

Introduction

3CR12, an acronym for Chromium Containing Corrosion Resisting 12% Chromium, has a dual phase microstructure after annealing between two critical temperatures determined, under equilibrium conditions, by the range of the α and γ phase field boundaries. The dual phase microstructure is produced by having the correct balance between the ferrite-forming elements (Si, Ti, Cr) and the austenite-forming elements (C, N, Ni and Mn). The microstructure resulting from the above treatment consists of a ferrite matrix with a finely dispersed second phase of martensite.

Empirically, the properties of dual phase steels can be understood in terms of a composite of two phases, ferrite and martensite (usually 10-20% by volume)[1]. The important parameters in controlling the properties of dual phase steels are the volume fraction and the strength of martensite, both of which are determined by the intercritical annealing temperature and the composition of the alloy; at equilibrium, these are found from the appropriate tie line construction. During intercritical annealing, alloying elements attempt to redistribute with time to reach chemical equilibrium, and this redistribution affects not only the final hardenability of the austenite in the dual phase structure, but also its growth rate during intercritical annealing.

Extensive research has been carried out on 3CR12[2-17] including that of Brink[4] and Schaffer[17]. The origin of this thesis stemmed from certain anomalies observed in their work which could not easily be explained.

The first question arose from Brink's[4] work. He observed, after the heat treatment and quenching of a hot-rolled and annealed 3CR12 specimen in the intercritical annealing region (figure 1.1.), that up to

840°C an increase in room temperature macrohardness of the material was evident and was largely controlled by the increase of the volume fraction of the martensite produced on quenching. Above this temperature the increase in macrohardness of the material is largely a result of the increase in the hardness of the martensite itself. This is shown by the fact that after heat treatment between 820°C and 840°C the volume percentage of martensite increases rapidly (fig. 1.2) with little change in the actual hardness of the martensite (fig. 1.1). Above 840°C the increase in the volume percentage of martensite measured at room temperature is much reduced but the hardness of the martensite increases significantly.

The reason why martensite hardness exhibited an increase after exposure at temperatures above 840°C is unclear. Being a titanium stabilised steel, 3CR12 contains titanium carbonitrides. Furthermore, 3CR12 has only 0.03% carbon added to the base melt. Therefore, it is expected that whatever carbon is available after titanium carbonitrides are formed will partition to the austenite. This suggests that very little

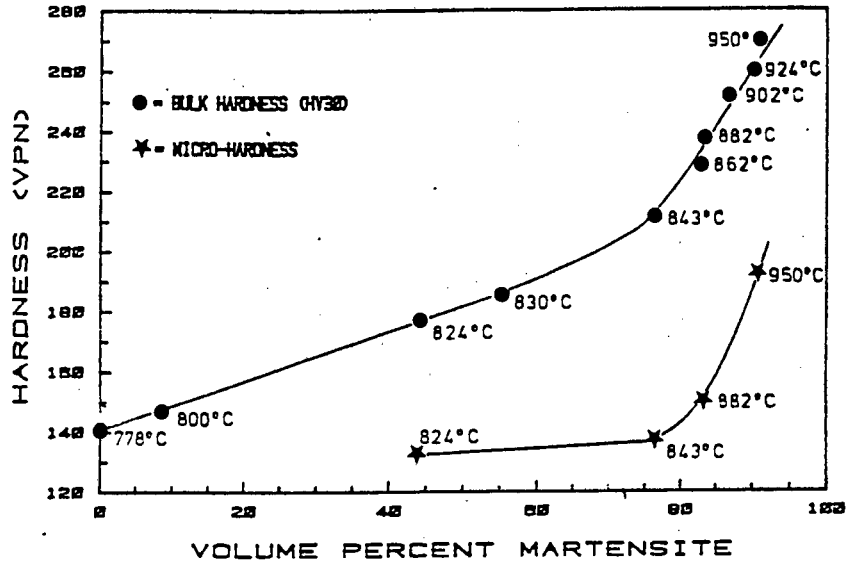

Fig. 1.1 The influence of annealing temperature on the hardness and volume fraction of martensite produced after soaking for 1 hour at the temperatures indicated. The bulk hardness and microhardness of the martensite phase are plotted separately to illustrate the contribution of martensite hardness to the overall hardness of the two-phase mixture. All specimens were oil quenched after annealing.[4]

free carbon would be available to partition to the austenite formed during intercritical annealing and that alternatives to interstitial diffusion have to be considered in order to rationalise the observed increase in martensite hardness.

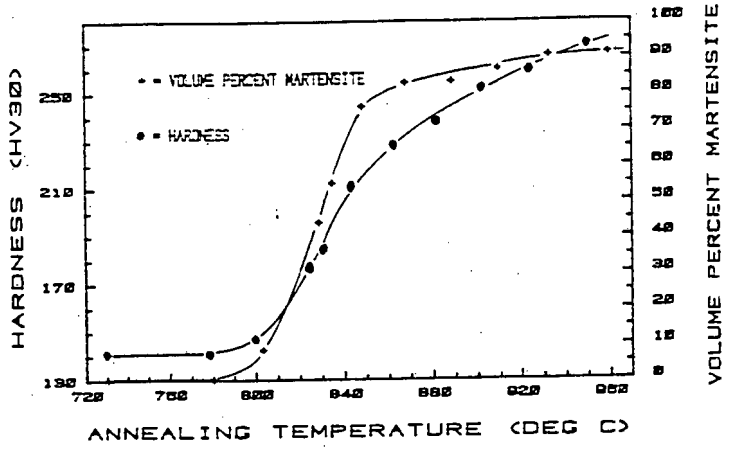

Fig. 1.2 The effect of annealing temperature (within the dual- phase region) on the bulk hardness and volume percentage of martensite for 3CR12. (All samples had undergone a prior treatment of hot rolling with subsequent annealing below 800°C)[4]

The results of Brink's work, illustrated in figure 1.1., unfortunately exhibit a clear quantitative error in that his reported microhardness data falls below the bulk macrohardness values. In addition to the fact that martensite, as the harder of the two phases present, must exhibit higher hardness values than the bulk, there is a well documented "load effect" associated with microhardness testing at low loads that produces an unexpectedly elevated hardness value. The reason for the inconsistency in Brink's data is associated with the instrumentation used to obtain microhardness values. However, the features of interest in figure 1.1. are the clear trends in both curves which are not invalidated by the comparative quantitative values. Fortunately, more reliable data produced during the course of the present work and also by Matthews[14] confirms the trends observed by Brink and is also quantitatively reliable (see figure 1.3).

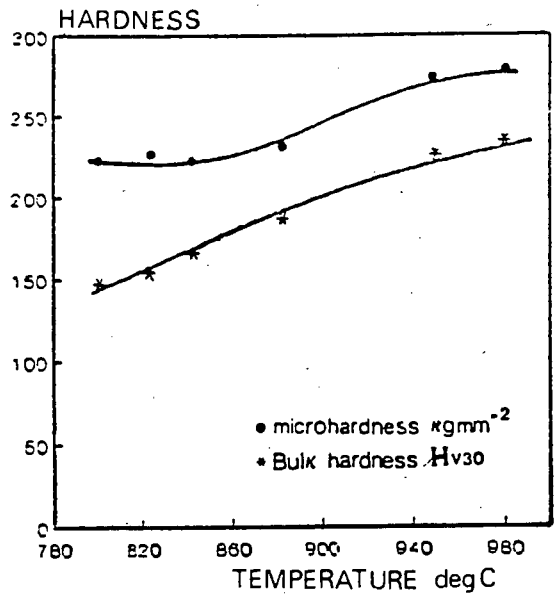

Fig.1.3 The variation in bulk hardness and microhardness of the martensite as a function of annealing for 1 hour at the temperatures indicated in order to confirm the trends obtained by Brink[4]. All specimens were oil quenched after soaking. The samples had undergone a prior treatment of hot rolling with a subsequent anneal below 800°C.

The second question to arise was from Schaffer's[17] work. Schaffer postulated that it can be reasonably assumed that carbon in solution will distribute preferentially to austenite rather than ferrite. Thus, for a given transformation temperature the more austenite formed, the lower the equilibrium carbon content of the austenite and thus the softer the subsequent martensite formed. However, the reverse effects were observed, see figure 1.4.

Therefore, as a result of the above, Schaffer[17] proposed that the hardness was initially affected by the diffusion of carbon and that any subsequent increase in the martensite hardness was attributable to substitutional elements partitioning to their respective phases. Substitutional solutes generally cause symmetrical distortion of the solvent lattice leading to relatively moderate strengthening effects.

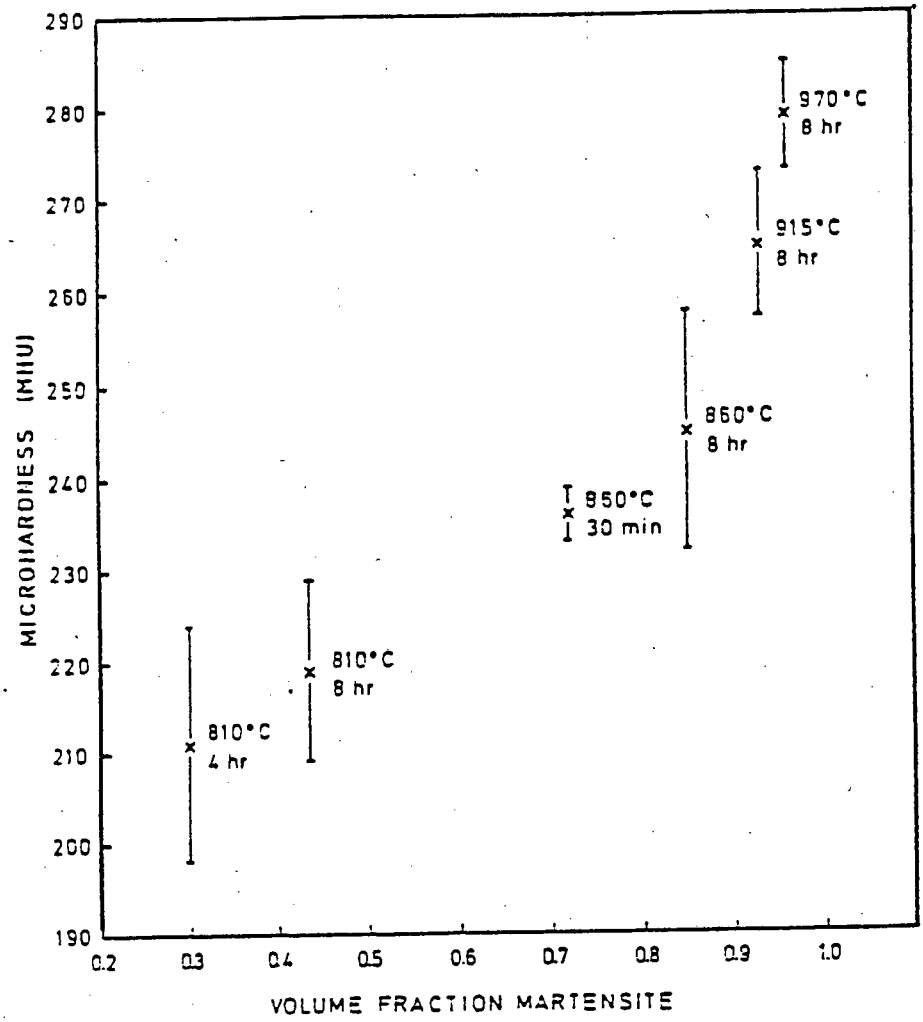

Fig. 1.4 The hardness of martensite vs volume fraction martensite for isothermal austenitisation transformations.The temperatures and duration of soaking time are indicated on the graph. All specimens were oil quenched after soaking. Prior treatment included hot rolling with a subsequent anneal below at 800°C [17]

This thesis is therefore predominantly concerned with substitutional element partitioning that is thought to occur during intercritical annealing. An understanding of these partitioning effects would give greater understanding and insight into the mechanisms by which microstructural control at elevated temperatures can determine room temperature properties; elucidated by their effect on the property of hardness.

The approach adopted in the present work has been to initially determine whether the trends introduced in this chapter were consistently obtainable. Subsequent experiments have involved using Scanning Electron Microscopy in order to determine substitutional element partitioning patterns. The duration of exposure at specific temperatures was considered important in order to identify whether any long term partitioning was evident. Alternative mechanisms to substitutional partitioning have also been considered and dilatometry has been used to examine the influence of annealing time and temperature on the transformations of interest.

CHAPTER 2

Literature survey

2.1 The constitution of stainless steels

The constitution of all the stainless steels plays an important role in controlling their metallurgical characteristics and mechanical properties.

The two main alloying elements namely, Ni and Cr, have opposing effects on the constitution; the former being an austenite former and the latter, a ferrite former. Hence, Fe-Ni alloys show an expanded temperature/composition range for austenite stability whilst Fe-Cr alloys show the reverse effect and a closed gamma loop (see fig.2.1 a and b below). Other alloying elements can conveniently be classed either as austenite formers, (C, N, Cu, Co, Mn) or as ferrite formers (Mo, W, Nb, Ti, V, Si, Al) which respectively increase or decrease the extent of the austenite phase field. In Fe-Cr alloys, the maximum Cr content of the gamma loop increases rapidly with increasing Ni, C or N content.[1]

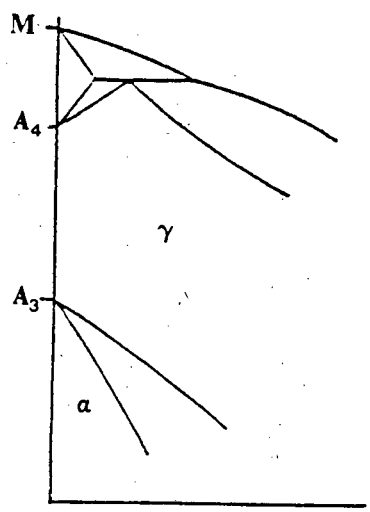

Fig. 2.1. Classification of iron-alloy phase diagram: open γ -field[1]

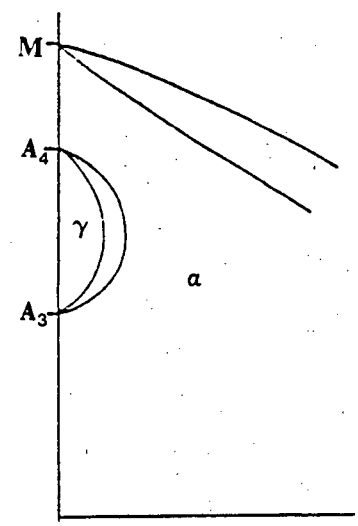

Fig.2.2. Classification of iron-alloy phase diagram: closed γ -field[1]

One of the most convenient ways of representing the effect of various elements on the basic structure of chromium-nickel stainless steels is the Schaffler diagram, in which the compositional limits at room temperature of austenite, ferrite and martensite are plotted in terms of nickel and chromium equivalents (figure 2.3).[1] At its simplest level, the diagram shows the regions of existence of the three phases for iron-chromium-nickel alloys. However, the diagram becomes of wider application when the equivalents of chromium and of nickel are used for the other alloying elements. The chromium equivalent has been applied using the most common ferrite-forming elements[18]:

$$\%Cr \text{ equivalent} = \%Cr + 2(\%Si) + 1.5(\%Mo) + 5(\%V) + 5.5(\%Al) + 1.75(\%Nb) + 1.5(\%Ti) + 0.75(\%W)$$

while the nickel equivalent has likewise been determined with the familiar austenite-forming elements[18]:

$$\%Ni \text{ equivalent} = \%Ni + \%Co + 0.5(\%Mn) + 0.3\%(Cu) + 25\%(N) + 30(\%C)$$

all concentrations being expressed as wt percentages.

Difficulty may be encountered in dealing with an element such as Ti in terms of its Cr equivalent value as it not only partitions to ferrite but also removes from solution the austenite formers C and N as titanium carbides\titanium nitrides. Equations have been suggested to take into account the carbide and nitride forming tendencies of Titanium,[19] for example:

$$\%Ti \text{ (effective)} = \%Ti - 4\,[(\%C - 0.03) + \%N]$$

When the carbide\nitrides are partially dissolved the constitution can be determined by elements in solution: these concentrations can be calculated from solubility data and then used individually with the appropriate Cr or Ni equivalent value[19]. Titanium in solution can be calculated from the following equation:

Ti_{ss} = (Ti) - 3.42(N) - 1.49(O) - 4(C)

where Ti_{ss} = Titanium in solid solution. (Ti_{ss} for 3CR12 is typically 0.15 to 0.2).[9]

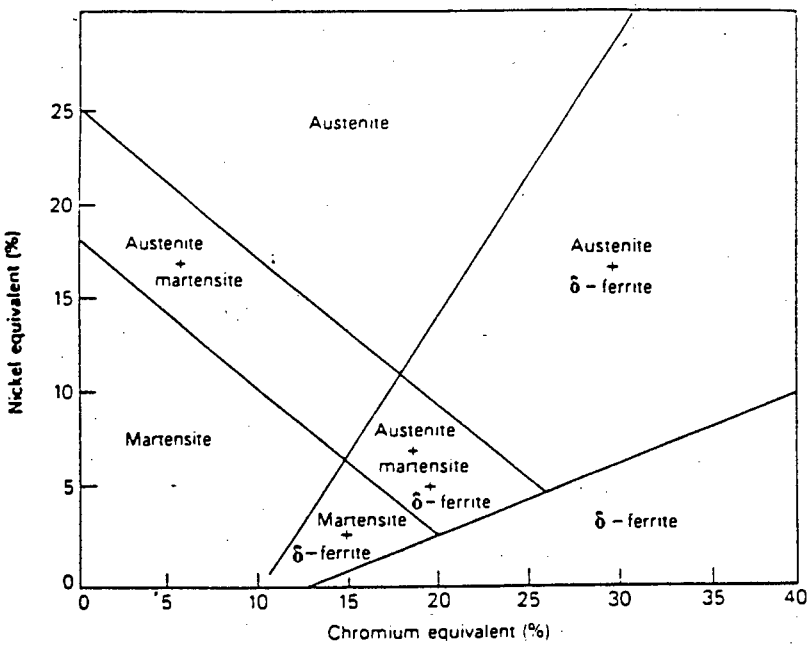

Fig. 2.3 Schaffler diagram. Effect of alloying elements on the basic structure of Cr-Ni stainless steels[1]

The partitioning of alloying elements is important as it controls the properties of the individual phases. The ratio of partitioning for a given element between austenite and ferrite is not constant, but depends on the composition of the steel and the width of the two-phase field; see figure 2.7 for example. Isothermal sections of the Fe-Cr-Ni system clearly show that a given ratio of austenite: ferrite, for example in a duplex steel, can be obtained by many different alloy compositions, but that in each the compositions of the austenite and ferrite will be very different. This is another means of predicting the phase constitution, i.e. using the Cr and Ni equivalent values which may be plotted on isothermal sections of the Fe-Cr-Ni diagram such as those shown in figures 2.4 and 2.5.

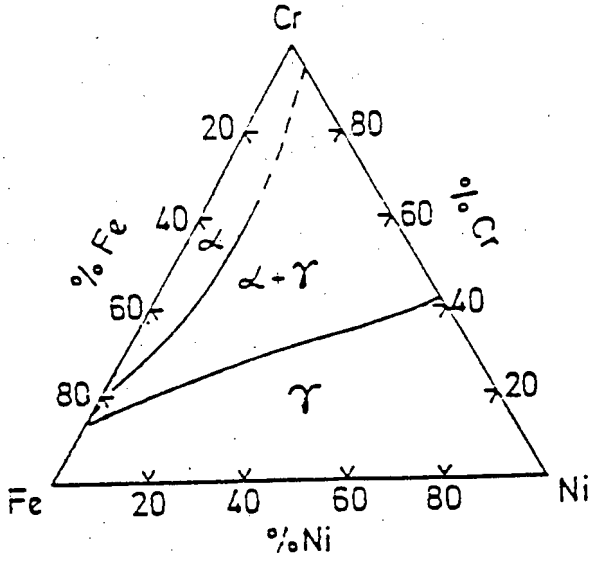

Fig.2.4. 1050°C isotherm of Fe-Cr-Ni ternary system[19]

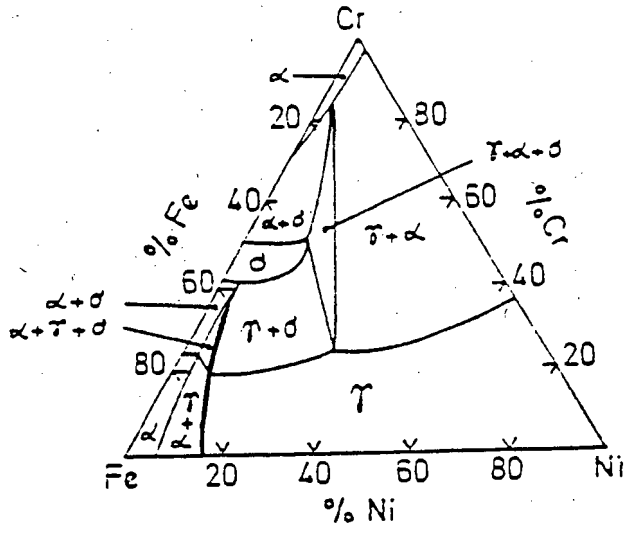

Fig. 2.5. 650°C isotherm of Fe-Cr-NI ternary system[19]

2.2 Dual phase steels

The typical composition range for conventional dual phase steels is:[21]

0.1 -0.2 C

0.4 -0.6 Si

1.3 - 1.7 Mn

0.04 - 0.07 V

Other possible additions being Mo and Cr.

The dual phase steels have a characteristic two-phase microstructure consisting of about 80 vol% ferrite (α-iron) and 20 vol% martensite. The term "dual phase" was coined in the mid-1970's to describe these ferrite-martensite microstructures,[13,20] but dual phase steels can contain more than the two phases implied by their name. The term "dual phase" refers to a class of low alloy steels which was originally developed to satisfy an increasing need, primarily in the transportation industry, for new high strength materials which permit weight reduction without sacrificing formability or dramatically increasing costs.[20,21]. The key feature of the annealing treatment in the two phase (α and γ) field, (i.e. in the production of dual phase steels,) is that the carbon content in the austenite pools will be substantially higher than in the ferrite. Thus on quenching the steel to ambient temperatures the martensite will be relatively hard due to carbon in solution and defect hardening[21] and the ferrite will be soft. The result is a dispersion-hardened structure with a highly ductile matrix. The martensite acts as a load carrying constituent in the soft ferrite matrix; the matrix supplies the system with the essential ductility[21].

3CR12 has a two-phase (α and γ) structure once it has been intercritically annealed. Although 3CR12 is a member of the dual phase steel family it is a special alloy in that it has 12% Cr and only 0.03 vol % Carbon added to the base melt. It is commercially available as a hot-rolled and annealed material having a ferrite\tempered martensite microstructure. The compositional limits for 3CR12 are tabulated on page 13, table 2.1.

2.2.1. The origin of 3CR12, the hot-rolled and annealed product

3CR12 is a titanium stabilised, weldable and corrosion resistant steel, with a composition arising from small but significant compositional deviations from that of AISI 409. A ferrite factor, using the Kaltenhauser formula[22] is calculated by balancing carefully the austenite and ferrite-forming elements. For 3CR12 this ferrite factor is in the range of 8-12[13]. Kaltenhauser[22] constructed an empirical formula which takes into account the relative austenite and ferrite-forming strengths of the various alloy elements and determines whether the steel will be austenitic, ferritic or duplex. The formula gives the so-called ferrite factor, FF, as follows:

ferrite factor = %Cr+6(%Si)+8(%Ti)+4(%Mo)+2(%Al)-2(%Mn) 4(%Ni)-40[%(C+N)]

The composition (table 2.1) of 3CR12 gives rise to a banded two-phase structure of martensite and ferrite after hot rolling, which, after tempering produces a ferrite and tempered martensite microstructure. The tempered martensite has a very low carbon content. The banded microstructure arises from the hot-rolling process being carried out in the duplex ferrite-austenite region[3]. The $\alpha \longrightarrow \gamma$ transformation occurs at approximately 800°C. This can be dilatometrically determined and depends upon the ferrite factor. The composition of 3CR12 at ≈12% on the Fe-Cr diagram is indicated in fig. 2.7. At 780°C the as-rolled material is almost completely ferritic. At 800°C a fine duplex microstructure is generated and retained until ≈1200°C, this structure becoming coarser with increasing temperature. The structure that 3CR12 possesses in the commercially available condition is a structure that has been transformed to a stable fine-grained ferritic and tempered martensitic structure by annealing at temperatures just below the dual phase (α and γ) boundary (the Austenite start (As) temperature), see fig. 2.7..

Table 2.1 Compositional limits for 3CR12 steel[12]

C	N	Ni	Mn	Si	P	Cr	Ti
0.03 max	0.03 max	1.5 max	1.5 max	1.0 max	0.03 max	11.0-12.0	4(C+N) min

Knutsen[10] has proposed that δ-ferrite is retained as δ-ferrite stringers in the final hot-rolled product. This is due to the transformation from δ-ferrite to austenite not going to completion and resulting in the presence of a stable residual δ-ferrite at room temperature. The origin of these δ-ferrite stringers can be explained briefly as follows: the transformation from δ-ferrite to austenite is a diffusional process and elemental partitioning occurs between the two phases. Hence the residual δ-ferrite phase becomes richer in ferrite-forming elements (Cr increases) whereas the transformed phase (austenite) becomes richer in austenite-forming elements (Ni increases). However Knutsen[10] has shown that this transformation does not go to completion and has identified a stable residual δ-ferrite at room temperature.

The thermal history of 3CR12 is schematically represented in figure 2.6. This is the production route of 3CR12 plates and has been included in order to illustrate the heat treatments and relative time involved in the different stages of the final hot-rolled and annealed product. The scrap and alloy material are melted and refined and then dispatched to the rolling mill for pretreatment and rolling. Here the slabs are rolled to their required size (or an intermediate size for cold rolling). The plates are then cooled and finally annealed in order to soften and homogenise the material after rolling.

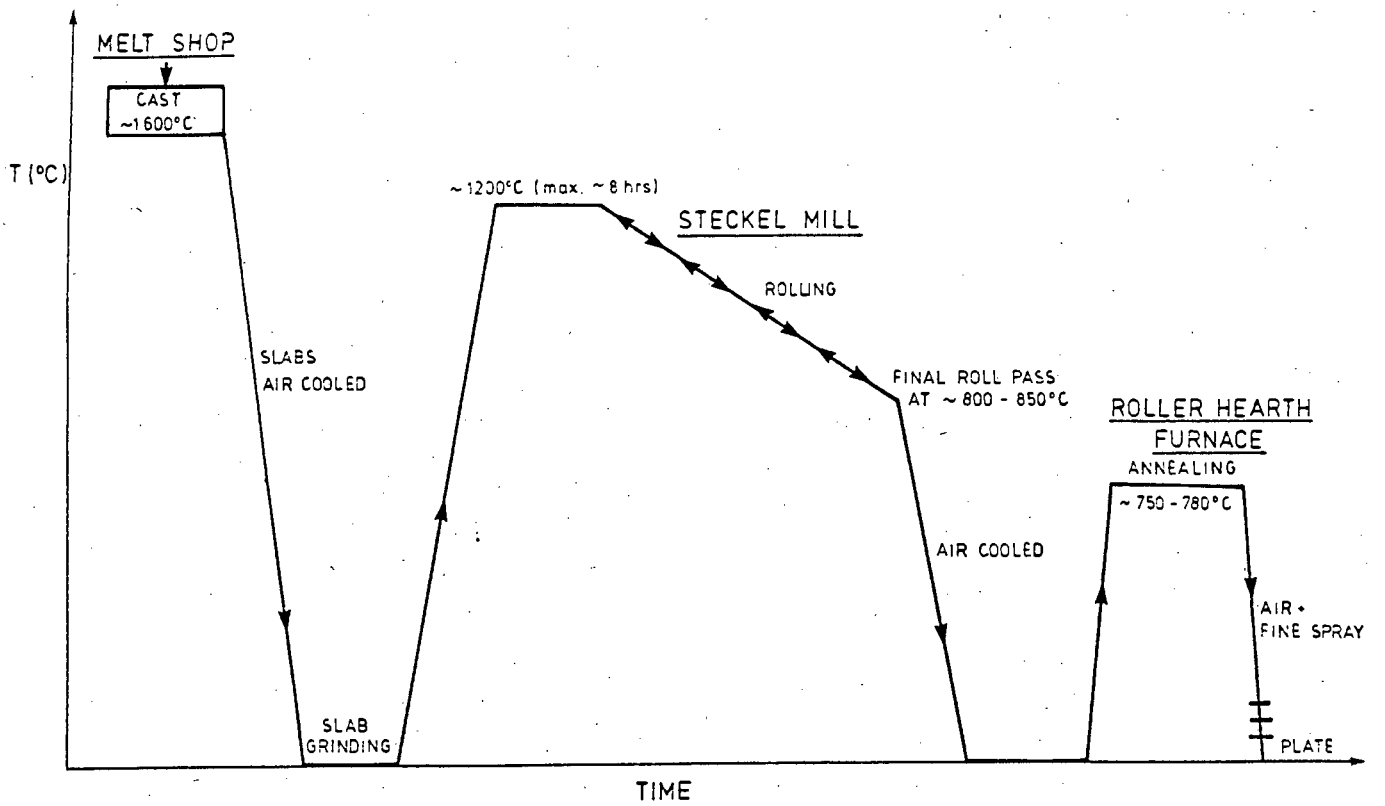

Fig.2.6 A schematic representation of the thermal history of 3CR12 during its production as plates

2.2.2. 3CR12 constitution according to the phase diagram

The pseudo-binary phase diagram (fig. 2.7) shows the composition of 3CR12. This phase diagram has been generated from isothermal sections of ternary diagrams for solid-phase equilibria in Fe-Ni-Cr systems for 85 wt% iron [10]. By using Cr and Ni equivalents calculated according to the equations shown in section 2.1, compositions having particular phases can be determined.[10] The compositional line for 3CR12 has been calculated from these equivalents and is shown in fig 2.7. The structure existing at 1400°C should be a homogeneous δ-ferrite phase. On cooling to 1150°C, the transformation from δ-ferrite to austenite should ultimately go to completion. This is verified in figure 2.7 which shows an Fe-Cr-Ni pseudo-binary diagram for a 85% wt% iron. At 1000°C the composition should lie within the γ -nose.

The transformation from δ-ferrite to γ is diffusion controlled involving the transformation of the δ-ferrite matrix into a dual-phase structure

consisting of the δ-ferrite phase and the new austenite phase. As the transformation from δ-ferrite to austenite is a diffusional process, elemental partitioning occurs between the two phases, i.e. the residual δ-ferrite becomes increasingly richer in ferrite formers (e.g. Cr increases) and the austenite becomes increasingly richer in austenite formers (e.g. Ni increases).

The composition of these phases is determined by the solvus lines as indicated in fig. 2.7. At temperature T1, the ferrite phase should have a composition of X1 whereas the austenite should have a composition X2. This indicates the respective partitioning of ferrite and austenite-forming elements to the ferrite and austenite phase. On further cooling, the slope of the solvus lines gives rise to a decrease in the amount of ferrite phase at the expense of austenite growth. This is shown by the

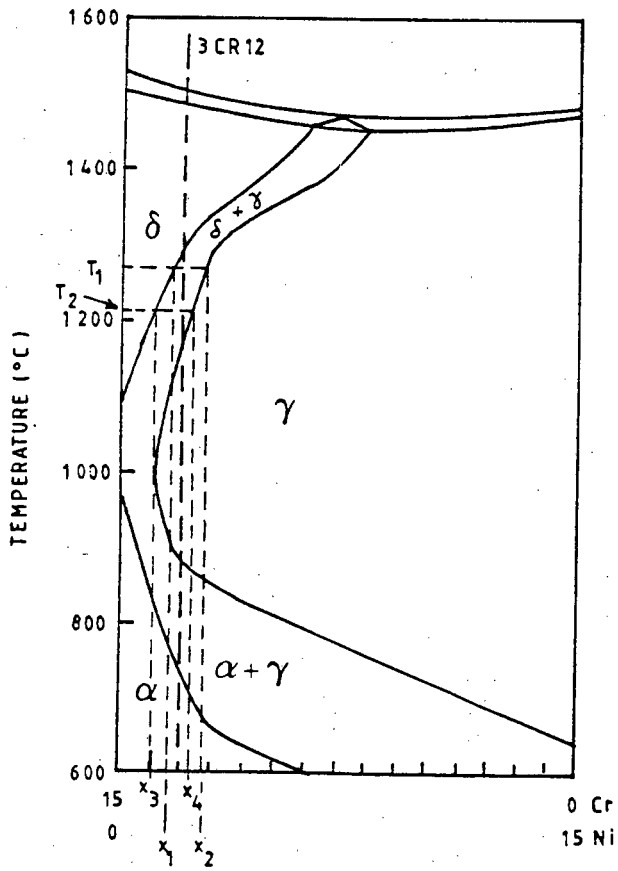

Fig 2.7 Pseudo-binary Cr-Ni equilibrium phase diagram for 85 wt %Fe[10]

tie-line at temperature T2. The composition of the ferrite and austenite has now changed to X3 and X4 respectively.

As stated above, the transformation is diffusion controlled and therefore the rate of transformation is expected to slow down as the temperature is decreased. At 1400°C the composition of the single δ-ferrite phase is expected to be homogeneous in view of the rapid homogenisation of ferrite at this temperature[23]. In 3CR12 the rate at which the subsequent diffusion controlled transformation to austenite occurs will be partially determined by the diffusion rates of the main substitutional elements, namely Cr and Ni, as well as C and N.

2.3. DIFFUSIONAL TRANSFORMATIONS

2.3.1 The formation of Austenite during Intercritical Annealing.

Dual phase steels can be produced in several ways and with a wide range of compositions. However, the first step in the development of the as heat-treated, dual-phase 3CR12 microstructure is the formation of a certain amount of austenite during intercritical annealing.

Annealing of a steel between its critical temperatures i.e. the Ae1 and Ae3, results in the formation of ferrite and austenite. All solutes present in the steel tend to partition between these phases, although to different extents. The amount of austenite in the steel at a given temperature is determined by the extent of partitioning and corresponds to equilibrium only when the annealing time is sufficient for complete partitioning of the alloying elements. The redistribution of substitutional alloying elements is much slower than that of the interstitial carbon and nitrogen as the diffusivities of the latter are nearly 10^5–10^6 times larger than those of the substitutional alloying elements. See table 2.2.

Table 2.2 Diffusivities of elements in γ- and α-iron [1]

Solvent	Solute	Activation energy Q (kJ mol^{-1})	Frequency factor D_0 (cm^2 s^{-1})	Diffusion coefficient $D_{910\,C}$ (cm^2 s^{-1})	Temperature range (°C)
γ-iron	C	135	0.15	1.5×10^{-7}	900–1050
	Fe	269	0.18	2.2×10^{-13}	1060–1390
	Co	364	3.0×10^{2}	24.0×10^{-12} (at 1050 °C)	1050–1250
	Cr	405	1.8×10^{4}	58.0×10^{-12} (at 1050 °C)	1050–1250
	Cu	253	3.0	15.0×10^{-11}	800–1200
	Ni	280	0.77	7.7×10^{-13}	930–1050
	P	293	28.3	3.6×10^{-12}	1280–1350
	S	202	1.35	1.5×10^{-9}	1200–1350
	W	376	1.0×10^{3}	12.0×10^{-12} (at 1050 °C)	1050–1250
α-iron	C	80	6.2×10^{-3}	1.8×10^{-6}	
	N	76	3.0×10^{-3}	1.3×10^{-6}	
	Fe	240	0.5		700–750
	Co	226	0.2	2.1×10^{-11}	700–790
	Cr	343	3.0×10^{4}		
	Ni	258	9.7	3.7×10^{-11}	700–900
	P	230	2.9	2.0×10^{-10}	860–900
	W	293	3.8×10^{2}		

The importance of studying austenite formation between the Ae1 and the Ae3 equilibrium temperatures is recognised because the austenite phase is of considerable technological interest and its occurrence plays an important role in several methods of thermal and thermomechanical treatment of steels. In addition, the influence of a fine austenite grain size on the structure and mechanical properties of the transformation products has been recognised for many years.[19]

It is well established[25] that the growth of austenite is controlled by diffusional mechanis including the diffusion of interstitials (i.e. C and N) as well as substitutional elements (i.e. Mn, Si, Cr, Ni, etc). Relevant models describing the growth of austenite involve:
(1) carbon diffusion control and (2) initial carbon diffusion control followed by substitutional alloying element diffusion control.[24]

In the binary Fe-C growth model the equilibrium compositions of α and γ are fixed for a given temperature in the intercritical region and the only independent diffusing species to be considered is carbon.

The latter model deals with the effect of alloying elements on the formation of austenite. Wycliffe et al [26] and Speich et al [27] studied the growth of austenite during the intercritical annealing of a dual-phase steel. They assumed that the process of austenite growth may be considered in three stages. The first two stages involve carbon diffusion control, and limited diffusion of Mn in α. The third and final stage involves the diffusion of Mn through γ .

As in the case of the binary growth model, the ternary[26,27] (i.e Fe-C-Mn) and quaternary[26] (i.e Fe-C-Mn-Si) growth models assume the existence of local equilibrium at the $\alpha\backslash\gamma$ interfaces. The local equilibrium model applies equilibrium thermodynamics to a kinetic phenomenon. It is assumed that the elements of two phases in contact with each other are in chemical equilibrium at the interfaces, but the bulk composition does not attain chemical equilibrium. Local equilibrium is one of the conditions which distinguishes between diffusion and interface controlled growth.[28]

A more detailed description of Speich, Demamest and Millerm's[27] theory of austenite formation involves; (1) an almost instantaneous nucleation of austenite at pearlite or grain-boundary cementite particles, followed by very rapid growth of austenite until the carbide phase is dissolved; (2) slower growth of austenite in ferrite at a rate that is controlled by carbon diffusion in austenite at high temperatures and by manganese diffusion in ferrite (along grain boundaries) at low temperatures and (3) very slow final equilibration of ferrite and austenite at a rate that is controlled by manganese diffusion in austenite.

The control of the austenite growth by manganese diffusion in the ferrite at low temperatures implies that manganese enrichment of the austenite phase must occur, which has been observed. Consideration of phase equilibria in the ternary Fe-Mn-C system also indicates that the austenite phase will be enriched in both manganese and carbon if true equilibrium is achieved during intercritical annealing. However, many

authors have assumed that because of the short annealing times only carbon redistribution occurs between the two phases, because substitutional manganese diffuses much more slowly than interstitial carbon. This situation is referred to as paraequilibrium.

2.3.2 Paraequilibrium

This basic concept was proposed by Hultgren[29] and is particularly useful when a fast diffusing species is prominent e.g. in some ternary systems. In this condition the substitutional elements do not contribute to the transformation. The transformation advances only by the interstitial element diffusion and local equilibrium of the interstitial element is attained across the interface.

Even in cases where there is no partitioning of substitutional solute between ferrite and austenite, the alloying element exerts considerable influence on the rate of transformation since it alters the relative activities of carbon in the two phases at the interface, affecting both the driving force for the reaction and the carbon diffusivity.[30]

Koch and Eckstein[31] using a Cr-26% Ni-6% stainless steel studied the growth of austenite from ferrite. Their results showed the transformation to be controlled by chromium and nickel diffusion which redistribute simultaneously during the transformation, resulting in an increase in the nickel content of the austenite and chromium content of the ferrite. Whereas Lenel[32] showed for an Fe-1.2% Mn-0.1% C alloy that the austenitisation reaction for "regions where both ferrite and austenite are stable," i.e. at temperatures between the Ae1 and Ae3 temperatures the reaction proceeds via two stages. The first stage was the direct transformation from ferrite to austenite and was carbon diffusion controlled. Further transformation to austenite during the second stage was manganese diffusion controlled. At temperatures above the Ae3, the first stage of austenite growth was controlled by solute drag at the austenite/ferrite interface,while the second stage was manganese diffusion controlled.

For a Fe-10%Cr-0.2%C alloy, Lenel found that the austenitisation also occurred via two stages. Firstly, the nucleation and growth of austenite was controlled by carbon diffusion through ferrite, while chromium partitioning did not occur. Secondly, alloy carbides dissolve in the newly formed austenite and at this stage the transformation is controlled by chromium diffusion.

Wycliffe, Purdy and Embury[26] determined for both a ternary and quaternary steel, that a rapid carbon diffusion controlled period of growth goes to completion in times of the order of a second, followed by much slower growth controlled by diffusion of substitutional alloying element(s) in ferrite. The rate and extent of austenite growth is related to the alloy chemistry, the scale of the microstructure and the partitioning coefficient(s) of the alloying element(s). However, during the same year, Koo et al[33] determined for an AISI 1010 steel, the partitioning of carbon and substitutional elements between ferrite and martensite during an intercritical anneal. They deduced that, as no preferential partitioning of Mn was observed, the change observed in the d spacing using lattice fringe imaging was entirely attributable to carbon partitioning to austenite. Likewise, Sarikaya et al[34] observed in a low to medium carbon lath martensitic structural steel that the existence of retained austenite at room temperature was attributable to carbon diffusion to the austenite and to the martensite\austenite interfaces. They also found no detectable change in substitutional alloying elements between martensite and austenite.

Garcia [24] found in his study on dual-phase steels that the formation of austenite from a ferrite-pearlite microstructure occurred in three stages: (1) formation of austenite at pearlite bands followed by (2) austenite formation outside the pearlite bands (i.e. at pearlite colony intersections) and finally (3) the austenite growth at ferrite grain boundaries i.e. austenite into ferrite. The initial section of this stage was adjudged to

be controlled by carbon diffusion first and then the final portion to be controlled by Mn diffusion.

Schaffer[17] observed in a low carbon dual phase steel, namely 3CR12, that the direct transformation from a body centred cubic crystal structure, α, to a face-centred cubic crystal structure, austenite, was the rate controlling step for the austenitisation reaction in this steel. The reaction was not controlled by long range diffusion and partitioning of the Ni, Mn and C to the austenite occurred after the crystal structure had changed.

Chaturvedi and Jena[35] determined for an Fe-1.0%Mn-0.5%Cr-0.5%Si-0.2%C steel that the martensite content of an intercritically annealed dual phase steel was the same as that calculated using a model of partial equilibrium. This implied that partitioning of carbon occurred without partitioning of substitutional solutes. However at higher intercritical annealing temperatures the experimental values departed from the calculated values and approached equilibrium. This he attributed to the partitioning of substitutional solutes.

2.3.3 The austenite decomposition reaction

The decomposition of austenite by nucleation and growth processes can result in a number of different phases, depending on the alloy composition, the reaction temperature and the time for which it is allowed to proceed.

2.3.3.1. Kinetics

The kinetics of a phase change can be illustrated by a TTT diagram. For a plain C steel the TTT curve for the decomposition of austenite has a simple, well defined "C" shape. The nose of the curve represents the temperature at which the reaction proceeds most rapidly, slowing down at higher and lower temperatures. The reasons for this shape are due to the interaction of the thermodynamic driving force governing the

reaction and the diffusivity of carbon. At high temperatures the driving force is low but the diffusivity of carbon is high, whereas at low temperatures these effects are reversed. At intermediate temperatures, i.e. the nose portion of the curve, the driving force and diffusion rate are optimised and the maximum reaction rate is achieved.

Honeycombe[36] suggests that at transformation temperatures above 700°C, nucleation of ferrite takes place predominantly at the austenite grain boundaries, because they are both energetically favourable nucleation sites and provide faster paths for diffusion. Ricks et al[37] when reporting on a study of a ternary Fe-7%Cr-2%Ni alloy observed two different ferrite reaction regions; that between 660 - ≈600°C where the ferrite reaction was observed to nucleate but was sluggish and the reaction never went to completion and one region below 600°C where a much faster reaction was observed.

The addition of alloying elements have been found to have a variety of significant effects. Ricks et al[37] showed that the addition of 7% Ni to an Fe-2% Cu alloy significantly retarded the reaction kinetics; Irvine et al[38] determined that the addition of 12 %Cr to a low carbon steel retarded the ferrite reaction and the steel became air hardened. These alloying elements retard the proeutectoid ferrite growth kinetics because they have lower diffusivities and also reduce the rate of diffusion of carbon in iron[1].

Schaffer[17] determined the TTT curve, (see figure 2.8) for the transformation between austenite and ferrite in 3CR12 which showed conventional "C" curve kinetics.

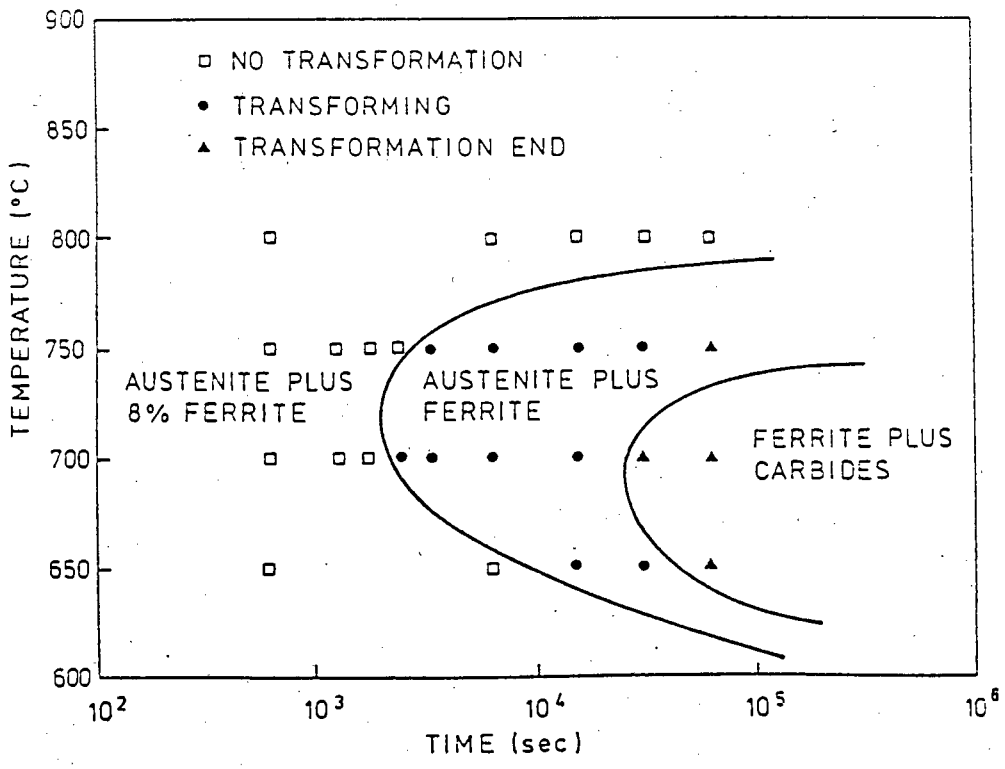

Fig.2.8 **The isothermal transformation for the decomposition of austenite to ferrite plus carbides in 3CR12[17]**

2.3.3.2. The partitioning of alloying elements

The relevant phase diagrams show that ferrite and austenite can dissolve different quantities of the various alloying elements. At equilibrium therefore, the alloying elements should partition between the two phases. Darken and Fisher(see [1]) suggested a theory of partitioning which assumed that austenite-forming elements partition preferentially to austenite, while ferrite-forming elements usually partition to ferrite. Thus, these elements may control the rate of transformation from austenite to ferrite. As the rate of carbon diffusion is more rapid than that of the substitutional elements, it is possible that the latter may control the reaction kinetics in Fe-C-X alloys, where X is Cr, Ni, Mn etc.

Aaronson et al[39] investigated the partitioning of alloying elements between austenite and proeutectoid ferrite in high purity Fe-C-X alloys, using electron probe analysis. They found that no partitioning occurred during the early stages of transformation at any temperature studied in

the Si, Mo, Co, Al, Cr and Cu steels. Partitioning however did occur for the Ni, Mn and Pt steels above an "individually characteristic critical temperature." Furthermore, there were no significant concentration profiles in the ferrite but often unequal concentrations of nickel were present on either side of an austenite grain. They found that the growth kinetics of proeutectoid ferrite were controlled by substitutional element diffusion when partitioning occurred and by carbon diffusion when it did not. Aaronson et al [39] formulated a thermodynamic theory of partitioning. They calculated a "no-partition" Ae3 curve which follows a temperature-composition path lying below the equilibrium Ae3 curve . At isothermal transformation temperatures lying between these curves, the occurrence of partitioning is a thermodynamic prerequisite for the formation of proeuctectoid ferrite. At temperatures below the "no-partition" Ae3 curve, the precipitation of ferrite, without partitioning is thermodynamically permissible. From the nature of the nickel concentration gradients, they concluded that the growth of "partitioned" ferrite is controlled by the diffusion of substitutional alloying elements in the austenite.

2.4. DIFFUSIONLESS TRANSFORMATIONS

2.4.1. The Martensitic transformation

Martensite is a product of diffusionless transformation and can occur in the form of thin, lenticular plates which often extend right across the parent austenite grains, or as packets of approximately parallel, fine laths whose size is generally less than that of the austenite grains. In both cases the parent and product crystals are related by an atomic correspondence and the formation of martensite causes the shape of the transformed region to change; this shape change is macroscopically an invariant-plane strain, the invariant-plane being the habit plane of the martensite. The nucleation of martensite is generally athermal; martensite can form at very low temperatures and its interface with the parent phase necessarily has to be glissile. Martensite forms at high undercoolings where the chemical free energy change for transformation

is generally very large, well in excess of that required to accomplish diffusionless transformation even when the stored energy of the martensite is taken into account.

The strength of martensite is affected by a variety of factors including;[17,24]

a. grain size; it has been shown [24] that the martensite structure can be related to a first approximation to the prior austenite grain size.

b. interstitial solid solution hardening; the strength of martensite depends primarily on the amount of carbon in solid solution. It has been shown that the strength of martensite changes linearly with the square root of carbon content.[40] This is probably due to the tetragonal distortion of the lattice by carbon atoms during the transformation from austenite to martensite. The amount of distortion increases with increasing carbon content.

c. precipitation or segregation of carbon; it is commonly accepted that the two dominant factors which appear to influence the degree of precipitation during martensite formation are the Ms temperature and the rate of quenching.

d. dislocation hardening; this mechanism is mainly operative in lath martensite. Kehoe and Keddy[41] found that the strength of lath martensite increased linearly with the square root of the dislocation density, this in turn being a function of the carbon content.

e. elements in substitutional solid solution; it is well known that substitutional alloying elements will affect the martensitic structure as follows:[40]

1. solid solution hardening
2. depression of Ms temperature and hence a reduction in the amount of precipitation during the quench, and
3. retardation of the tempering process.

However, the overall contribution of substitutional alloying elements to solid solution hardening is very small. It has been shown that the Ms is related to composition by the following equation:[1]

$$M_s\ (^\circ C) = 502 - 810(C) - 1230(N) - 13(Mn) - 30(Ni) - 12(Cr) - 54(Cu) - 46(Mo)$$

where ( ) is weight percent alloy addition.

Summarising, it appears that the strength of martensite can be attributed to two main contributions. The one being a structural contribution which is largely independent of carbon content. The other is due to the redistribution, segregation and amount of carbon in solid solution after quenching.

2.5. Effect of alloying elements on mechanical properties

Ideal dual-phase steels must possess such properties as low yield stress, high tensile strength, high work hardening rate and large uniform and total elongations.[42] In order to obtain such properties, the ferrite matrix must be very clean i.e. free from interstitial impurities and precipitates in so far as is possible, and fine martensite islands must be dispersed throughout. Extensive research on all types of dual phase steels has been performed[43-53] in order to obtain optimum properties and features using the concept of two phases behaving in a mutually beneficial mode.

The effect of alloying elements on the structure and properties of 12% Cr steels has been extensively studied.[2-17] The critical control of alloying elements can be appreciated from these studies. By altering the

equilibrium diagram alloying elements will affect the microstructure obtained and hence the mechanical properties. Alloying elements will also affect the martensite transformation range, usually depressing the transformation temperature. The effect of carbon on the Fe-Cr equilibrium diagram is seen in figure 2.9. The addition of carbon increases the austenite loop and significantly broadens the ferrite-plus-austenite region.[22]

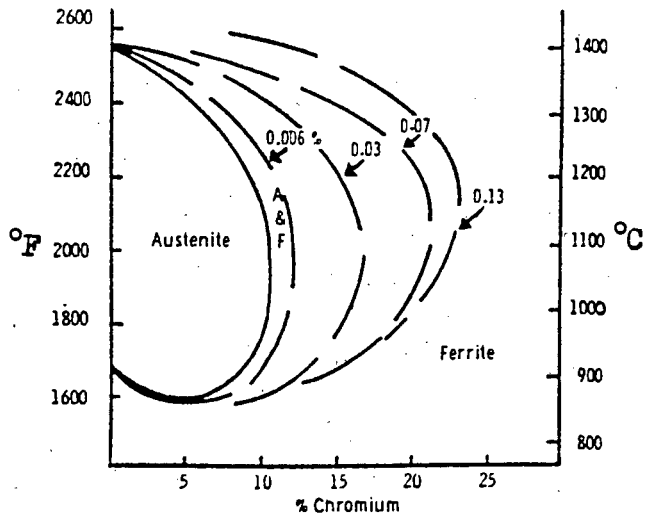

Fig. 2.9. Effect of percent carbon and nitrogen (given equal weight) on austenite and ferrite regions.[22]

Austenite-forming elements invariably increase the strength of an alloy by increasing the amount of austenite, which subsequently transforms to martensite. The interstitial solutes, C and N, increase the strength of martensite and their effects seem to be more or less a linear function of concentration[41]. Increasing amounts of austenite (which subsequently transforms to martensite), cause a linear increase in tensile strength (figure 2.10)[54]. Increasing amounts of martensite, however, first lower the yield stress, but more than 15-20% martensite causes the proof or yield stress to increase (figure 2.11). This is observed in several Cr containing dual-phase alloys.

Grain refinement has long been known as one of the most effective means of improving the toughness of a steel and in addition, increasing the hardness. Dual phase steels have the advantage of being able to

attain a fine grain size since growth of one phase is impeded by the other and vice versa. Lanzillotto and Pickering[55] carried out detailed studies on the martensite constituent of dual phase steels and found that decreasing the size of the austenite grains markedly increased the work hardening rate relative to the flow stress.

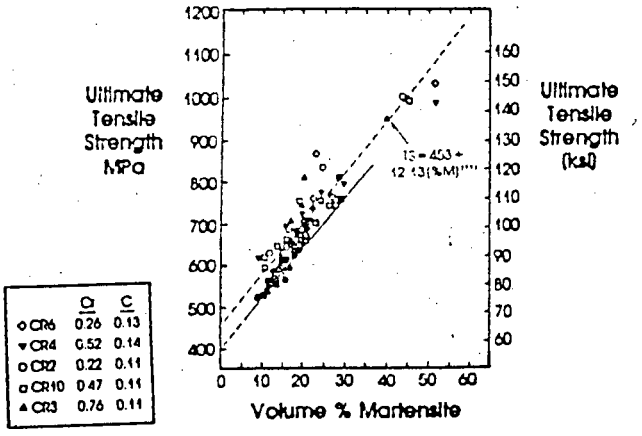

Fig. 2.10 The effect of volume percent martensite on the ultimate tensile strength of several Cr dual phase alloys.[54]

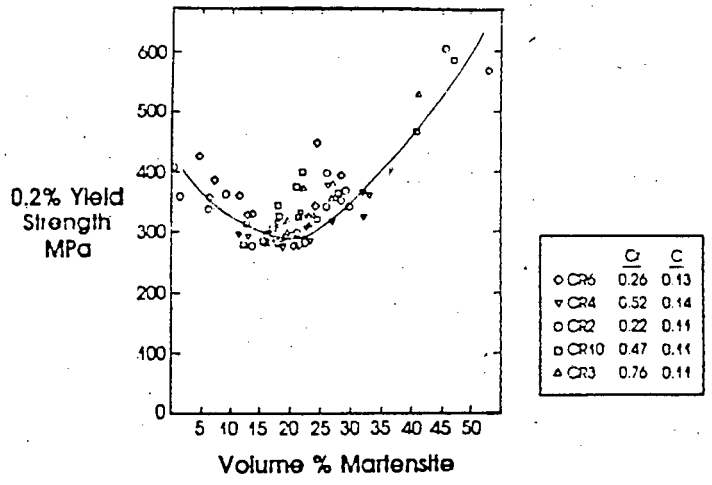

Fig. 2.11 The effect of volume percent martensite on the 0.2% yield strength of several Cr dual-phase alloys.[54]

Extensive work has been performed to determine the effect of adding alloying elements on dual phase steels. Several previous investigations have been concerned with the additions of vanadium, molybdenum and chromium, in enhancing the properties of dual phase steels.[54] Cr additions were found to improve the hardenability of dual phase steels. A 0.5% Cr addition lowered the critical cooling rate at which dual phase properties were obtained, and Marder[54] found that increasing Cr and Mn content both increased the hardenability of the steel. Figure 2.12 demonstrates the effect of Mn on hardenability.

Koo et al[56] observed that Si seemed to increase the carbon content of the austenite formed during intercritical annealing, while Kato et al[57] investigated the influences of Si, Mn and Cr on a variety of dual phase steels. Si was found to accelerate the ferrite transformation and stabilise the austenite by enriching the carbon content; while Mn and Cr also stabilise austenite, but when the content was too large the ferrite

transformation was suppressed. Furthermore Si was found to improve the ductility of these steels.

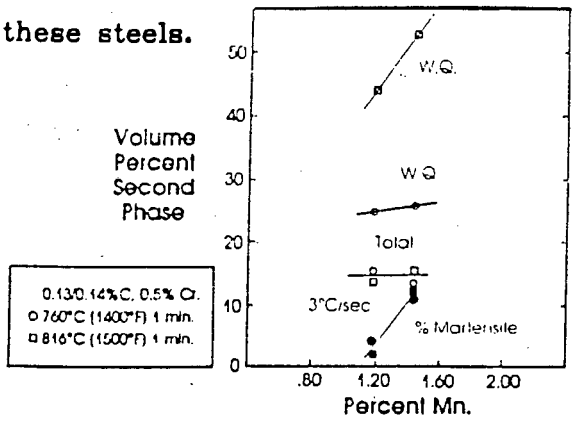

Fig. 2.12 The effect of Mn on the volume percent second phase produced after intercritical annealing at 760°C (1400°F) and 816°C (1500°F) and water quenching of cooling at 3°C/sec.[54]

Hansen et al[58] also performed studies on C-Mn-Si steels. They determined that carbon content plays a significant role on tensile strength on water quenched samples; for example, for a 0.037 %C alloy, an increase in annealing temperature from 760°C to 820°C increases the tensile strength by 69 MPa, whereas at 0.145 %C this change in annealing temperature results in a strength increase of 345 MPa.

Messiem et al[59] found that the carbon content of martensite increased with the Mn and Si contents of the steel depicted in figure 2.13. The increase in these elements resulted in increases in U.T.S. without a significant loss of ductility (figure 2.14).

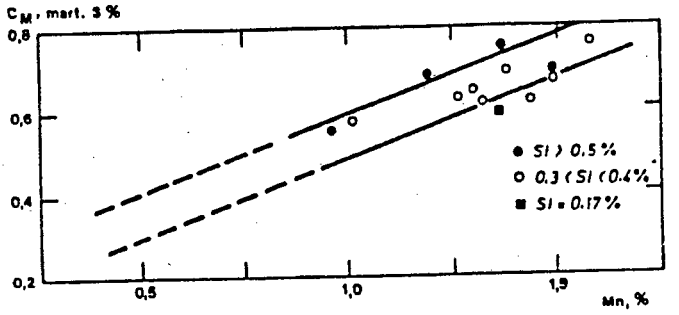

Fig. 2.13 Influence of the manganese and silicon contents of the steel on the carbon content (CM) of the martensite for an amount of 3 percent of martensite in the microstructure of dual-phase steels.[59]

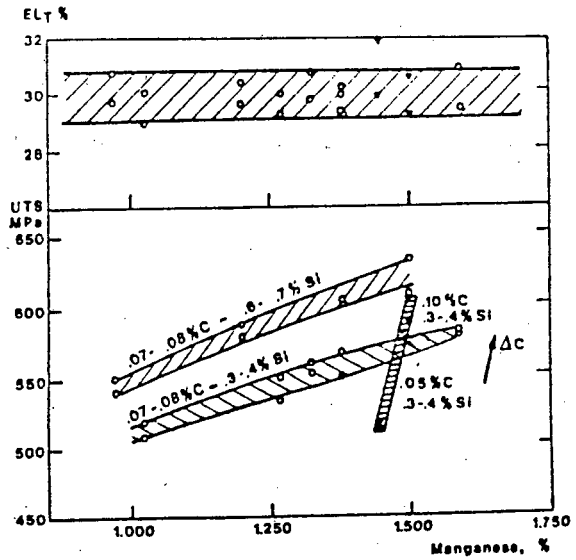

Fig. 2.14 Influence of the steel composition (carbon, manganese and silicon) on mechanical properties. Annealing at 825°C (1517°C) for 2 min30sec and cooling at 48°C/sec (86°F/sec).[59]

The above illustrates some examples of various investigations into the effects of the addition of alloying elements on mechanical properties.

It can be seen that the alloy composition and the effect of thermal treatment markedly influence the properties and behaviour of steels. Thus, it is important to have a reliable and accurate knowledge of the behaviour of elements, both interstitial and substitutional, during heat treatment and their effect on the mechanical behaviour of 3CR12.

CHAPTER 3

Experimental methods

3.1 Materials used

All the materials investigated were manufactured by Middelburg Steel and Alloys. Three 3CR12 alloys were studied and were obtained from a commercial production route. However, each was supplied at different stages of production. Alloy I was received in its final hot-rolled and annealed condition. Alloy II was received from the middle of an as cast slab and alloy III was received in various stages of the production route. These stages included two samples; one from the edge (designated C1) and the other from the centre (designated C2) of an as cast slab. The next stage included two samples again from the edge and centre (designated B1 and B2 respectively) of a slab in the hot-rolled condition. The final stage included two samples again from the edge and centre of a slab in its hot-rolled and annealed condition (designated A1 and A2 respectively). These are diagrammatically represented in section 4, figures 4.15-4.17. The production route is depicted in section 2.2.1., figure 2.6. The compositions of the steels are given in Table 3.1.; these having been determined in the laboratories of Middelburg Steel and Alloys.

Alloy	C	Mn	P	S	Si	Cr	Ni	Mo	Ti	N	FF
I	0.021	1.15	0.02	0.013	0.42	11.28	0.59	0.04	0.37	0.012	10.97
II	0.019	1.17	0.023	0.015	0.45	11.15	0.57	0.02	0.40	0.03	10.55
III	0.027	1.22	0.025	0.006	0.48	11.40	0.58	0.03	0.35	0.013	10.94

Table 3.1 Chemical Composition of test alloys; wt%; Balance Fe

3.2 Dilatometry

A dilatometer was used to determine the As (the austenite start),Af (the austenite finish), the Ms (the martensite start) and the Mf (the martensite finish) temperatures for alloy,I. The specimens were cut to dimensions of 4x4x50mm. The specimen was heated to 1050°C at a rate of 3°C\min and then furnace cooled. The cooling rate varies with temperature as illustrated in figure 3.1. The transformation temperature was taken at that temperature at which the slope of the dilation curve started to change, since this represents the onset of the phase transformation (see figure 3.2.).

Dilatometry is an established technique in the determination of equilibrium phase diagrams. This method utilises the change in volume associated with nearly all phase changes. For instance, the transformation from ferrite to austenite produces an increase in density and hence a decrease in specimen length which is monitored by the dilatometer. It is applied by measuring the change in length of a specimen heated or cooled at a given rate.

As the technique is a system to simulate transformations occurring under equilibrium conditions, it is necessary that the equipment used must be reliable and consistent under both the cooling and heating cycle. It has been determined[10] that a 3°C/min heating rate and a cooling rate as shown in figure 3.1., allow transformation approximating to equilibrium conditions for 3CR12. Raynor[60] comments that "the chief advantage of the method (dilatometry), as with the electrical conductivity technique, is that heating and cooling rates may be made sufficiently slow to give an approximation to equilibrium, while if this is not possible, the temperature may be controlled at a given value until equilibrium is indicated by a steady state."

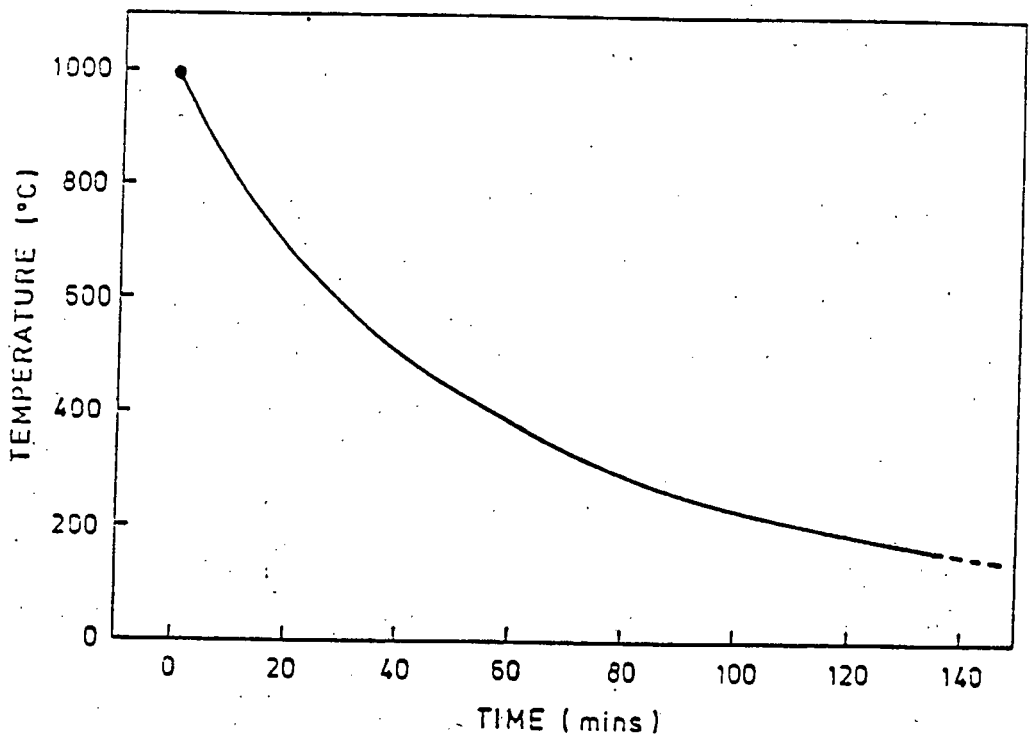

Fig.3.1 **The determination of the cooling rate for a particular temperature and time**

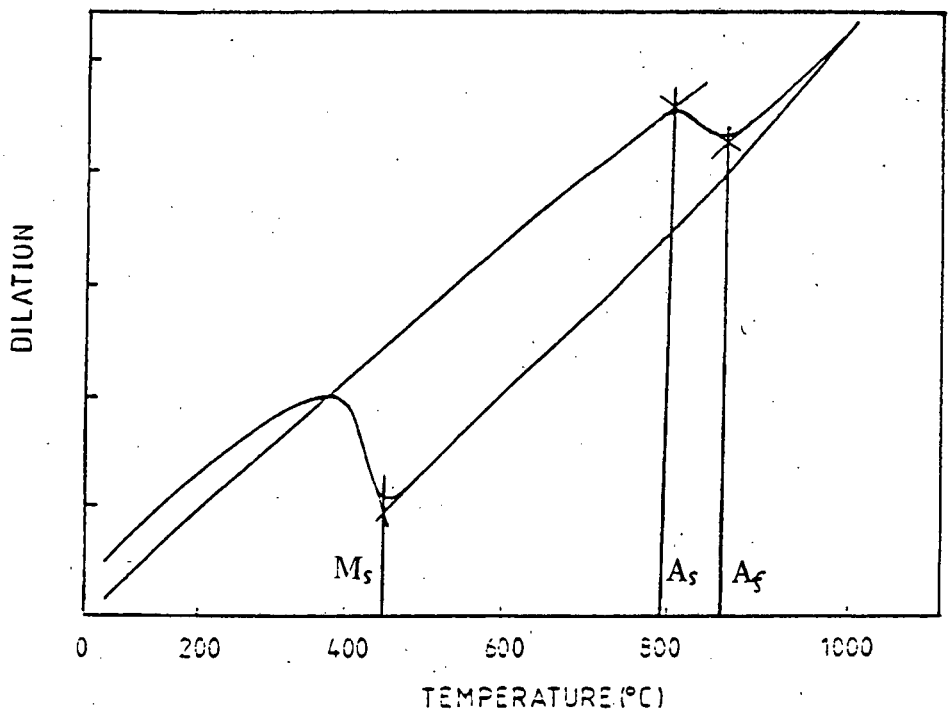

Fig.3.2 **A dilatometric trace showing the transformation changes occurring under equilibrium conditions for an alloy of 3CR12 and how these changes are measured for empirical observations.**

3.2.1. The effect of interstitials on the martensite start (Ms) and the martensite finish (Mf) temperatures

Further dilatometry was performed on test alloy I. The specimens were heated at a rate of 3°C/min and again furnace cooled. Specimens were heated to various temperatures in the dual phase region (see section 3.3.).They were held at temperature for 1 hour. This set of treatments was used to determine the Ms and Mf temperature of these samples.

3.3 Heat treatments

Two horizontal tube furnaces connected by a porcelain tube were used. Specimen dimensions were 10x15x5mm. They were attached by a thin nichrome wire to an AISI 316 stainless steel rod. This enabled quick and reliable extraction from the furnaces to the quench bath. The quench medium being oil. All specimens were coated in two high temperature ceramic coats, aniscol and isomol, to prevent oxidation .

Alloy I (see table 3.1.) was the only material to undergo heat treatment. As the temperature is altered in the dual phase region, so the volume fraction of both the ferrite and austenite alters. The effect of temperature on the volume fractions of each phase can be seen in the pseudo-binary phase diagram for 3CR12 (section 2.2.2., figure 2.7.). The heat treatment temperatures considered were both between and outside the dilatometrically determined As and Af temperatures; namely 815°C, 835°C, 870°C, 900°C, 950°C, 1000°C and 1050°C. This allowed for samples of a purely ferritic structure as well as samples with a maximum amount of austenite to be studied. Three holding times were considered; 1 hour, 4 hours and 20 hours. For the 1 hour treatment, other temperatures included were 823°C, 843°C and 882°C.

3.4 Metallography

3.4.1 Macroetch

The as cast samples were etched in aqua regia in order to obtain a macroetch. The etchant consisted of 3 parts HNO_3 : 1 part HCl : 1 part H_2O. The samples were swabbed for 10 -15 minutes at room temperature.

3.4.2 Optical metallography

All specimens were mounted in a cold-curing resin. polished and finished with a 0.25μm diamond paste. A variety of etchants were tested. The most effective for characterising microstructures was a tint etch of the following chemical composition:

A. 100 ml of 1:5 v\v HCl
2g ammonium bifluoride
1g potassium metabisulphite

B. 10 ml HNO_3
20 ml HCl
30 ml H_2O

Stage 1 required a pre-etch with etchant B to reveal the general microstructure and ferrite grain boundaries plus martensite structure. Immersion of 2½ minutes at room temperature was sufficient. Stage 2, using etchant A, tinted the specimen. A good contrast between the ferrite and martensite was obtained. The ferrite phase colours a blue\brown colour whilst the martensite phase is not etched. Immersion for 10-20 seconds at room temperature sufficed. Between the two stages the samples are washed in water. They were never allowed to dry. Final washing was with water followed by ultrasonic cleaning in alcohol.

A third etchant; C. 3.0g potassium metabisulphite
1.5g sulphamic acid
0.7g ammonium biflouride
100 ml H_2O

was used to enhance the microstructure identified in figures 4.15 (a) and 4.16 (a) and (b). Immersion for 10-20 seconds at room temperature results in the martensite being etched while the ferrite remains unetched.

3.5 Microanalysis

Specimens for the Scanning Electron Microscope(SEM) were usually the same specimens used for the optical microscopic investigation. They were all carbon coated for microanalyses.

The SEM is fitted with an energy dispersive X-ray spectrometer capable of detecting X-rays emitted by the specimen during electron-beam excitation. These X-rays carry a characteristic energy and wavelength, which when measured will reveal the elemental composition of the specimen. Limitations of energy dispersive X-ray analysis include the inability to analyse light elements (e.g C,N,O).

Energy-dispersive spectrometers are most efficient for the analysis of X-rays having energies between ≈ 0.7 and 15 keV.Spectrometer resolution at energies below 0.7 keV is degraded by absorption of the X-rays in the beryllium window and other factors such as the thin gold film at the face of the diode and the thin inactive layer at the surface of the diode [61]. Analysis of an element having a lower atomic number than sodium (11) is not considered possible. Hence, it was not possible to analyse interstitial elements (i.e C and N) using the available equipment. However, the area of interest was the partitioning of substitutional elements which could be detected.

The characteristic X-rays of some elements overlap on an energy spectrum and this may be a serious problem if the region of interest on a spectrum contains several closely spaced peaks. An example of this overlapping is the Kα peak of manganese ($K\alpha_{Mn}$ =5.9 keV) which will be hidden by the Cr Kβ ($K\beta_{Cr}$ = 5.9 keV) peak, and the manganese Kβ peak ($K\beta_{Mn}$ = 6.5 keV) will be hidden by the iron Kα peak ($K\alpha_{Fe}$ = 6.4 keV).Thus spectrometer resolution needs to be very high to differentiate between these peaks.

The composition of the ferrite and austenite (now martensite) phases was determined using energy dispersive spectrometry (EDS) on a semi-quantitative basis (SSQ). These analyses were performed using a Cambridge S200 scanning electron microscope equipped with a Tracor-EDS system. It must be remembered that SSQ results are not absolute but can be used to accurately compare relative phase compositions. Within a single analysis system the results are reproducible and it has been established that microanalysis is a reliable semi-quantitative method for determining the relative concentrations of an alloying element in different regions of the same phase or between phases.[12] It is necessary to select optimum parameters that best suit a particular material. 3CR12, as seen in figure 2.7 (section 2.2.2.), shows very small amounts of partitioning of substitutional elements (Cr and Ni) occurring between the two phases. It is therefore fundamental to have reliable parameters to obtain accurate results. Parameters include accelerating voltage, probe diameter and X-ray aquisition time.

It has been established [10,11] that those parameters most suited to 3CR12 on the Cambridge S200 are:

1. an accelerating voltage (kV) of 20 kV, where the background contribution, based on Kramers' law is at its lowest.

2. an acquisition time of 400 seconds. This was found to give the best resolution of the X-ray spectrum, which produced a greater statistical accuracy of analyses.

3. as small a probe diameter as possible in order to obtain the smallest interaction volume. Naturally, an acceptable x-ray count rate has to be achieved (monitored by the dead time percentage). The parameters chosen for this work were a working distance of 25mm (i.e. the distance from the sample to pole piece in the

SEM) and (for the X-ray detector configuration on the SEM, i.e. a tilt angle of 30°) a take off angle of 58°. To minimise detector dead time and simultaneously optimise counts the dead time was adjusted manually to be about 25-26%.

3.6 Hardness measurements

The bulk hardness of all specimens was measured using a Vickers pyramid indenter at a 30 kg load. Each result is the average of four separate indentations. These measurements are found to be accurate with a high reproducibility.

Microhardness measurements were performed in order to monitor any change in the hardness of the martensite phase. The hardness of martensite changes as a function of chemical composition - particularly interstitial content[49] - and can thus reflect the influence of elemental partitioning. The microhardness of all specimens was measured using a Shimadzu microhardness tester. It was necessary to use the smallest possible load to prevent an overlap of the indentation on the adjoining grains. Experimental error, however, is rapidly increased when small test loads are used due to the nature of the reading of the indentations. The relative accuracy with which an observer can evaluate a series of measurements is naturally increased the greater the number of measurements taken. Thus the quoted results are an average of ten separate indentations.

3.7 Volume fraction analysis

Volume fraction analysis was carried out on all specimens to determine the amount of martensite and ferrite formed at the transformation temperatures of interest. This was performed using a point counting technique described by Hillard, Cahn and Underwood (see ref. 11). A 9X9 graticule was fitted to the Scanning Electron Microscope. This was a perspex graticule made according to the dimensions of the SEM

screen. This allowed for greater comfort for the operator and hence increased accuracy. The volume fraction (VFM) was determined according to the following relationship:

V.F.(Pp) = number of grid intersections lying on a martensite phase/ total number of grid intersections.

THe grid superimposed on the SEM screen was such that the magnification relative to the grid spacing did not allow the martensite phase to occupy more than one grid intersection. This naturally was not always possible but the highest accuracy was achieved by two operators using identical operating conditions. Each operator applied the graticule 32 times to each specimen i.e. a total of 5184 points per specimen were counted. This gave an accuracy of greater than 10% with a 95% level of confidence.

3.8 X-ray diffraction

This technique is useful for the investigation of phase changes in the solid state. It was hoped that monitoring of carbon concentrations using this technique was feasible. However, the difficulty of differentiating the various phases resulted in some degree of inaccuracy. The similar crystal structures, i.e ferrite, a body centred cubic structure, and martensite, a body centred tetragonal crystal structure, mean that there is considerable overlapping of these peaks which cannot be differentiated by the available facility. Furthermore, as the carbon content of this steel is low (0.03%) the distortion of the ferritic and martensitic lattice parameters is minimal thereby further reducing the ability to clearly distinguish the two peaks.

CHAPTER 4

Results

4.1. The transformation temperatures of 3CR12

The hot-rolled and annealed material, alloy I (see section 3.1.,table 3.1) was used in order to dilatometrically determine the As, Af, Ms and Mf temperatures of this alloy. This dilatometric trace, see figure 4.1., was obtained only to determine these transformation temperatures thus allowing for an accurate assessment of the extent of the dual phase region for this alloy. A heating rate of 3°C/min has been considered adequate[10] for identification of equilibrium transformation temperatures in 3CR12. The high temperature diffusional transformation temperatures observed are considered a reasonable approximation to equilibrium. The cooling rate is shown diagrammatically in section 3.2, figure 3.1. A maximum temperature of 1000° was achieved, whereupon the specimen was immediately allowed to furnace cool. No soaking at any temperature for any length of time occurred. The As and Af temperatures obtained from the trace were 842°C and 940°C respectively. The Ms temperature, on furnace cooling, was 539°C, while the Mf was 467°C.

The trace of figure 4.1. indicates that specimens annealed above 940°C should be fully austenitic. However metallography of the specimens annealed at 1000°C showed that 3CR12 never became fully austenitic.

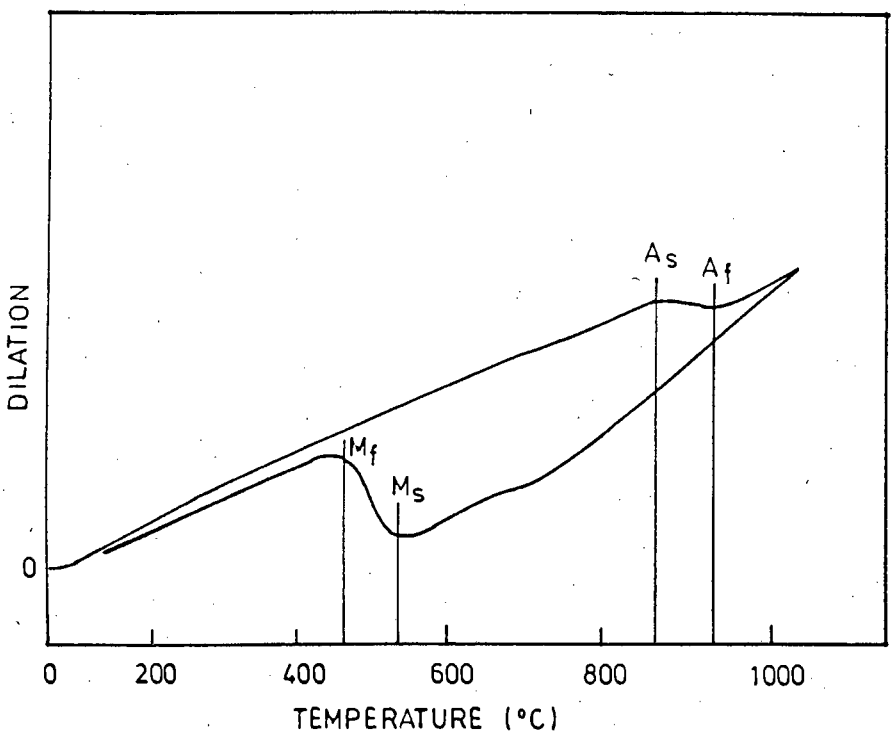

Figure 4.1 A dilatometric trace of 3CR12 showing the phase transformation temperatures.

(As represents the austenite start temperature; Af represents the austenite finish temperature; M_s represents the martensite start and M_f the martensite finish temperature on furnace cooling)

The microstructures of heat treatments at 835°C, 900°C and 1000°C for 1 hour, 4 hour and 20 hour holding times are shown in figures 4.2, 4.3 and 4.4. The microstructures of the specimens treated for 1 hour and 4 hours at each test temperature showed no significant change with respect to the size of the ferrite grains, whilst after 20 hours at 1000°C significant growth of the ferrite grains had occurred.

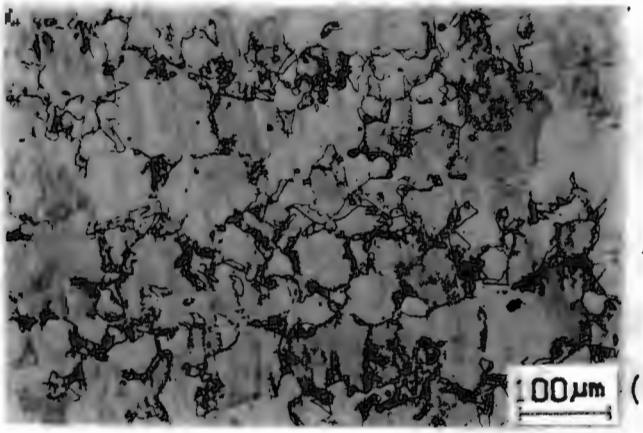

(i)

(ii)

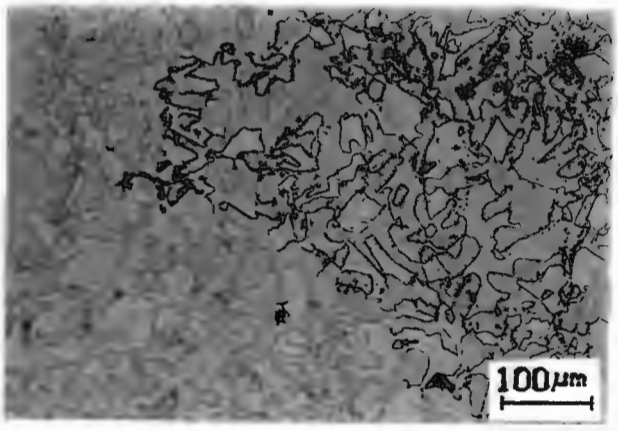

(iii)

Fig. 4.2 Isothermal annealing of 3CR12 at 835°C for (i) 1 hour (ii) 4 hours (iii) 20 hours, and oil quenched. Starting material was the hot-rolled and annealed condition.

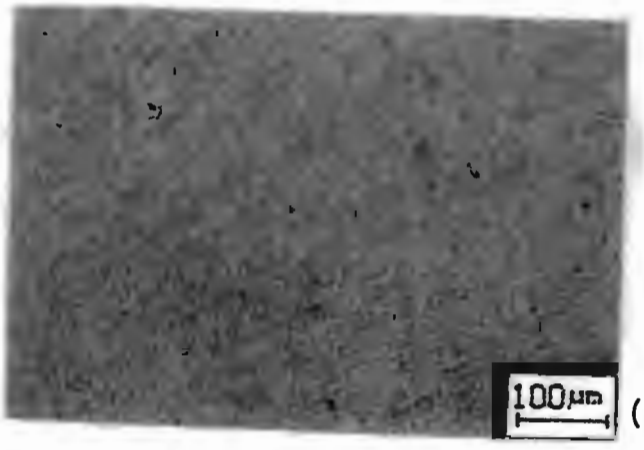

(i)

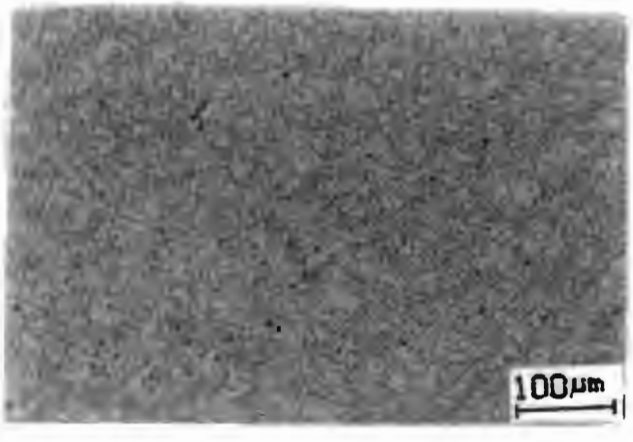

(ii)

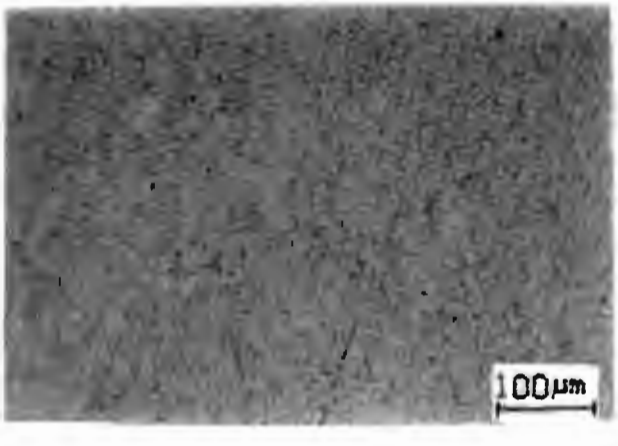

(iii)

Fig. 4.3 Isothermal annealing of 3CR12 at 900°C for (i) 1 hour (ii) 4 hours (iii) 20 hours, and oil quenched. Starting material was the hot-rolled and annealed condition.

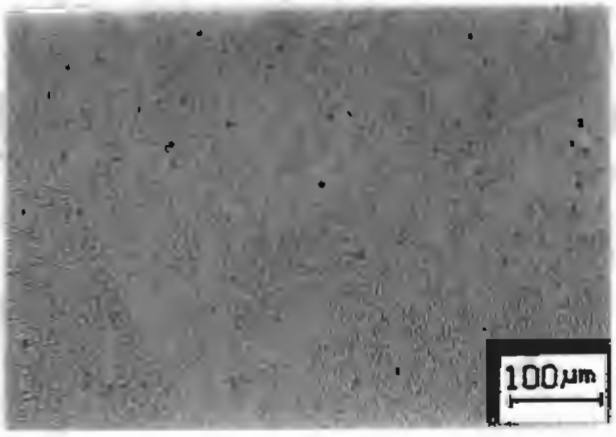

(i)

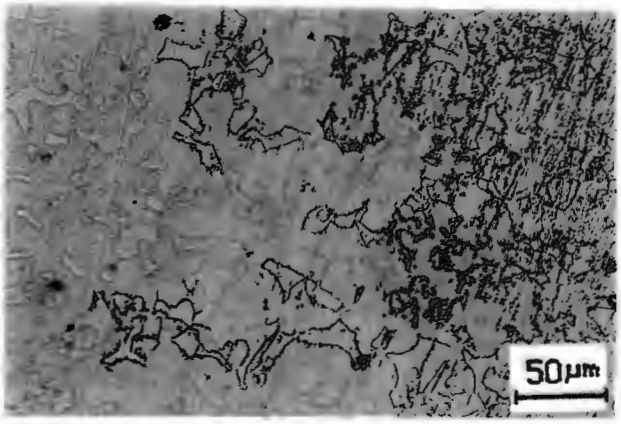

(ii)

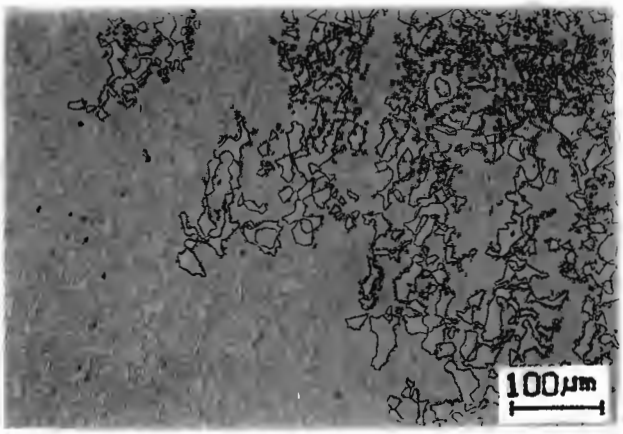

(iii)

Fig. 4.4 Isothermal annealing of 3CR12 at 1000°C for (i) 1 hour (ii) 4 hours (iii) 20 hours, and oil quenched. Starting material was the hot-rolled and annealed condition.

The following results refer to the hot-rolled and annealed condition (i.e. alloy I, section 3.2). These samples having been annealed for 1,4 and 20 hours at various temperatures both "within" and "outside" the dilatometrically determined dual phase region, and then oil quenched. This was performed in order to study the changes in bulk hardness, microhardness of martensite and ferrite, volume fraction of martensite (VFM) and microstructural changes as a function of these temperatures.

4.2. Macrohardness

The bulk hardness trends from the heat treated and quenched specimens are presented in figures 4.5, 4.6 and 4.7. The macrohardness values are presented in tables 1.1-1.3, appendix A. There is a very clear trend of macrohardness for all three holding times. The hardness increases steadily through the dual phase region. No dramatic increases are observed and specimens from the three holding times reach a maximum value at 1050°C of 251.8 $kgmm^{-2}$, 243.5 $kgmm^{-2}$ and 257.0 $kgmm^{-2}$ for the 1, 4 and 20 hours holding times respectively. The values are similar and holding time appears to have had little effect, indicating that hardness is a temperature and not time dependent property.

4.3. Martensite microhardness

The microhardness values for the martensite and ferrite phases are shown in tables 1.1-1.3, appendix A. Only martensite microhardness values are presented in a graphical form as it is the property of this phase that is of particular interest.

Generally, the tabulated ferrite microhardness (see tables 1.1-1.3) values show a general increase in ferritic hardness as VFM increase. The fluctuations observed, particularly for the 4 hour heat treatment, could be due firstly to the increase in martensite content affecting the plastic flow in ferrite grains due to the nature of the microhardness testing; and secondly, due to increased martensite content causing high

dislocation density in ferrite due to the greater expansion of austenite grains upon martensite formation.

In figure 4.5, the microhardness values for the 1 hour annealed and oil quenched specimens initially show a region of relatively small change until 900°C, although a general increase in martensite microhardness is observed, but then a sharp increase in martensitic microhardness until 1000°C, whereupon a general levelling of values occurs. The data points of 823°C, 843°C, and 882°C were included in order to attempt to reproduce Brinks[4] results. However, although the values he obtained were lower than the values obtained in this series of results, the trend is similar. As stated in the introduction, his values are not fundamentally correct. The "load effect" associated with the microhardness testing at low loads further produces elevated hardness measurements.

The 4 hour annealing treatment shows again the two regions; - the first being a region of little change in microhardness, with a slight increase occurring toward 900°C. However, the increase in annealing temperature from 900 -1050°C shows a steep rate of increase in the microhardness values reaching a maximum value of 362 $kgmm^{-2}$ at 1050°C.

The 20 hour anneal again shows the trend described above. A slight dip occurs around 870°C with the microhardness value reaching a low at 237.0 $kgmm^{-2}$. However, this falls within the experimental error. Again, the steady increase in microhardness from 900°C reaching a maximum at 1050°C is evident.

Generally, the values of the martensite microhardness for the 1 hour and the 20 hour annealing times show the very distinct trend that Brink[4] observed. The values for the 4 hour treatment are slightly lower, however the trend is clear.

4.4. Volume fraction of martensite (VFM)

The volume fraction of martensite (VFM) values for the three holding times are presented in tables 1.1-1.3 in appendix A. The transparencies over figures 4.5, 4.6 and 4.7 present these values graphically.

The VFM curve for the 1 hour treatment show little increase in VFM at the lower annealing temperatures but after 835°C there is a sharp increase in VFM until ~870°C whereupon a levelling of the curve results with little subsequent change.

The 4 hour anneal shows a more steady, consistent increase as can be seen in figure 4.6. Again the curve levels from 900 to 1050°C.

The 20 hour anneal again demonstrates this familiar shaped curve. A steady increase is observed until 870°C, whereupon a general levelling of martensite percentage occurs.

4.5 Summary of the relationship between bulk hardness, microhardness and volume fraction of martensite

The relationship between bulk hardness and VFM in figures 4.5-4.7 can be generally separated into two distinct regions within the temperature range of 800-1050°C. From 0% to 50% VFM there tends to be a gradual increase in hardness with a steep increase in VFM. From 50% VFM and greater the increase of hardness is still gradual, but the VFM function hardly changes. There is a slight increase but overall the tendency is that of an unchanging function.

The general trend of the microhardness values can also be categorised as having two regions. Initially this function is relatively unchanging, but after 950°C there is a rapid increase of martensitic hardness. Thus

the trend overall is apparent. The bulk hardness values at the lower temperatures can be attributed to VFM increase but at the higher temperatures it would appear to be affected by the martensite hardness increase alone.

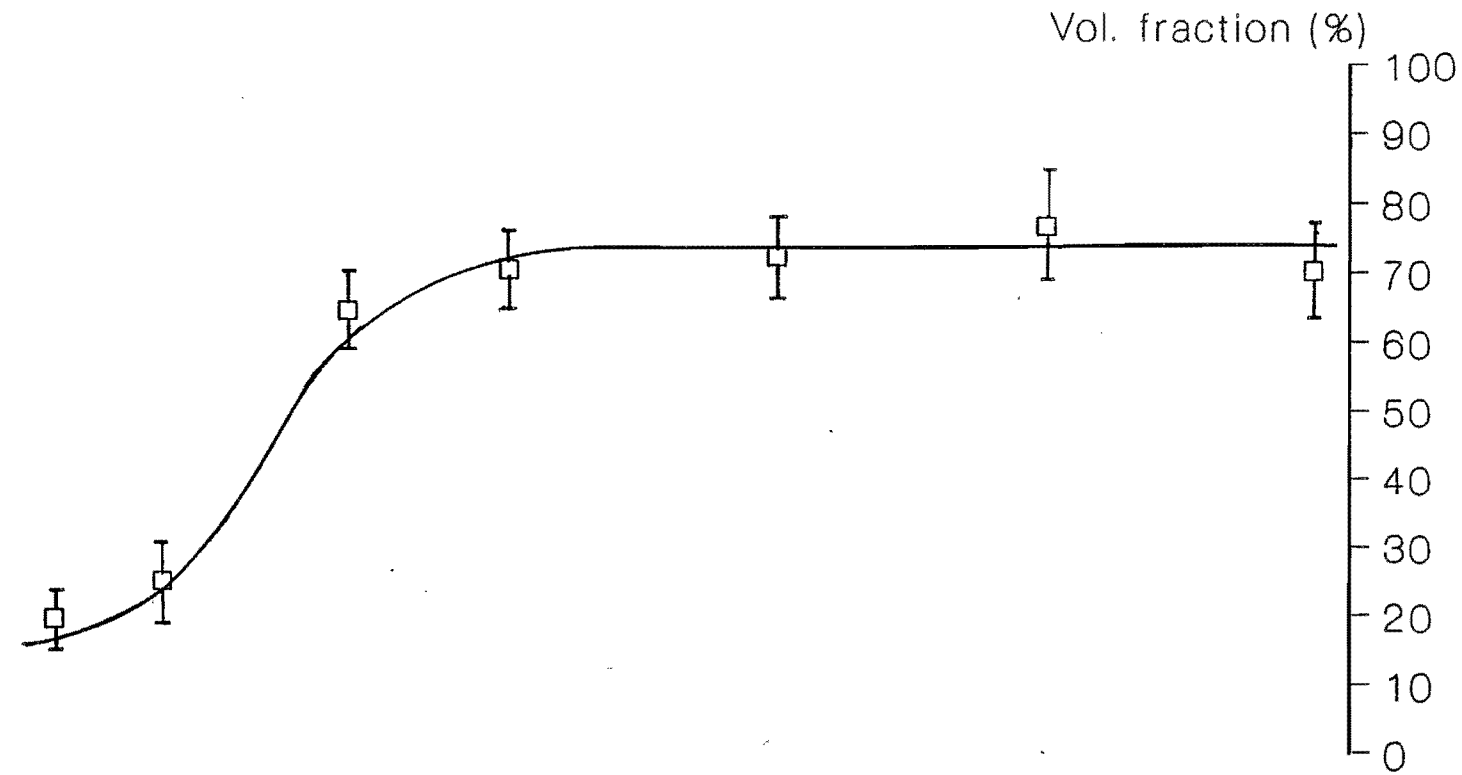

□ Volume fraction (%)

FIGURE 4.5.

Annealing time: 1 hour

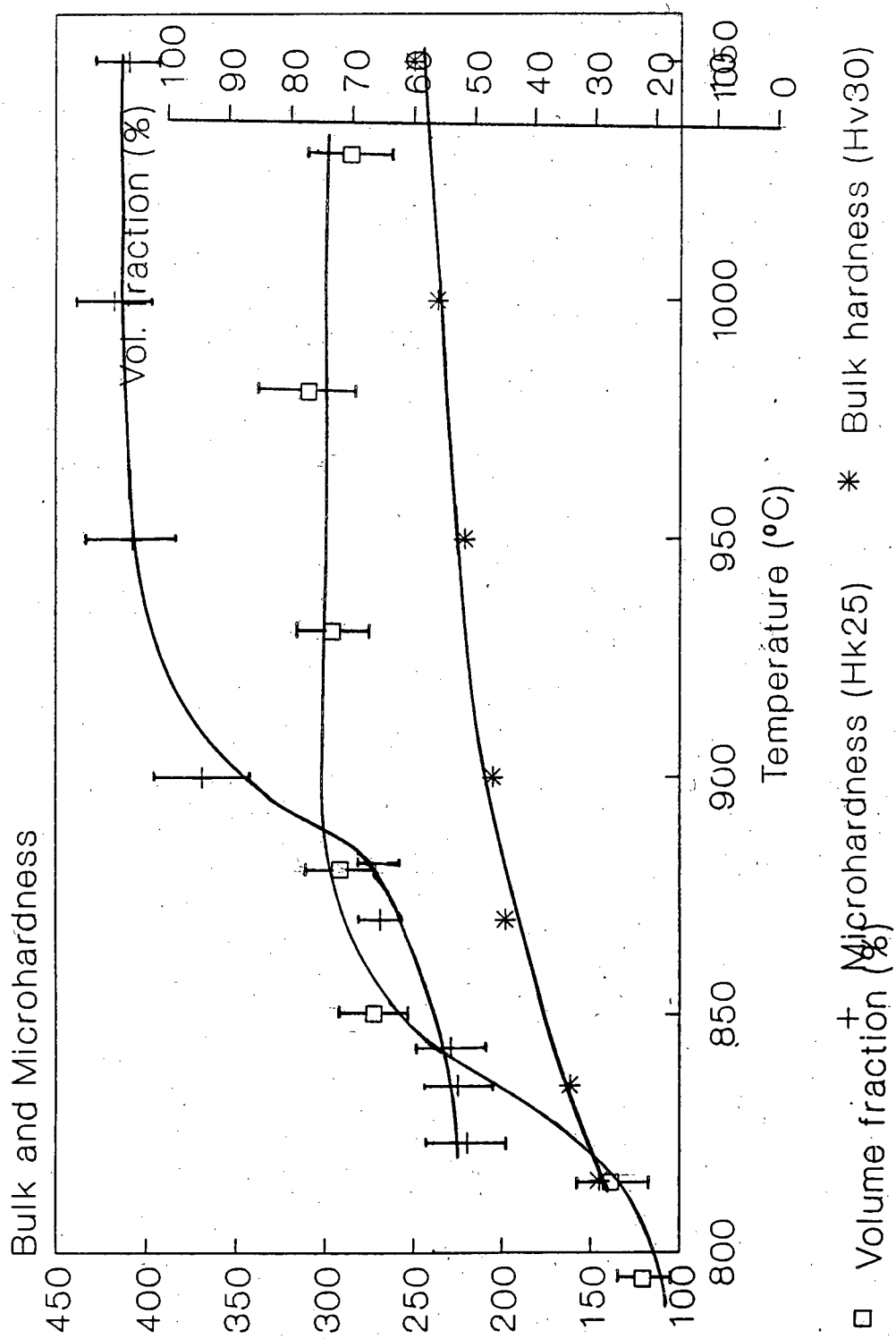

Vol. fraction (%)
0
10
20
30
40
50
60
70
80
90
100
Volume fraction (%)

FIGURE 4.6.

Annealing time: 4 hours

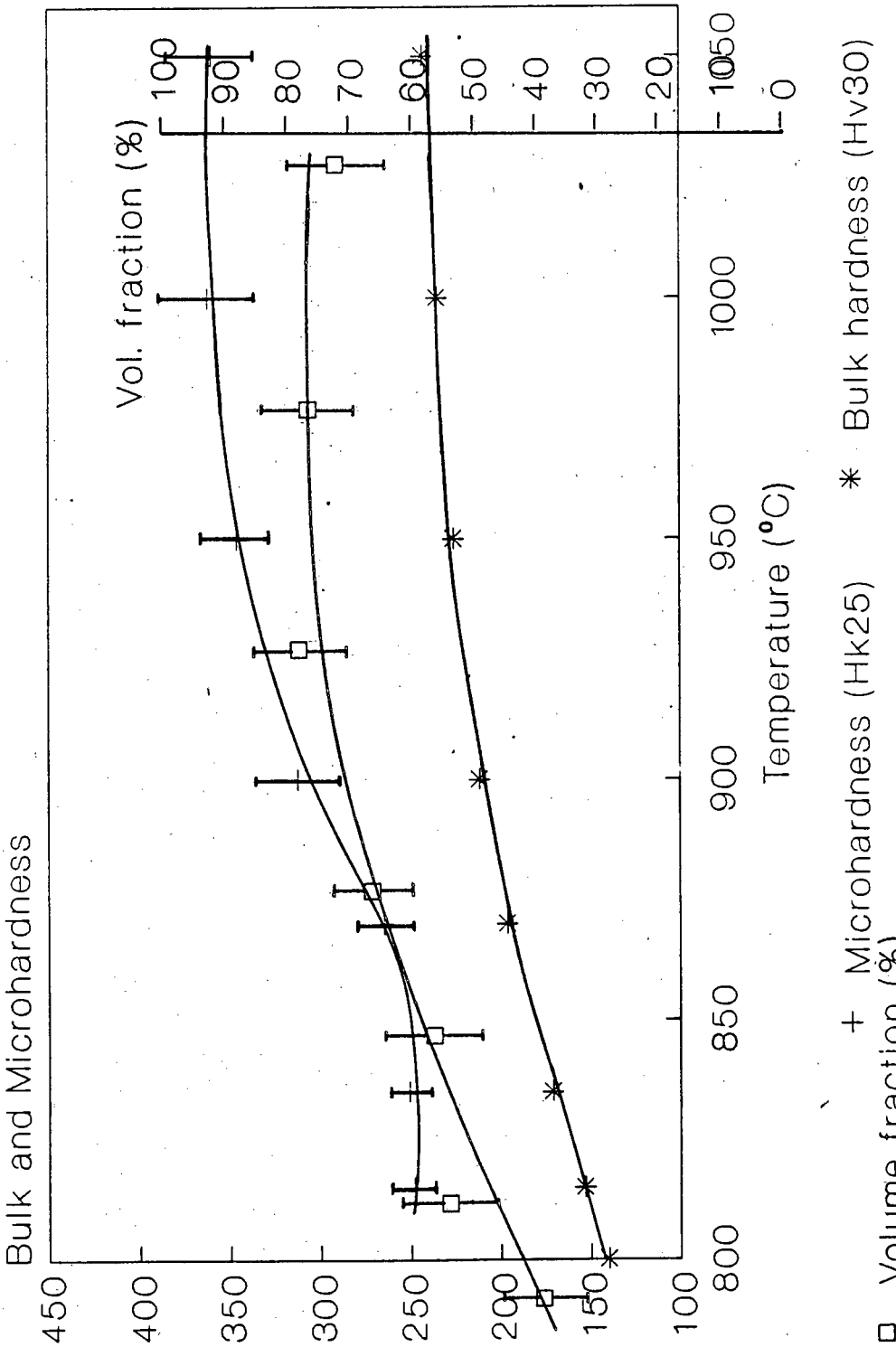

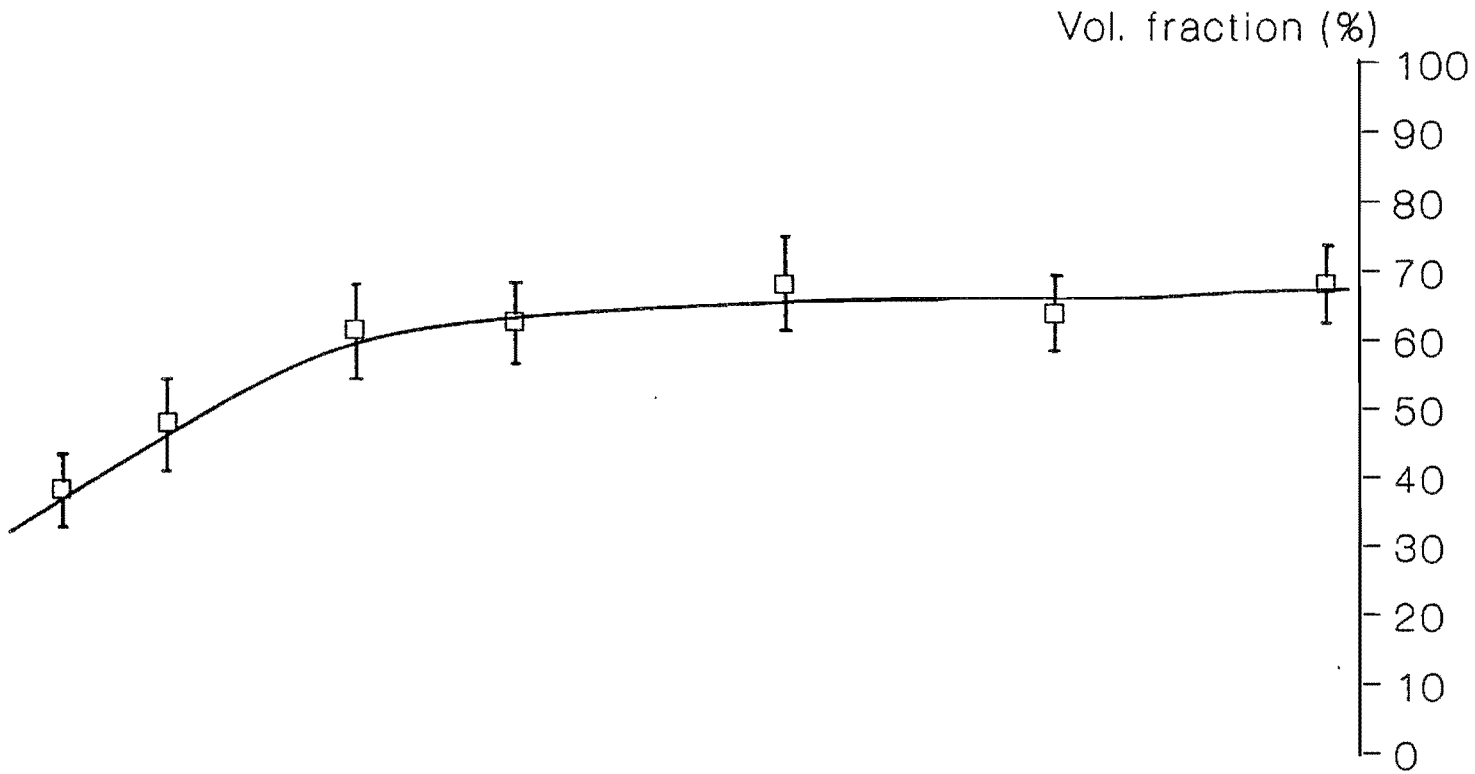

□ Volume fraction (%)

FIGURE 4.7.

Annealing time: 20 hours

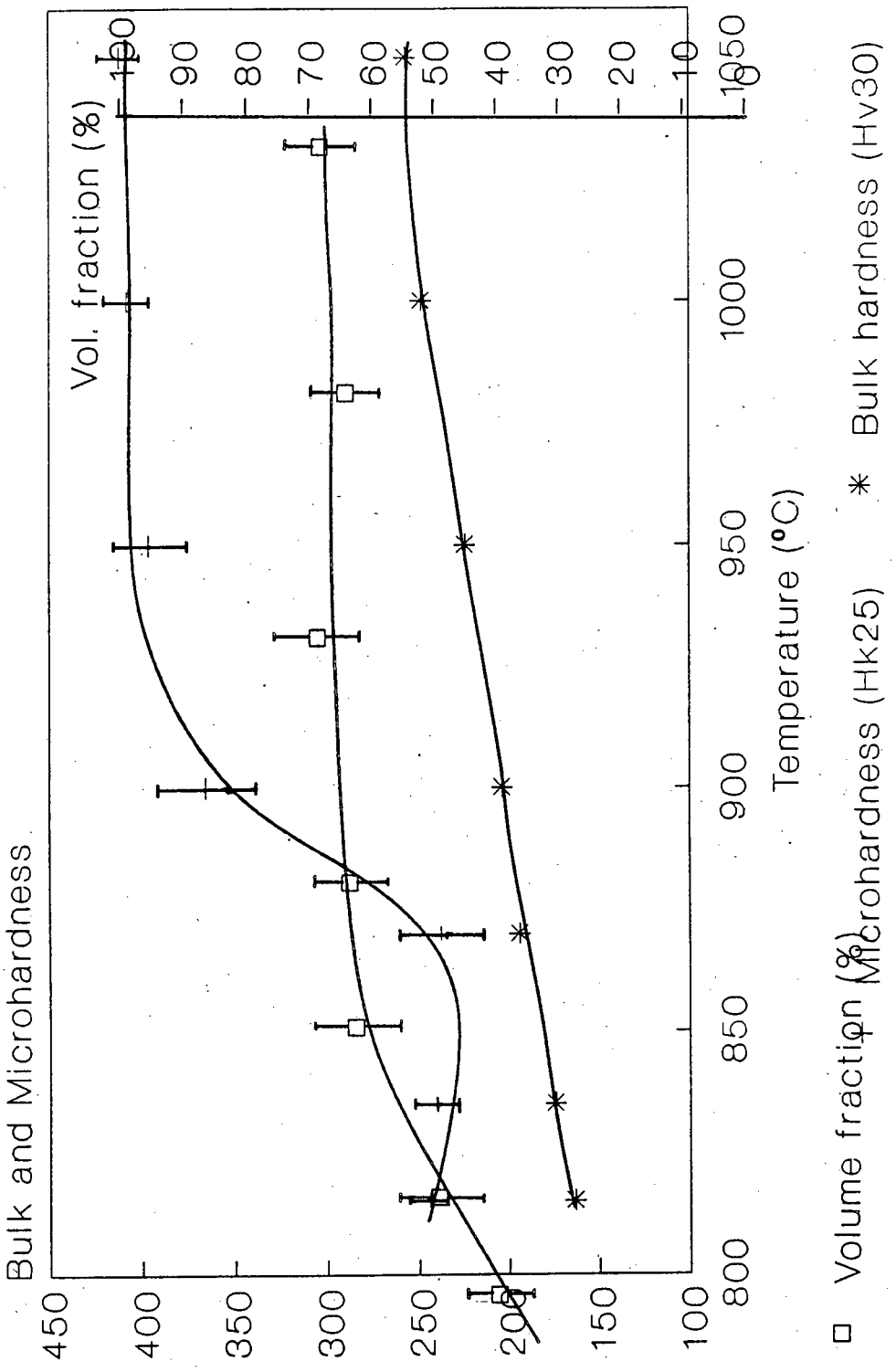

4.6. Element concentration

The values for the concentration of elements in each phase is shown in tables 1.1-1.7 appendix A. Each table gives the element concentration at a particular temperature for the different annealing holding times. The graphs (figures 4.8 -4.13) present these values as the ratio of element concentration in martensite with respect to the element concentration in ferrite, defined as the partitioning coefficient.

In figures 4.8 - 4.13 the relationship between partitioning coefficients of the ferrite-forming elements, Cr and Si and the austenite-forming elements, Ni and Mn and the intercritical annealing temperature is shown. The partitioning coefficient of Cr and Si remains relatively constant with increasing intercritical temperature and also with increasing holding time. The composition appears closely similar to that of the bulk composition of 3CR12. The partitioning coefficients of the austenite-forming elements, Mn and Ni show the greatest variations. However within the statistical error of the SSQ package these fluctuations are not significant.

For Ni, after a one hour anneal the ratio values show fluctuations between 1.25 and 1.70; while the four hour anneal shows between 1.35 and 1.75 and the 20 hour between 1.55 and 2.04. The Mn curves again show slight inconsistencies, being particularly noticeable in the 20 hour anneal. The Mn ratios for this annealing time fluctuate between 1.25 and 1.55. However, as shown in section 3.5, the Mn peaks are overlapped by both the Cr and Fe peaks hence difficulty in accurately assessing the element concentration arises.

Table 4.1. presents a tabulated form of the ratio of the titanium content in martensite to titanium content in ferrite. No particular trends are observed and these values fluctuate considerably.

It is clear that partitioning of substitutional elements occurs at all

temperatures. The general trend is one of no significant change of partitioning occurring as a function of holding time and intercritical temperature. Generally all graphs appear linear within experimental errors.

Table 4.1. The ratio of titanium content in the martensite to the titanium content in the ferrite phase. Annealing times of 1, 4 and 20 hours at the temperatures indicated are given.

TEMPERATURE (°C)	ANNEALING TIME (hours)		
	1	4	20
815	0.85 ± 0.08	0.61 ± 0.04	0.70 ± 0.06
835	0.77 ± 0.23	0.64 ± 0.04	0.59 ± 0.06
870	0.58 ± 0.07	0.60 ± 0.03	0.62 ± 0.10
900	0.48 ± 0.12	0.50 ± 0.06	0.53 ± 0.07
950	0.72 ± 0.25	0.75 ± 0.17	0.58 ± 0.05
1000	0.67 ± 0.04	0.80 ± 0.22	0.63 ± 0.07
1050	0.60 ± 0.01	0.67 ± 0.01	0.58 ± 0.01

The ratio of element content in martensite with respect to element content in ferrite
Annealing time : 1 hour

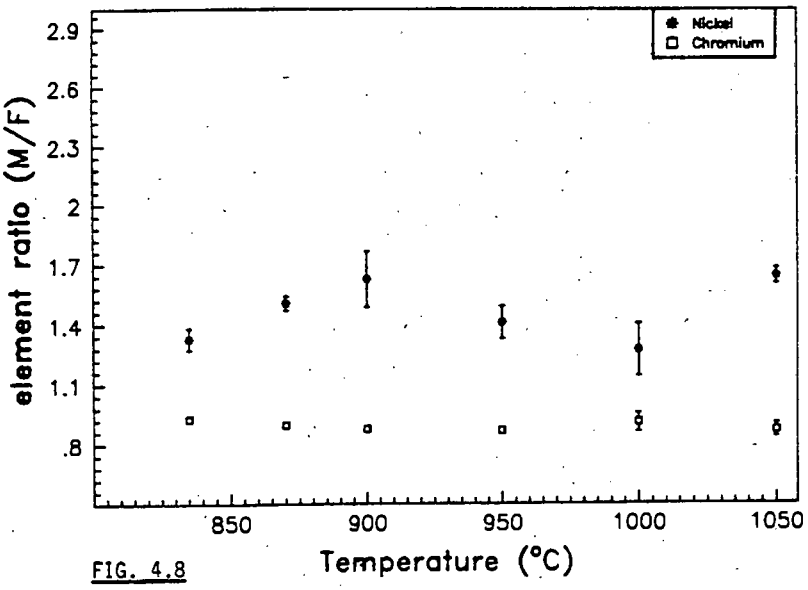

FIG. 4.8

Annealing time : 4 hours

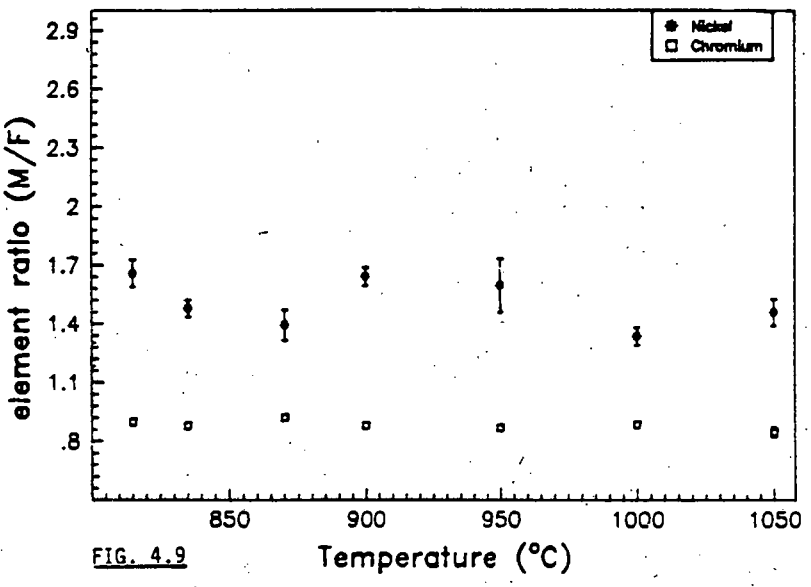

FIG. 4.9

Annealing time : 20 hrs

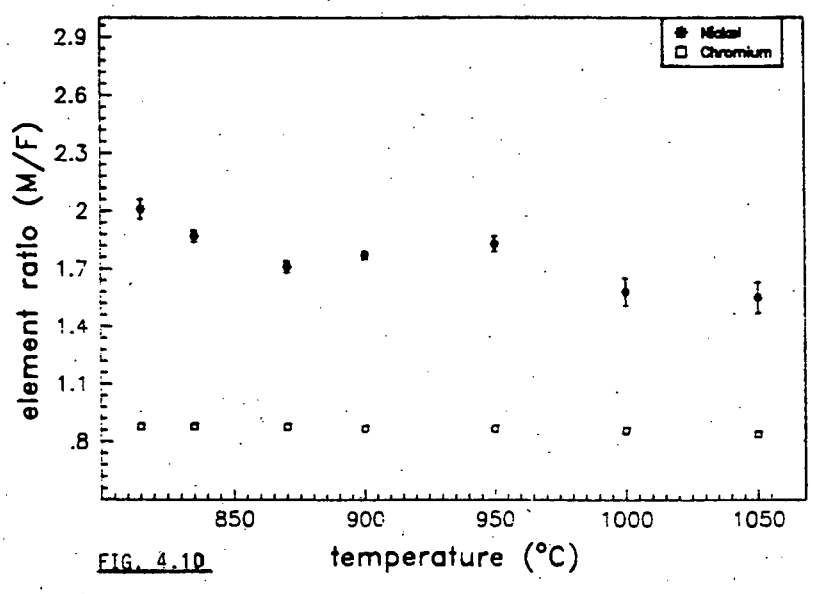

FIG. 4.10

The ratio of element content in martensite with respect to element content in ferrite
Annealing time : 1 hour

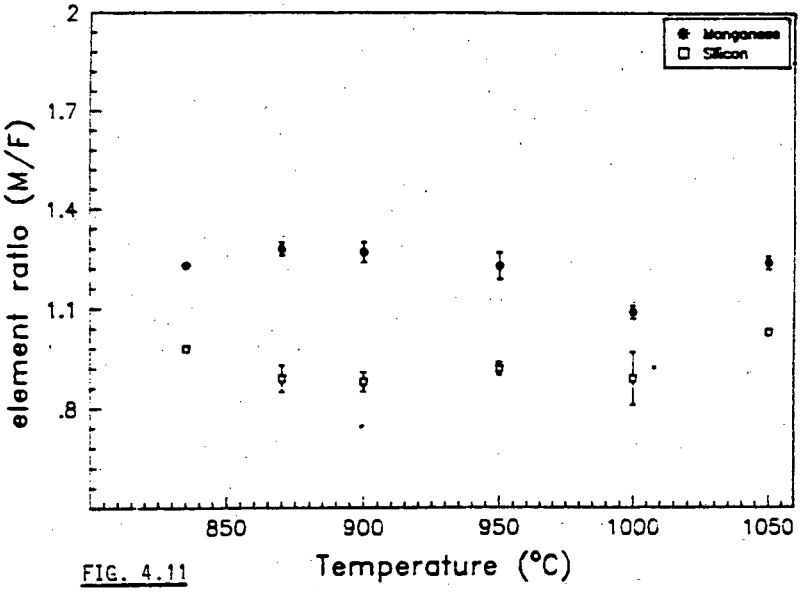

FIG. 4.11

Annealing time : 4 hours

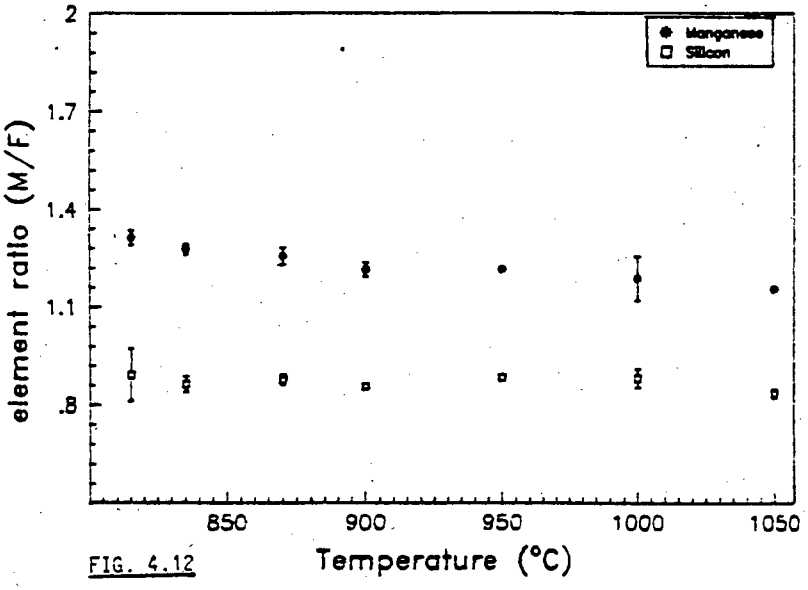

FIG. 4.12

Annealing time : 20 hours

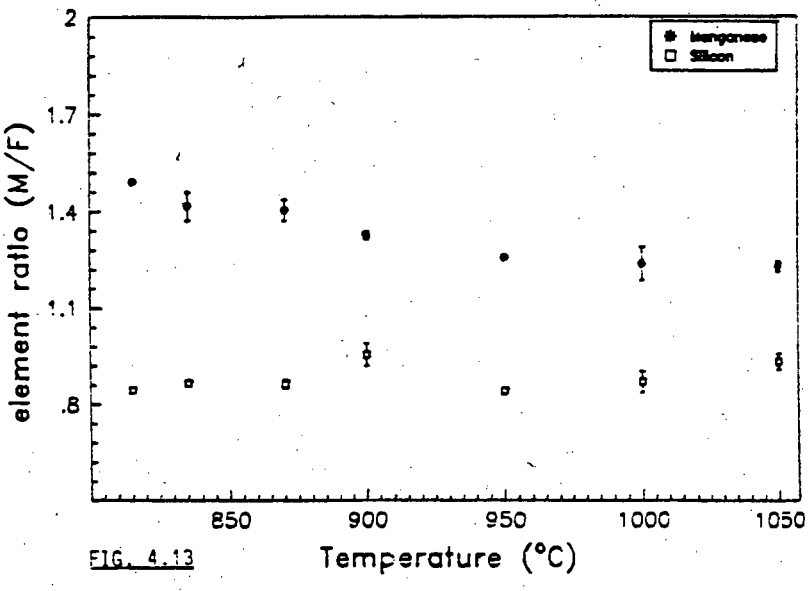

FIG. 4.13

4.7. The structure of the as cast slab, the rolled and the final hot-rolled and annealed state.

Introduction

This section of work was performed on alloys II and III (see section 3.1). These were examined microscopically, SEM analyses were performed and martensite hardness and volume fraction were measured. This was performed in order to determine whether any partitioning of substitutional elements was occurring prior to the hot-rolled and annealed condition. These tests were only performed through a vertical section of a commercially produced slab. This section has been diagrammatically presented in figures 4.15–4.17.

4.7.1. The macrostructure of the as cast slab

Three different zones can be distinguished in solidified alloy ingots:

1. the outer chill zone of equiaxed crystals
2. the columnar zone of elongated or column-like grains, and
3. a central equiaxed zone

Figure 4.14 shows the macrostructures of two different areas from the as cast slab. The shaded regions on the diagram of figure 4.15 represent the above areas. Figures 4.15.(a) and (b) represent the encircled areas on figures 4.14.(a) and (b) respectively. In figure 4.14.(a), the outer edge area, shows very large longitudinal grains of δ-ferrite with transformation to austenite occurring at the grain boundaries (see figure 4.15.(a)). This represents the columnar zone. No outer chill zone is visible. In figure 4.14.(b). the inner central region, shows a thin chill zone near the edge of the sample where rapid cooling has occurred, but small regular equiaxed grains are predominant.

4.7.2 The microstructure of the as cast slab, -the "meltshop samples"

Figure 4.15 shows the microstructure of samples CI and CII from alloy III. From sample CI, it is evident that a single phase (δ-ferrite) existed at the elevated temperatures where the initial heat treatment process occurs during the production of 3CR12 (see figure 2.6.). This resulted in extensive grain growth. Transformation of δ-ferrite to austenite is visible at the grain boundaries as Widmanstatten side-plates. Transformation of this kind indicates that the cooling rate is fast, but not sufficiently fast to prevent diffusion occurring and a transformation product being formed.

The microstructure of CII shows an extension of growth of the Widmanstatten type compared to that observed in CI; indicating that further transformation from δ-ferrite to austenite has occurred. However during the cooling of this slab, not all the δ-ferrite is transformed to austenite and some point is reached where the driving force for austenite formation no longer occurs and δ-ferrite remains in the microstructure. Knutsen[16] attempted to reconstruct the commercial plant production route in the laboratory and he observed that this transformation of δ-ferrite to austenite occurred , but was incomplete. The micrographs show this incomplete transformation.

4.7.3 The microstructure of BI and BII, the hot-rolled structure -"the Steckel samples"

The hot rolling procedure now results in the δ-ferrite becoming "stringered" parallel to the rolling direction. This martensite-δ-ferrite structure can be seen in figures 4.16.(a) and (b). Transformed α-ferrite, as recrystalised grains, is not expected as the hot rolling procedure is terminated above 850°C, well above the temperature determined by Schaffer[17] (see section 5. figure 5.3.) where any transformation from austenite to α-ferrite occurs. Therefore, these micrographs show a martensitic-δ-ferritic microstructure.

4.7.4. The microstructure of the hot-rolled and annealed structure, - "the Shear samples".

The microstructural condition of this sample of 3CR12 after a hot-roll and anneal process, is illustrated in figure 4.17. A banded δ-ferrite and recrystallised α-ferrite grain structure is evident. This banded structure results from the rolling process at the previous stage of the production route; the martensite has been tempered The bulk hardness and α-ferrite microhardness are presented in table 4.4 .

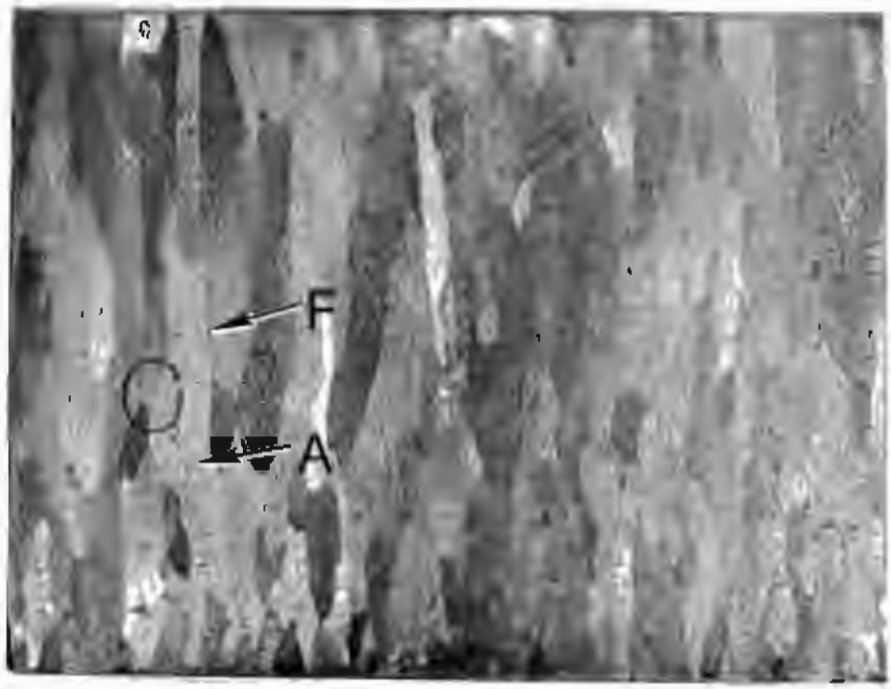

Fig. 4.14 (a) An area from the edge of the slab of 3CR12 in the as cast condition.
Large, longitudinal δ-ferrite grains, (F), with transformed Widmanstatten austenite, (A), in the δ-ferrite grains, are indicated.
Magnification: 1.2x

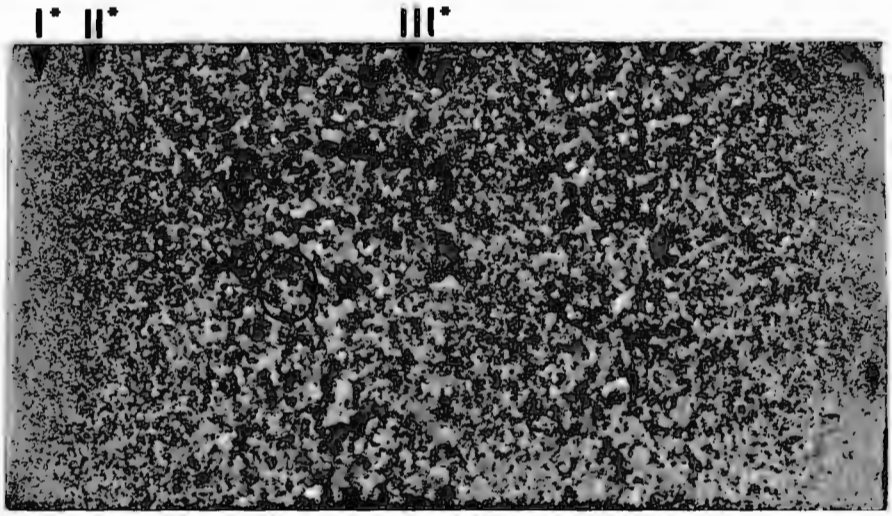

Fig. 4.14.(b) An area from the centre of the slab of 3CR12 in the as cast condition.
δ-ferrite grains are equiaxed and a thin chill zone is visible. Regions I*, II*, III* are indicated (see text, section 4.8.1.)
Magnification' 0.5x

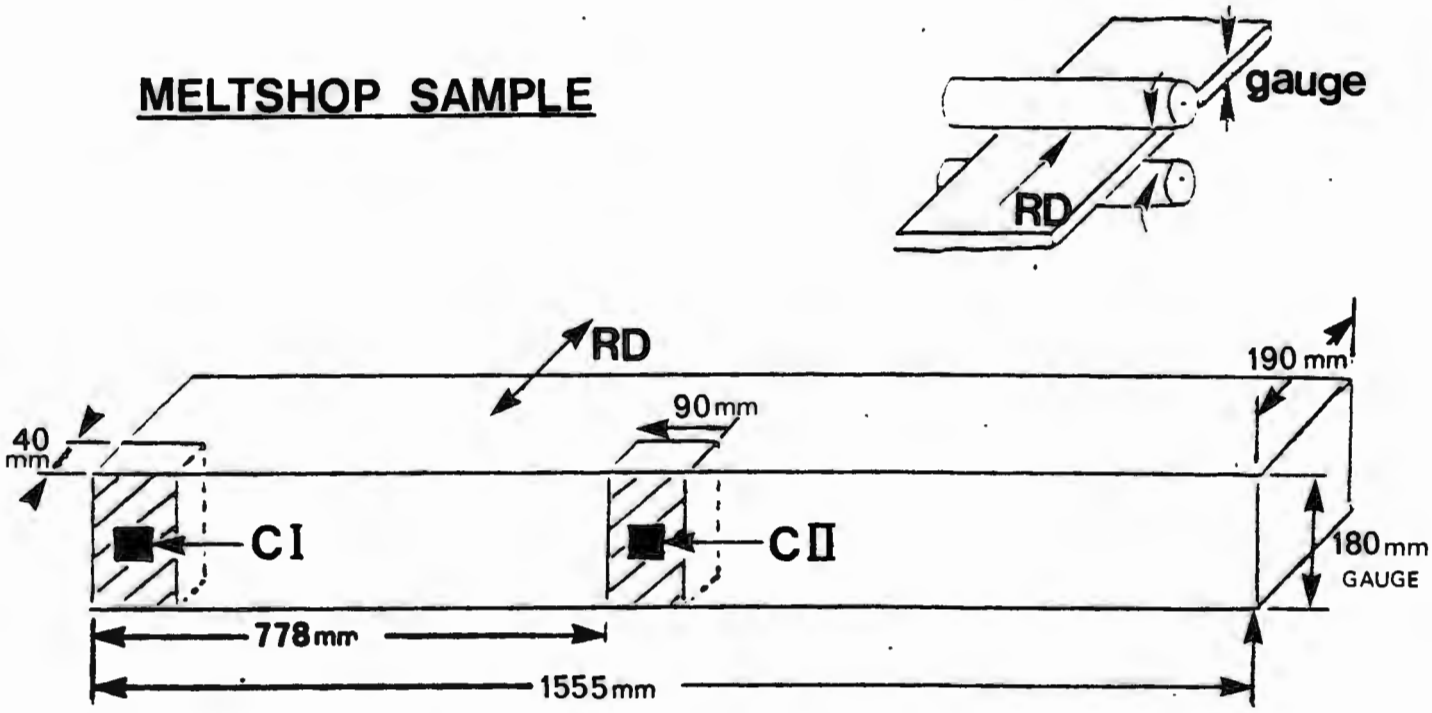

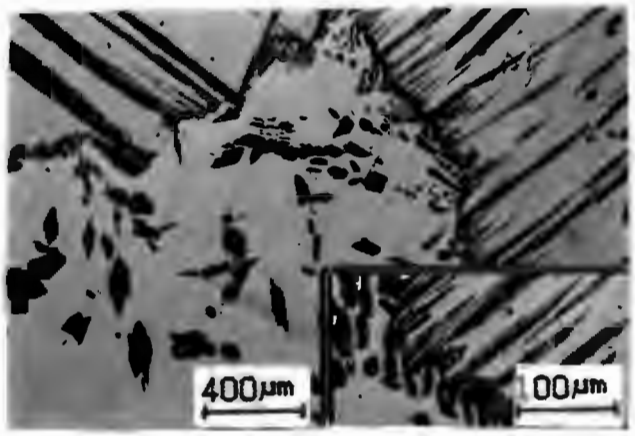

Fig. 4.15 (a)
Sample CI: The microstructure of a sample of 3CR12 taken from the edge of the as cast slab. Transformed Widmanstatten austenite (dark) is visible at the grain boundaries of the large δ-ferrite grains.
Hv30: 189

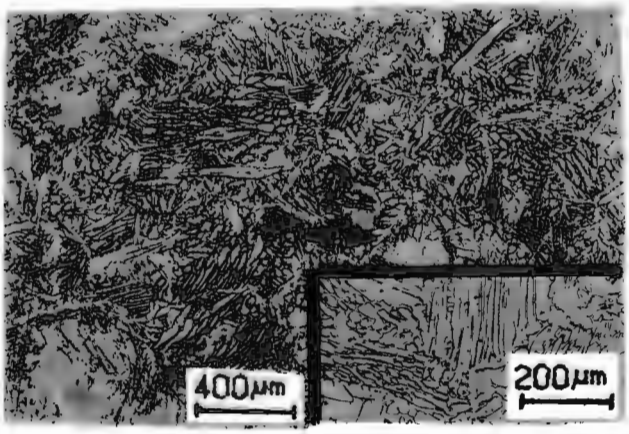

Fig. 4.15 (b)
Sample CII: The microstructure of a sample of 3CR12 taken from the centre of the as cast slab. The Widmanstatten austenite growth indicates further transformation of δ-ferrite to Widmanstatten austenite. δ-ferrite grains are smaller and are equiaxed compared to the above structure.
Hv30: 209

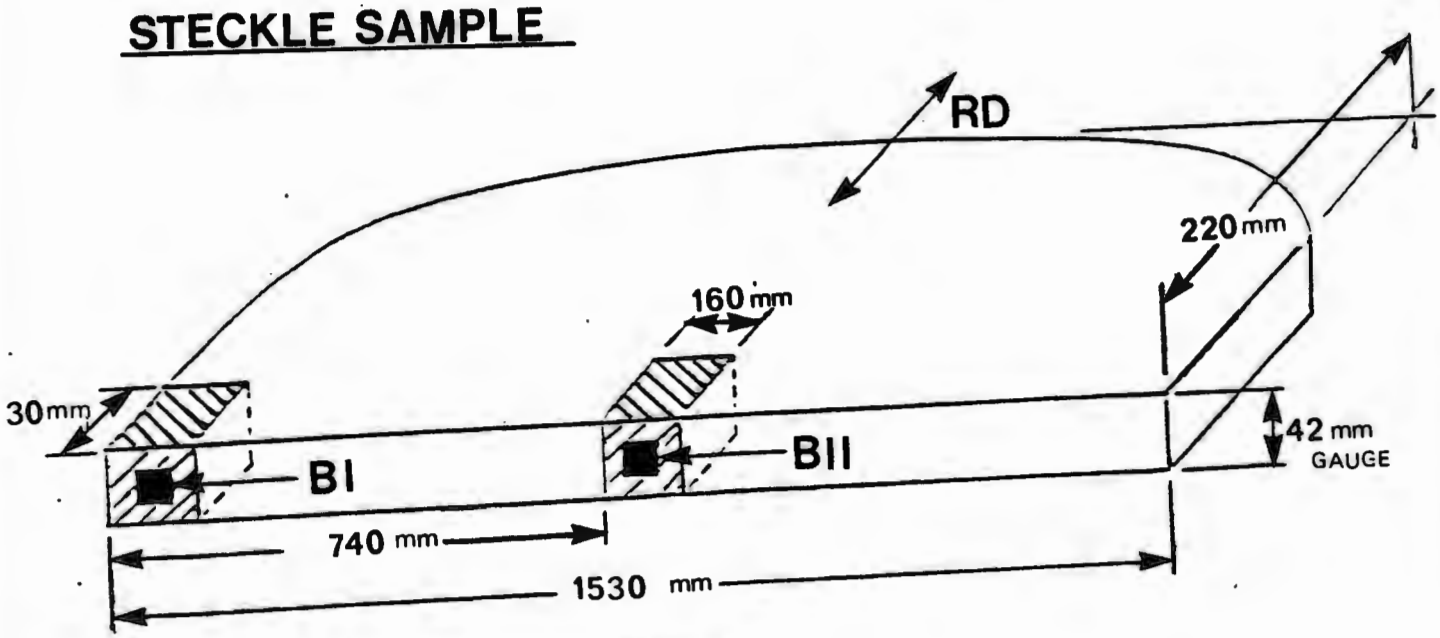

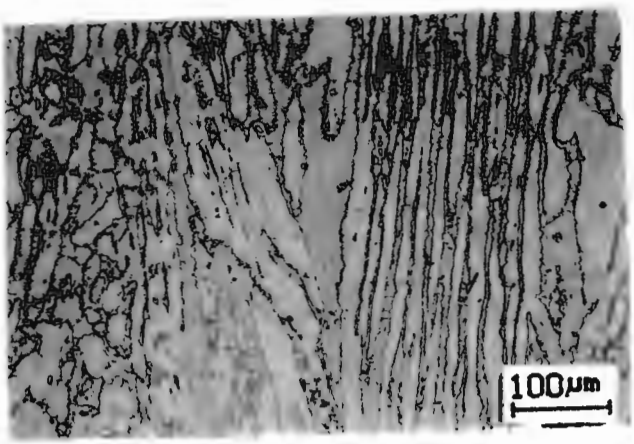

Fig. 4.16(a):
Sample BI: The microstructure of a sample of 3CR12 taken from the edge of the hot-rolled slab. A banded two-phase ferrite-martensite microstructure is visible.
Hv30:252

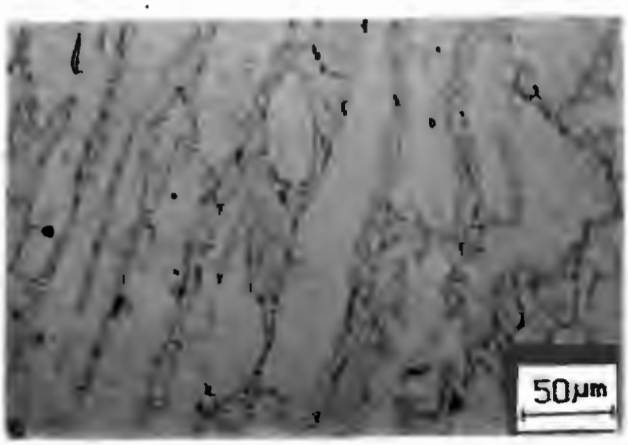

Fig. 4.16(b):
Sample BII: The microstructure of a sample of 3CR12 taken from the centre of the hot-rolled slab. The banded two-phase microstructure is again clear.
Hv30:225

SHEAR SAMPLE

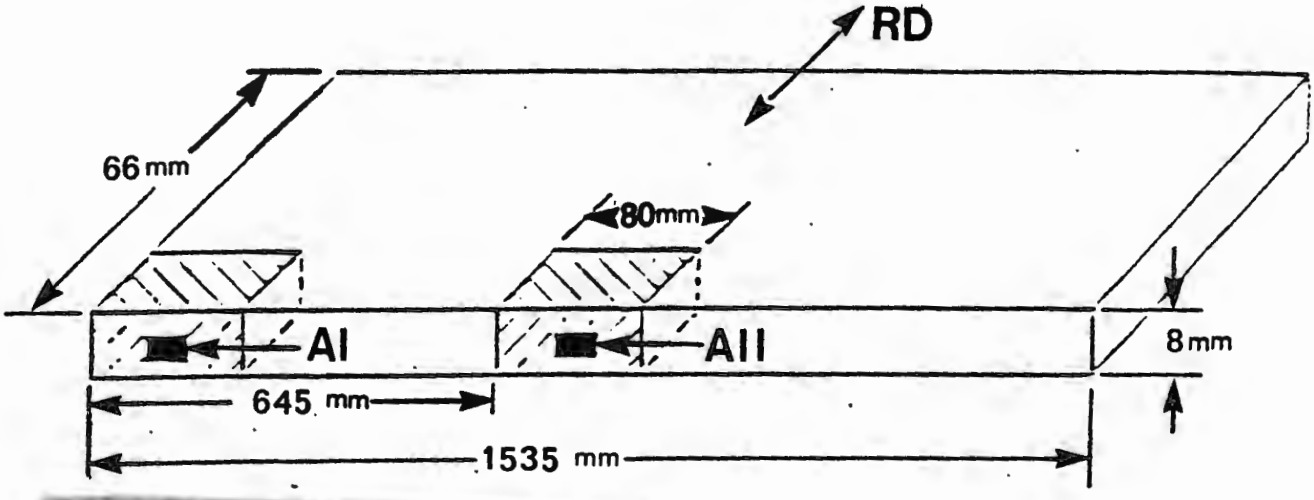

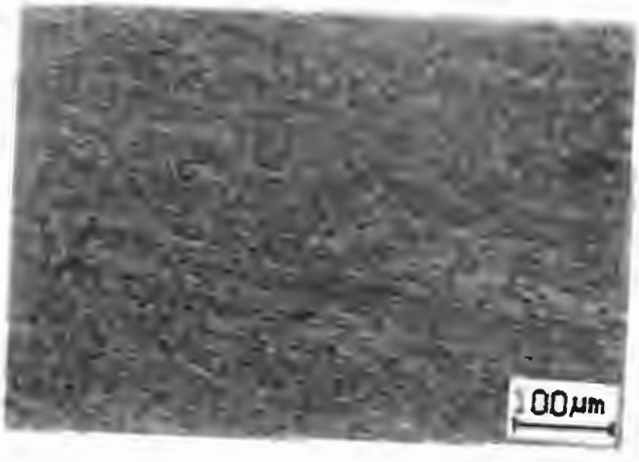

Fig. 4.17(a):
Sample AI: A sample of 3CR12 taken from the edge of the hot-rolled and annealed slab.
Hv30:181

A banded δ-ferrite and α-ferrite microstructure is indicated.

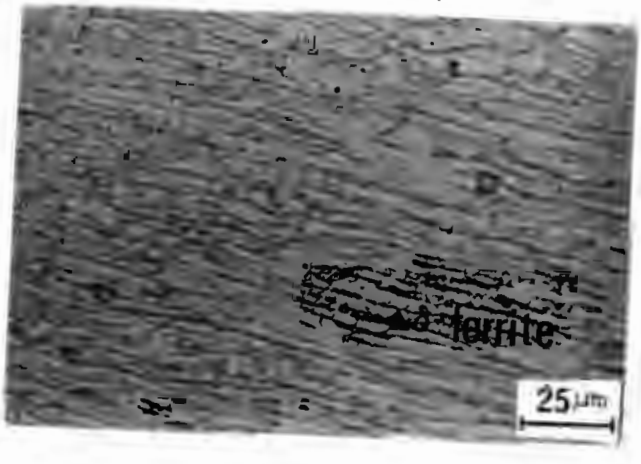

Fig. 4.17(b):
Sample AII: A sample of 3CR12 taken from the centre of the hot-rolled and annealed slab.
Hv30:224

Recrystalised α-ferrite grains with δ-ferrite bands is visible.

4.8. Microanalyses of the as cast slab, the hot-rolled and the hot-rolled and annealed samples

4.8.1. Microanalysis of regions CI and CII, alloy III

Energy dispersive X-ray analyses of regions CI and CII are tabulated in table 4.2. The substitutional elemental partitioning values of CI show Cr enriched and Ni depleted phases with respect to the bulk 3CR12 composition (see section 2.2.2., figure 2.7). Whereas, the substitutional partitioning values obtained for sample CII suggest solidification having occurred according to the bulk composition of 3CR12 as shown in the equilibrium phase diagram for 3CR12.

These results for the substitutional elements indicated that segregation has occurred during the solidification of the as cast slab.

Table 4.3 shows the substitutional partitioning values for alloy II. The regions I^s, II^s and III^s, see figure 4.14(b), show no significant differences in values occurring from the chill region, I^s, to the equiaxed region of III^s. It is apparent that the sample of CII and alloy II show solidification partitioning of substitutional ferrite-forming elements to the ferrite phase and austenite-forming elements to the austenite phase as shown for the bulk 3CR12 equilibrium composition on the phase diagram in section 2.2.2., figure 2.7.

The titanium values for sample CI show very little Ti in the sample area. There were large clusters of Titanium Carbonitrides observed in sample CII, which were not evident at all in sample CI. It is proposed, that during the melting process, Titanium Carbonitrides form[16]. During the pouring of the melt, due to the "flow effect" of the melt into the ingots, the Titanium Carbonitrides become concentrated in the centre and during the solidification and subsequent rolling process these Titanium Carbonitride clusters remain in the centre of the slab. Thus, energy dispersive X-ray analysis shows Ti in the centre of the slab and not at the edge.

4.8.2. Microanalysis of BI and BII, the hot rolled structure

The partitioning values obtained for BI and BII can be seen in table 4.2. Again partitioning of the ferrite-forming elements to the ferrite phase and austenite-forming elements to the austenite phase has occurred. The amount of partitioning is of the same order as that of sample CII and alloy II, and the relative ratios are of the same order. Schaffer[17] showed that austenite will not transform to α -ferrite above 800°C and if it were to, it would be an exceedingly slow reaction (see section 5, figure 5.3). As hot rolling is terminated around 850°C, it seems unlikely that any α-ferrite would form. Thus partitioning has occurred between retained δ-ferrite and austenite (now martensite).

4.8.3. Microanalysis of AI and AII, the hot-rolled and annealed state

The results are shown in table 4.2. Two different phases, see figure 4.17 (b), are evident i.e. residual δ-ferrite and recrystallised α -ferrite grains. Compositional analyses of the two regions show similar values to those obtained in the previous stages of the production route, the exception being the edge of the as cast sample, CI.

Table 4.2 **Substitutional element partitioning values of the ferrite and austenite (now martensite) phases for the Meltshop (CI and CII),Steckle (BI and BII) and the Shear samples (AI and AII).**

Area	Cr		Si		Mn		Ni		Ti	
	Ferrite	Martensite	Ferrite	Martensite	Ferrite	Martensite	Ferrite	Martensite	Ferrite	Martensite
CI	16.50±0.08	16.58±0.32	0.68±0.03	0.69±0.07	0.68±0.04	0.69±0.07	0.17±0.03	0.18±0.04	0.02±0.01	0.05±0.01
CII	12.02±0.43	10.45±0.06	0.39±0.06	0.42±0.06	1.18±0.04	1.36±0.05	0.51±0.08	0.65±0.03	0.37±0.03	0.22±0.02
BI	11.73±0.47	10.98±0.40	0.60±0.01	0.53±0.02	1.22±0.07	1.41±0.07	0.48±0.08	0.65±0.14	0.30±0.03	0.22±0.05
BII	11.87±0.12	10.40±0.15	0.62±0.05	0.57±0.04	1.20±0.05	1.388±0.05	0.52±0.07	0.75±0.05	0.28±0.03	0.20±0.02
AI	11.73±0.47	10.98±0.34	0.55±0.02	0.53±0.07	1.34±0.04	1.42±0.07	0.57±0.05	0.71±0.08	0.26±0.05	0.24±0.03
AII	12.30±0.17	11.31±0.21	0.55±0.07	0.53±0.04	1.29±0.04	1.46±0.03	0.47±0.04	0.66±0.04	0.28±07	0.26±0.04

Table 4.3 **Substitutional element partitioning values of ferrite and austenite phases for the as cast slab of alloy II, regions I*, II*, and III*.**

Area	Cr		Si		Mn		Ni		Ti	
	Ferrite	Martensite	Ferrite	Martensite	Ferrite	Martensite	Ferrite	Martensite	Ferrite	Martensite
I*	11.98±0.26	10.54±0.14	0.36±0.03	0.32±0.03	1.18±0.03	1.42±0.05	0.50±0.04	0.73±0.03	0.37±0.03	0.26±0.02
II*	11.31±0.14	10.64±0.21	0.32±0.02	0.31±0.02	1.21±0.03	1.41±0.02	0.55±0.03	0.72±0.04	0.35±0.02	0.31±0.05
III*	11.60±0.25	10.43±0.12	0.45±0.05	0.45±0.04	1.18±0.04	1.36±0.05	0.54±0.07	0.70±0.06	0.33±0.04	0.21±0.02

Table 4.4 **The bulk hardness, microhardness and the volume fraction of martensite for the different stages of alloy III**

SAMPLE	REGION	BULK HARDNESS (HV30)	MICROHARDNESS ($Kgmm^{-2}$)	VOLUME FRACTION MARTENSITE (%)
AS CAST	CI	189	212 ± 12	36 ± 18
	CII	209	283 ± 15#	70 ± 7
HOT ROLLED	BI	252	357 ± 21#	83 ± 8
	BII	220	347 ± 28#	70 ± 7
HOT ROLLED & ANNEALED	AI	181	198 ± 20	5
	AII	224	243 ± 29	5

* matrix hardness, unless otherwise indicated
\# martensite hardness

4.9. Dilatometry results

Figures 4.18 (a)-(g) show the dilatometry traces obtained for the 800°C, 835°C, 870°C, 900°C, 950°C, 1000°C and 1050°C heat treatments respectively. All specimens were held at temperature for 1 hour.

4.9.1 Figure 4.18 (a), specimen heated to 800°C

During the soaking of this specimen at temperature new austenite forms. This transformation from ferrite to austenite produces an increase in density and hence a decrease in specimen length which is monitored by the dilatometer, and is indicated on the trace. During cooling, the new austenite begins to transform to α-ferrite at 655°C and finishes at 615°C. Cooling below this temperature showed no further transformation i.e. no martensite formation is apparent.

4.9.2. Figure 4.18 (b), specimen heated to 835°C

Soaking at this temperature shows a larger amount of new austenite forming. On cooling, this austenite begins to transform to α-ferrite at 683°C and finishes at 636°C, indicated by x' and y' respectively on the trace. Again, cooling below this temperature showed no further transformation.

4.9.3. Figure 4.18 (c), specimen heated to 870°C

Soaking at this temperature showed a very similar trace to figure 4.18 (b). On cooling, the transformation, commenced again at 683°C, x', and finished at 636°C, y'. Further cooling showed no subsequent transformation.

4.9.4. Figure 4.18 (d), specimen heated to 900°C

Soaking at this temperature showed transformation of α-ferrite to austenite to occur with increased amounts of new austenite forming during soaking. On cooling, it can again be seen that some austenite transforms to α -ferrite at 717°C and finishes at 649°C. On further cooling martensite formation occurs at an Ms temperature of 587°C and finishes at 515°C.

4.9.5. Figure 4.18 (e), specimen heated to 950°C

Soaking at 950°C showed further formation of new austenite. This could mean that the heating rate is too fast for complete transformation to austenite to occur and hence further transformation occurs at the holding temperature. On cooling, again an austenite to α-ferrite transformation temperature is evident at 731°C, x', finishing at 663°C, y'. Further cooling shows an Ms at 575°C and an Mf at 508°C.

4.9.6. Figure 4.18 (f), specimen heated to 1000°C

The heating curve showed the same trend as figure 4.18(e) and little further transformation occurred during the soaking time. On cooling, an x' of 722°C and a y' of 653°C was evident. Further cooling showed an Ms of 547°C and Mf of 477°C.

4.9.7. Figure 4.18 (g), specimen heated to 1050°C

The heating curve showed the same pattern as that obtained for 1000°C. Transformation to new austenite was evident during holding at 1050°C, again indicating that the heating rate was to fast to allow all austenite to form during the heating. On cooling there is no evidence of a decomposition of austenite to α-ferrite and only a martensitic transformation is identifiable. The Ms occurs at 537°C and ends at 458°C.

Table 4.5 presents the transformation temperatures i.e. the As, the reaustenitisation start temperature and the Af, the reaustenitisation finish temperatures; x', the austenite to α-ferrite start transformation temperature, and y', the austenite to α-ferrite finish temperature. Ms, the martensite transformation start and Mf, the martensite transformation finish temperature are also depicted. The microhardness of the martensite formed during cooling and the bulk hardness of the specimens are also tabulated.

The microhardness results show a clear trend of increasing martensitic hardness as the temperature is increased through the dual phase region. A maximum hardness of 279.1 $kgmm^{-2}$ being obtained for the 1050°C temperature.

Table 4.5 The dilatometrically determined A_s, A_f, M_s and M_f temperatures for the hot-rolled and annealed alloy. The split transformation has been designated the letters "x^1" and "y^1". The microhardness of the martensite formed on cooling is included.

TEMPERATURE (°C)	As(°C)	Af(°C)	x^1(°C)	y^1(°C)	Ms(°C)	Mf(°C)	MICROHARDNESS ($Kgmm^{-2}$)*
800	-	-	655	615	-	-	171±8#
835	-	-	683	636	-	-	180±7#
870	-	-	683	636	-	-	187±6#
900	848	-	717	649	587	515	193±12
950	842	932	731	663	575	508	226±18
1000	847	932	722	653	547	477	238±15
1050	842	940	-	-	530	455	279±20

* microhardness of martensite unless otherwise indicated
# ferrite microhardness

FIGURE 4.18 DILATOMETRIC TRACES OF 3CR12 HELD AT VARIOUS TEMPERATURES FOR A 1 HOUR HOLDING TIME

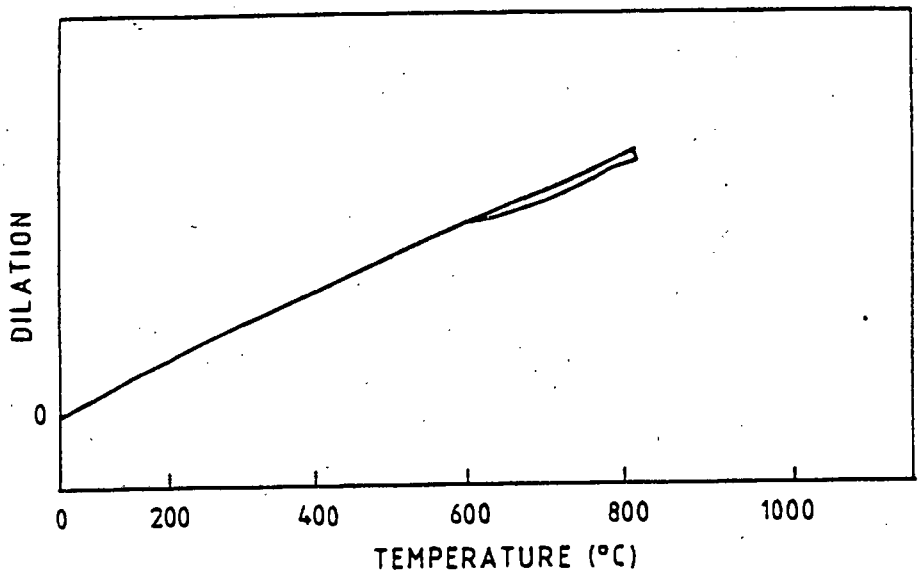

a) specimen held at 800°C

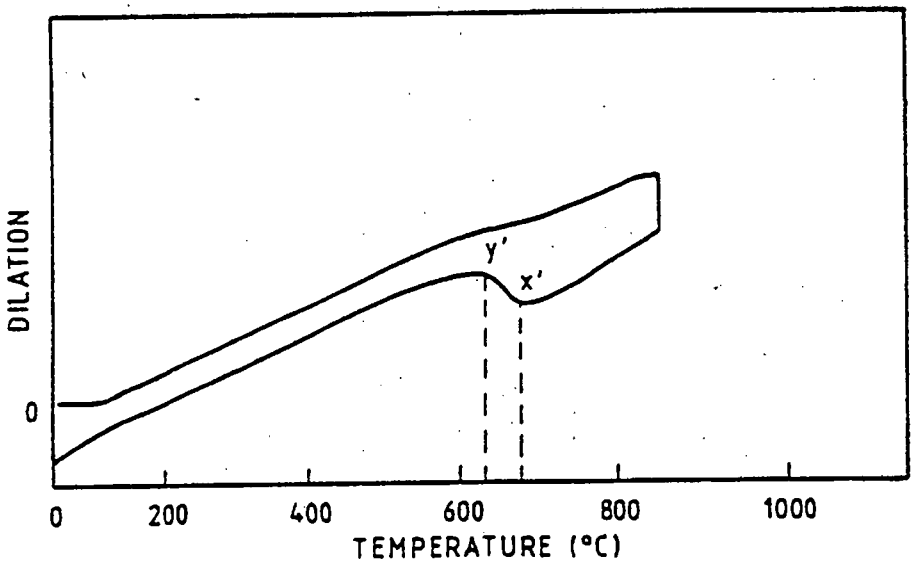

b) specimen held at 835°C

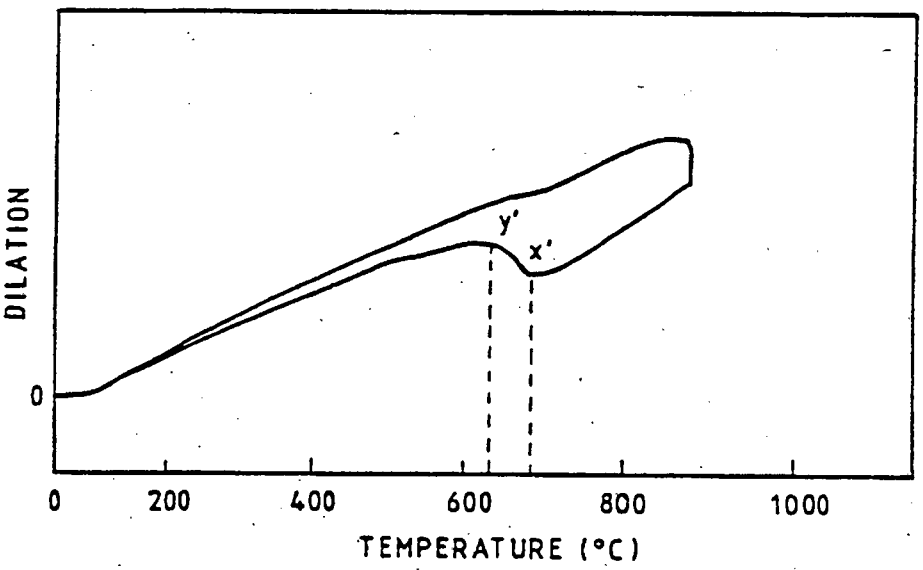

c) specimen held at 870°C .

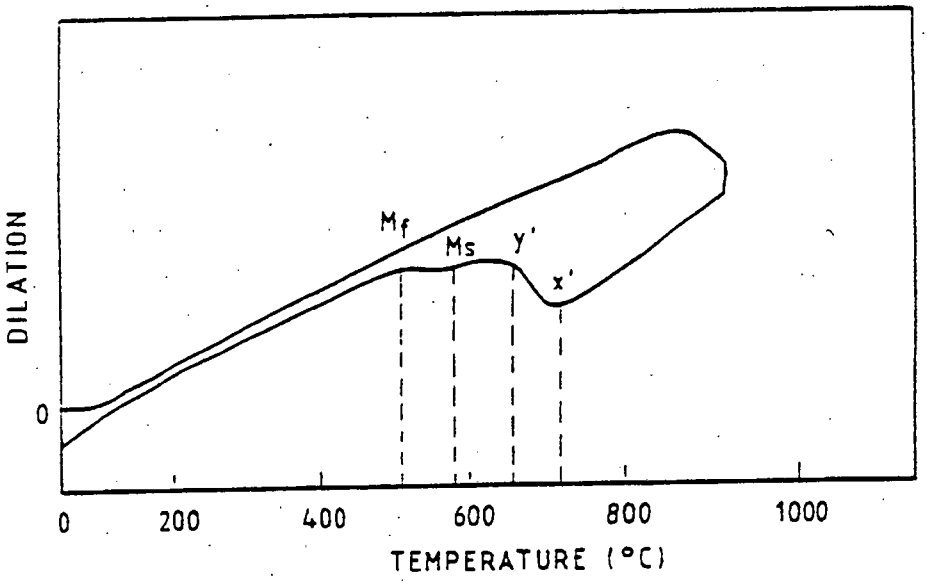

d) specimen held at 900°C

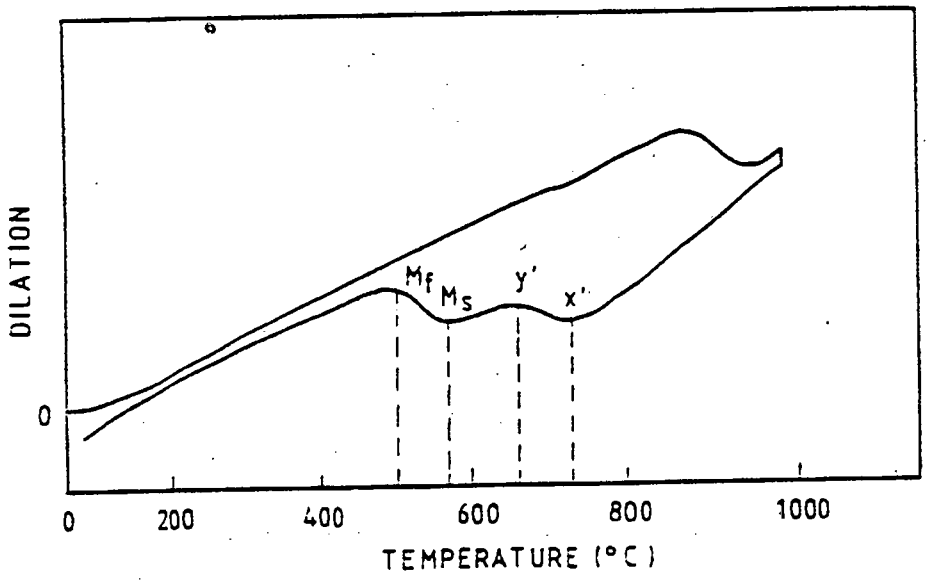

e) specimen held at 950°C

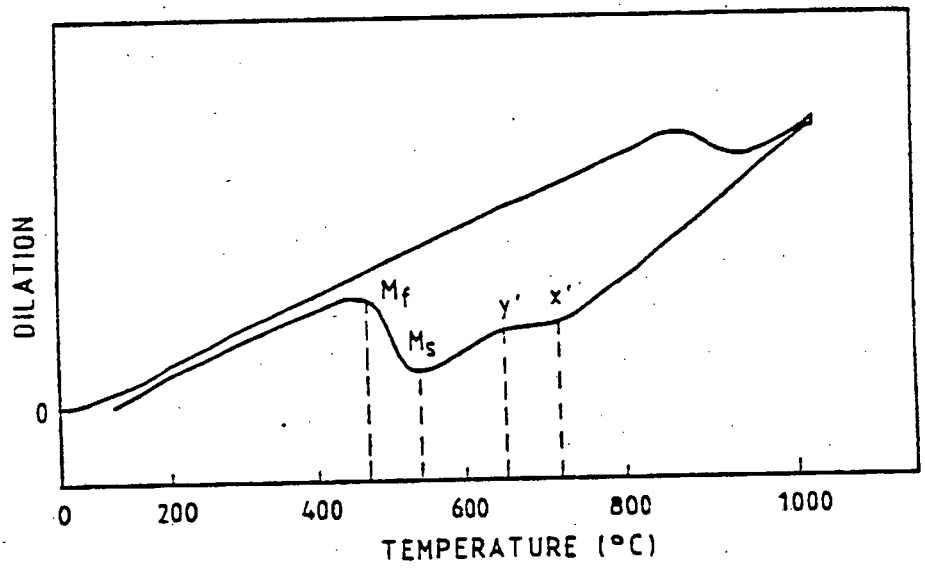

f) specimen held at 1000°C

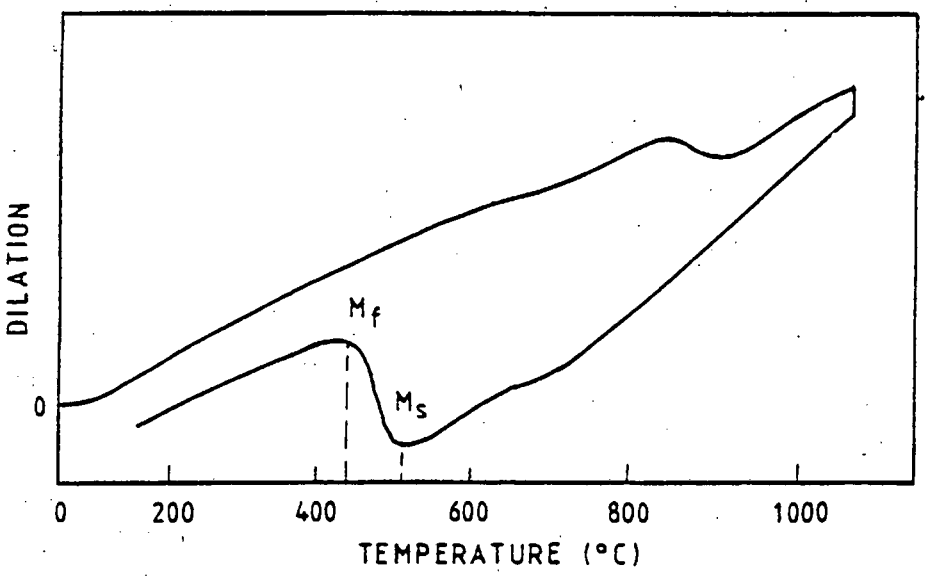

g) specimen held at 1050°C

CHAPTER 5

Discussion

3CR12 was never found to be fully austenitic. Although an austenite-start (the As) and an austenite-finish (the Af) temperature were observed, this did not imply that 3CR12 had become fully austenitic, as can be seen from the microstructures, figures 4.2 - 4.5, section 4. The high Ms temperature and the fact that martensite forms during furnace cooling is indicative of the high hardenability of 3CR12 and hence austenite is never present at room temperature. The lath martensite structure present is of the same shape, size, composition and distribution as the prior austenite grains and hence information on the austenite phase can be obtained.

As the intercritical annealing temperature increases through the dual phase region, so the macrohardness of the specimen was observed to increase (see figs.4.5-4.7, section 4.). The volume fraction of austenite (now martensite), increases as the intercritical temperature increases until ≈900°C, whereupon the volume fraction of martensite (VFM) showed no further volume increase. The VFM values are obtained by SEM point counting techniques (see section 3.7) and hence error would be expected, but the results relative to each other are reliable and accurate. The increased amount of martensite could therefore account for the increased macrohardness in the lower regime of figures 4.5-4.7. After 900°C it appears that the consistent increase in microhardness of the martensite itself, for all three time durations considered, directly affects the macrohardness. The trends introduced in chapter 1, i.e. a delineation of two regions namely; an initial region where the increase in macrohardness is attributed only to the increase of VFM; and then a second region where the continued increase of macrohardness now is affected by the increase in the microhardness of austenite (now martensite), only, seems evident.

However, as stated previously, the 3CR12 alloy has a very low carbon concentration. Under equilibrium conditions, it would be expected that the martensite transformed in these steels would have a correspondingly low carbon content and thus at any one temperature, the more austenite formed the lower the overall concentration of carbon within the austenite, i.e. the less the carbon content per grain and hence the softer the subsequent martensite on cooling. This was not observed. Furthermore, Schaffer[17] argued that, from the Fe-C diagram, the higher the transformation temperature in the dual phase austenite plus ferrite region, the less carbon will be in solution in the austenite at equilibrium, while above the Af, the austenite can dissolve the same volume of carbon with increasing temperature. The resulting martensite formed from higher transformation temperatures would be softer than that formed from the lower transformation temperatures and reach a constant value at temperatures above the Af. This however was again, not observed.

Because the carbon content of the austenite is fixed by the intercritical temperature, the hardenability of the austenite phase varies with intercritical annealing temperature[62]. Thus at low temperatures where the carbon content of the austenite is high, see figure 5.1., the hardenability of the austenite is high. Similarly, at high temperatures where the carbon content of the austenite is low, the hardenability of the austenite is low. The graphs of figure 4.5-4.7, section 4, show an increase in the hardness of the martensite phase until a pre-quench holding temperature of approximately 900°C has been reached, whereupon no further increase is observed. Carbon and nitrogen may therefore be the only controlling factor in affecting these properties of macrohardness, microhardness of the martensite and volume fraction of martensite. However the effects of substitutional elements partitioning to their respective phases cannot be disregarded.

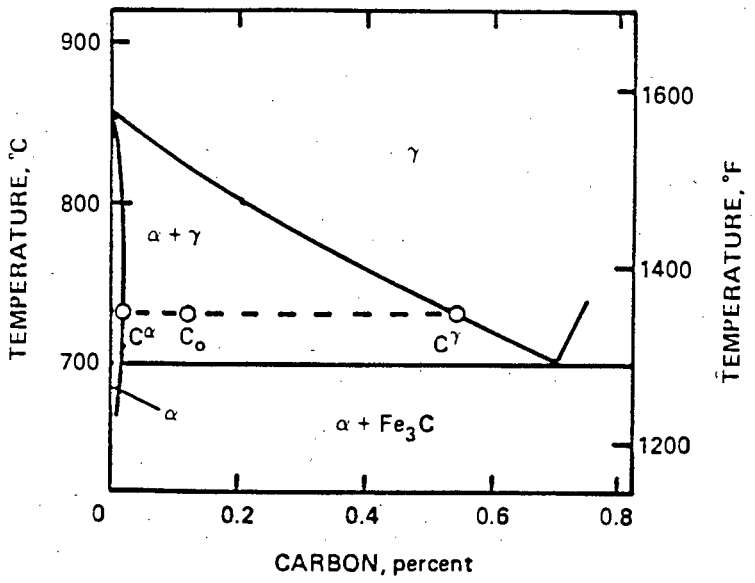

Figure 5.1. Phase diagram for a 1.5Mn steel (para-equilibrium conditions)[63]

It has been determined by Schaffer[17] (see figure 5.2.) that for 3CR12 at a temperature of 810°C, the maximum amount of austenite formed took approximately 20 hours, whereas at 915°C the maximum amount forms in less than 10 minutes. Therefore it can be expected that the 1,4, and 20 hours holding times would adequately allow for the equilibrium situation to be approached and furthermore for partitioning of substitutional elements to occur.

Speich et al[27] discussed the formation of austenite in which the starting microstructure was a ferrite-pearlite structure. In the early stage, growth of austenite is controlled by carbon diffusion due to the low diffusivities of the substitutional alloying elements, while in the later stage growth of austenite is proposed to be controlled by both substitutional alloying elements and carbon.

Schaffer[17] proposed that the formation of austenite in 3CR12 occurred by a Hultgren type para-equilibrium mechanism. The rate controlling process was the structural change from the body centred cubic crystal structure of ferrite to the face centred cubic crystal structure of

austenite. He claimed that the reaction was not controlled by long range diffusion; i.e. the partitioning of Ni, Mn and C to austenite occurred after the crystal structure had changed.

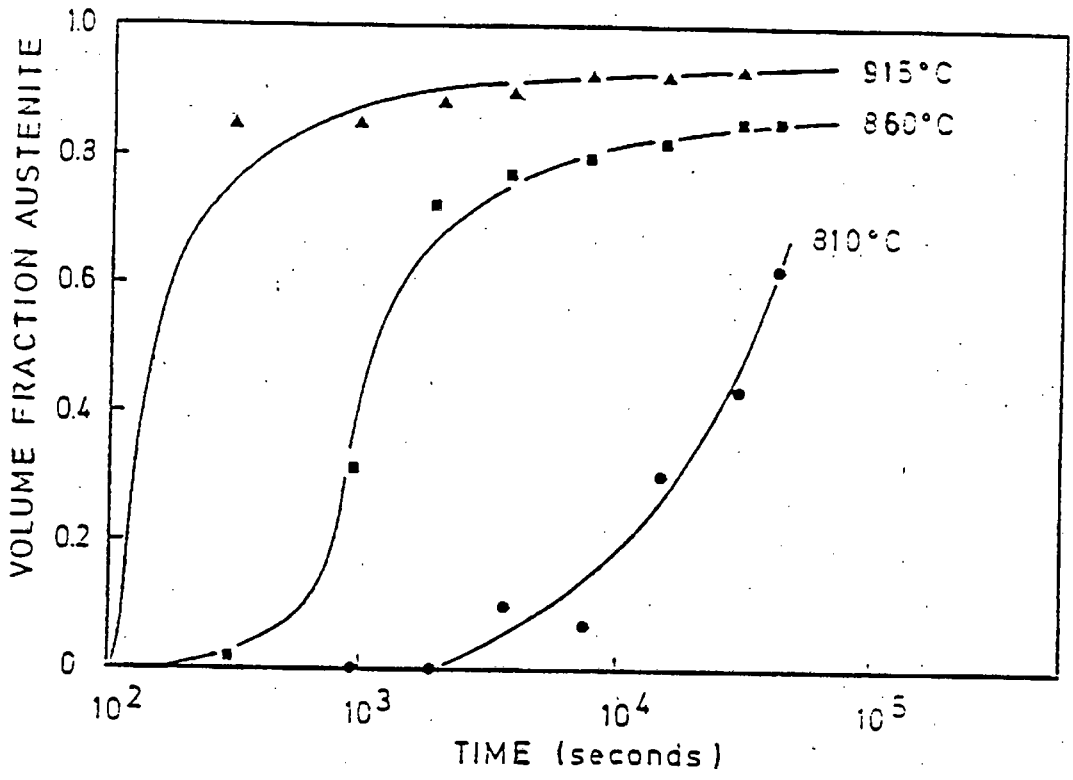

Figure 5.2. The volume fraction of austenite vs. time for the isothermal test temperatures indicated.[17]

Thus, it is proposed that once austenite formation has occurred in 3CR12, the partitioning of substitutional elements would then occur. The duration of holding time at an intercritical annealing temperature might be expected to affect the concentration of these elements and it was hoped that this would explain the microhardness values that have been obtained in this study.

The results for the substitutional element partitioning obtained in this study showed a clear partitioning trend occurring; i.e. the ferrite-

forming elements; Cr, Si and Ti were partitioning to the ferrite phase and the austenite-forming elements; Ni and Mn, to the austenite phase. Taking a temperature in the dual phase region; e.g., 870°C; the Mn partitioning coefficient was 1.25 for both the 1 and 4 hour treatment and 1.42 for the 20 hour duration. The Ni partitioning coefficients at 870°C were 1.5, 1.4 and 1.8 for the 1,4 and 20 hours respectively. Schaffer[17] obtained partitioning coefficients for Ni and Mn after 15 and 30 minutes at a temperature of 860°C. These coefficients were effectively unity for both Ni and Mn for the 15 minute treatment, and 1.24 Ni and 1.11 Mn after 30 minutes. Comparing these partitioning coefficients with those obtained in this study show that although there is a change in concentration of these elements from 15 minutes to 1 hour, there is little significant change subsequent to a 1 hour hold. A change of 0.4 for the Ni values from a 1 hour holding time to a 20 hour holding time could not be considered a real effect in causing the marked increases in martensite microhardness that have been observed in this study.

The temperature dependence of diffusivity follows the standard exponential relationship:[21]

$$D_x = D_o \exp - Q/RT$$

where D_x is the diffusion coefficient of the alloying element,X (cm^2s^{-1}),
Q the activation energy ($kJmol^{-1}$),
D_o the frequency factor (cm^2s^{-1}),
T the temperature (K) and
R the universal gas constant(J/molK).

Using data obtained from table 2.2 section 2.3, the following values were obtained for Ni diffusing in ferrite and austenite at 800°C and 1000°C :(from table 2.2., it can be seen that the temperature range for Ni diffusing in ferrite was 700-900°C, whilst that for Ni diffusing in austenite was from 930-1050°C. Therefore the values below for Ni diffusing in ferrite at 800°C and Ni diffusing in austenite at 1000°C

are not entirely correct as the activation energy, Q, and the frequency factor, D_o, are correct for the above temperature range and not for those used to obtain the results below. However these values have been used to approximate the type of values for the diffusivities of Ni at these temperatures).

D_{Ni} in α (800°C) $=2.7 \times 10^{-12}$ cm^2s^{-1}
D_{Ni} in γ (800°C) $=2.1 \times 10^{-13}$ cm^2s^{-1}
D_{Ni} in α (1000°C) $=3.14 \times 10^{-11}$ cm^2s^{-1}
D_{Ni} in γ (1000°C) $=2.5 \times 10^{-12}$ cm^2s^{-1}

For a particular temperature, diffusion of both substitutional and interstitial solutes (see table 2.2 for carbon and nitrogen diffusivity values) occur much more rapidly in ferrite than in austenite[1]. This could be due to the close -packed structure of γ-iron compared to that of the α-iron. The α-iron, being more loosely-packed responds more readily to thermal activation and allows easier passage through the structure of vacancies and associated solute atoms. In all cases, the activation energy, Q, is less for a particular element diffusing in α-iron, than it is for the same element diffusing in γ-iron. Therefore, at a particular temperature, the more ferrite in the sample, the easier it would be for a substitutional element like Ni to diffuse to the austenite phase and hence the more Ni there should be at that temperature in the austenite. This would be less feasible at lower temperatures because thermal activation is not sufficient and diffusion is far more rapid at higher temperatures. But at the higher temperatures where δ-ferrite starts to nucleate (according to the equilibrium phase diagram, figure 2.7.) not only are the effects of elevated temperatures being experienced, but also the fact that δ-ferrite, being a loosely packed structure can assist the rapid diffusion of substitutional elements to the austenite. Thus, the effect of the microstructure of this alloy at these elevated temperatures and the effects of the elevated temperature itself, allowing for faster diffusivities of substitutional elements, would seem to indicate that a greater concentration of substitutional elements should

be evident in the austenite phase at these temperatures. This however is not apparent. The concentration of substitutional elements, irrespective of whether a low or high temperature in the dual phase region was studied, have the same values for both ferrite and austenite phases with respect to these phases at other temperatures.

Generally, the Ti values vary considerably from one temperature to another (see table 4.1., section 4.). EDS analysis showed that there is free Ti in solution. However, dissolution of Titanium Carbonitrides should not occur within the temperature range used in these set of experiments.[10] Chauhan[7] showed that heating at 1300°C for 3 hours produced no change in the volume fraction of Titanium Carbonitrides and furthermore, heating up to 6 hours showed no dissolution of Titanium Carbonitrides to occur in 3CR12.

From figure 5.3, it can be seen that the limit of solubility of titanium carbides in stainless steels for between 0.01 and 0.02 wt% C occurs between the approximate temperatures of 900°C and 1000°C. (It is not known exactly the content of free carbon in solution in 3CR12 due to the gettering effect of Ti, but for a 0.01 - 0.02 wt% C alloy, it is apparent that titanium carbides go into solution between the above stated temperatures). Therefore, although titanium carbonitrides are not dissolving, titanium carbides which exist[10] in 3CR12 do dissolve and could account for the amount of free Ti observed. Precipitation of titanium carbides will reduce the matrix carbon content. This could explain the microhardness results; i.e. below 900°C, the microhardness values are considerably lower than above this temperature. By reducing the matrix carbon, there is less carbon to partition to austenite during annealing and hence the subsequent martensite formed would reflect this in the microhardness values. Above ≈ 900°C, titanium carbides go into solution, according to the diagram, figure 5.3., and free Ti and carbon become available, which again, is indicated by the microhardness values obtained.

The amount of Ti necessary for effective stabilisation is four times the carbon concentration (both expressed as wt%). However, this simple representation does not take the effect of heat treatment and the presence of nitrogen into account. One empirical formula that does take these effects into account is;:[64]

$$\text{combined carbon} = f\ \frac{\left(\text{Ti} - 3.43\ (\text{N} - 0.01)\right)}{4}$$

where f is a factor which depends on the heat treatment, and 3.43, the coefficient for the nitrogen term, is the stoichiometric relation between Ti and N.

These formulae are important in the development and improvement of all types of alloys as, in principle, it is required to have sufficient Ti so that all the carbon is "combined carbon."[64]

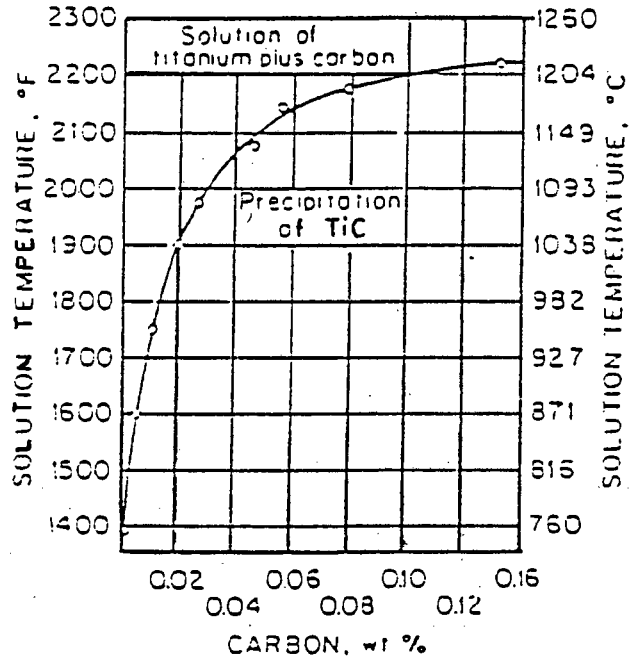

Figure 5.3 The solubility of Titanium Carbide in 321 stainless steels[64]

Titanium Carbonitrides in 3CR12 have been shown to predominantly consist of more nitrogen than carbon (see reference 10). Furthermore, Titanium Nitrides have been found to withstand temperatures reaching at least 1250°C[10] and do not dissolve at these temperatures. Thus it seems

unlikely that dissolution of Titanium Carbonitrides would occur at the temperatures considered in this study of 3CR12.

From empirical evidence, Follstaedt[65] demonstrated that titanium implanted in α-Fe getters carbon upon post-implantation annealing and precipitates as titanium carbides near the surface of the sample. At 800°C he noticed an increase in the size of the titanium carbides for increasing annealing times between 1-64 hours. Two factors were thought to govern the transport of titanium by substitutional diffusion in the iron matrix between precipitates, viz. the solid solubility of titanium in equilibrium with titanium carbides and the titanium diffusivity. At 860°C ripening occurred prior to 1 hour and was then followed by a decrease in precipitate size due to dissolution and diffusion of titanium into the underlying bulk material. This indicates further that free Ti, from Titanium Carbides going into solution, is liberated at temperatures of ≈860°C.

It has been established so far, that although partitioning of substitutional elements occurs the concentration of these elements neither changes appreciably as a function of temperature nor as a function of holding time. It can be postulated that there are sufficient interstitials in solution to cause the martensite microhardness values to increase above 900°C; i.e. C and N are actively diffusing to austenite grains. The relationship between bulk hardness and volume fraction martensite are thus such that the original increase in bulk hardness is attributable to the increased volume fraction of martensite and the grain refining effect that the nucleation of new austenite has within the dual phase region. Initially, the ferrite grains are unrefined and relatively large encompassing, at room temperature, isolated islands of martensite. With increasing volume fraction martensite the presence of martensite becomes more universal within the grain structure and as such the grain refining effect becomes common to the entire microstructure. Thus the increase in hardness can be partially attributed to a decrease in

ferrite grain size together with an increase in the dislocation density. With the higher volume fraction of martensite levels, the areas of dislocation activity surrounding martensite grains begin to interact. Subsequently, once no more austenite forms, the further increase in martensite hardness is attributed to the increase in carbon solubility in austenite with increasing annealing temperature.

It can also be postulated that, as the solubility of carbon in austenite increases with increasingly elevated temperatures, at the lower temperatures not all the available carbon is being dissolved in the austenite and for the given experimental conditions it would seem that below ≈900°C there is little change in this solubility. Above this temperature the amount of carbon which can dissolve in austenite is significantly increased. An increase in the carbon content of the austenite then causes a corresponding increase in the hardness of the transformed martensite.

A paraequilibrium situation seems relevant to 3CR12. Substitutional elements are partitioning to their respective phases but the partitioning coefficients are remaining constant irrespective of changing intercritical temperatures and holding durations being increased. Thus it would appear that equilibrium between the ferrite and austenite phases is only established with respect to carbon and nitrogen and not with respect to the substitutional elements.

5.1. Partitioning trends observed in the prior and final state of the as received hot-rolled and annealed sample

The departure from equilibrium can be effected by altering the solidification rate, the cooling rate subsequent to solidification and /or modifying the chemical composition. Whichever the effect, it can result in δ-ferrite remaining in the microstructure at room temperature[66].

The solidification morphologies of the as cast structures studied in this work are shown in figures 4.14 (a), (b) and 4.15 (a) and (b). Figure 4.14 (a) shows the macroscopic solidification morphology of the edge sample of the as cast slab whilst that of figure 4.14 (b), the morphology of the central area of this slab. Castings frequently exhibit a columnar-to-equiaxed grain transition during solidification; i.e. columnar grains growing inward from the mould wall and a central equiaxed zone. Figure 4.14 (a) shows this large columnar zone which then grows inwards towards those equiaxed grains depicted in figure 4.14 (b).

For relatively rapid cooling the δ-ferrite to austenite transformation has been alternatively referred to as producing a Widmanstatten or acicular morphology[66]. Figure 4.15 (a) and (b) show this morphology, although this is more clearly represented in the former. This Widmanstatten structure has been described as a thermally activated and diffusion controlled reaction in which an orientation relationship between the parent and product phases is established[66]. At slower cooling rates the mode of δ-ferrite to austenite transformation has been termed "equiaxial". Figure 4.15 (b) shows this morphology although the magnification might be too high for absolute clarity of the shape of these grains. Figure 4.14 (b) show the equiaxial grains more clearly.

The morphology of figure 4.14 (a) and 4.15 (a) have resulted from a rapid cool and not a slow cool, as indicated by the results tabulated in table 4.1 of the substitutional element partitioning values. These results, (i.e. those from alloy III, sample CI) show that the resulting structure

has formed from a Cr enriched and Ni depleted composition with respect to the bulk 3CR12 composition (figure 2.7, section 2.2.2) i.e. substitutional elemental partitioning values obtained are the same for both the δ-ferrite and austenite phases. The cooling rate is far too rapid for these elements to partition. Thus the transformation of δ-ferrite to austenite, being a diffusion controlled transformation occurs as a result of interstitial diffusion only.

The central area of the slab , depicted in figure 4.14 (b) and 4.15 (b) shows that progressive growth of austenite into the primary δ-ferrite has occurred. According to the values obtained for the substitutional elements at this stage, (see table 4.2., sample CII), the partitioning of these elements now shows a composition similar to that of the bulk 3CR12 equilibrium composition. This further transformation of δ-ferrite to austenite is as a result now of not only interstitial diffusion, but also of substitutional duffusion as a result of the cooling of the material being sufficiently slow to allow for these elements to diffuse. Further segregation of ferrite-forming elements to the δ-ferrite would further stabilise this structure against any further transformation. Furthermore, it has been postulated[19] that a certain point is reached after which the driving force for further transformation of δ-ferrite to austenite is no longer sufficiently strong for the reaction to occur and is proposed as being due to a combination of the partitioning effects on the two phases and the decrease in diffusivity. This results in a stable residual δ-ferrite being present at room temperature.

The Titanium results, (see table 4.3 section 4), indicate that although Titanium Carbonitrides form in the melt (see previous section) there appears to be a "melt-flow" effect. This means that during the pouring of the melt into the ingots, the Titanium Carbonitrides that have formed flow to the centre of the melt and result in an inhomogenous Titanium Carbide distribution in the as cast microstructure. The titanium values show a titanium-depleted zone at the edge of the as cast structure and a titanium rich zone towards the centre.

The hot rolled material, (figures 4.16 (a) and (b)), show residual δ-ferrite (as identified by Knutsen[10]) and martensite parallel to the rolling direction. The microanalyses of these areas, (i.e. samples BI and BII, tabulated in table 4.2), show a substitutional elemental composition according to the equilibrium phase diagram for the bulk 3CR12 composition. From the thermal history, (figure 2.6) the cast slabs, once cooled to room temperature, are then reheated to 1200°C where they remain for a maximum of 8 hours. This allows for a continuation of substitutional elemental partitioning to occur. This structure is then hot rolled with a final roll pass occurring at a temperature of 850°C. Schaffer[17] showed, figure 2.8., that above 800°C no transformation of austenite to α-ferrite would occur. According to this diagram no transformation of austenite to α-ferrite would be expected to occur during this hot rolling procedure. The substitutional element partitioning values for the hot rolled structure show an equilibrium composition of the bulk 3CR12 composition.

The further and final treatment of the alloy, i.e. cooling and annealing at ≈750–780°C, occurs in the α-ferrite region of the phase diagram. The martensite is tempered and the final structure is a mixture of ferrite and tempered martensite. However, the ferrite is of two origins; new nucleated α-ferrite grains from the austenite and residual δ-ferrite. From the results (table 4.2, samples AI and AII) the two types are further indicated by their differences in composition. The residual δ-ferrite being richer in ferrite-forming elements than the transformed α-ferrite. It would therefore appear that the δ-ferrite phase remains in the material in spite of the treatments the material undergoes in the commercial production route. This phase becomes richer in ferrite-forming elements and has been termed "residual δ-ferrite"[10].

From the results obtained it is apparent that substitutional elements are not in fact contributing to the microhardness of the martensite, and that carbon and nitrogen appear to be responsible for the hardness effects.

Thus in order to clarify this, dilatometry was performed in order to ascertain whether any changes were observed in the Ms, the martensite start temperature. This was decided as a result of the knowledge that many elements cause increased austenite stability, and thus lower the transformation temperature on cooling. As it has been established that substitutional elements in this alloy are not likely to cause any change in this transformation temperature; if any changes were observed through dilatometry, it could therefore be postulated as being a result of interstitial concentrations only.

There are two systematic effects that appear as the carbon content of a steel is increased:[62]

1. The effect of dissolved carbon in making austenite stable at lower temperatures is reflected in progressively lower temperatures for martensite formation as the carbon and nitrogen content increases. This is evident in figure 5.4. below. 3CR12 never has sufficient carbon to allow for retained austenite to be present, however, the effect of these interstitials in solution in the austenite should be reflected by their effect on the Ms transformation temperature.

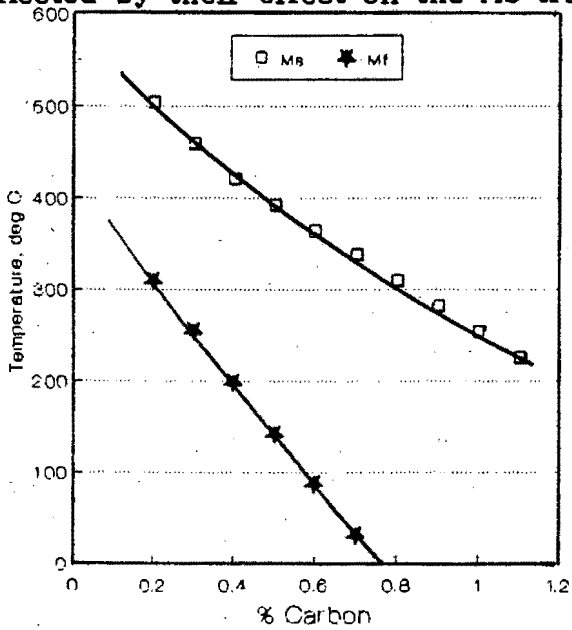

Figure 5.4. Variation of M_s and M_f Temperatures with Carbon content of plain-carbon steels.[62]

2. Since all the carbon originally present in the austenite is retained in martensite produced from it, the extent to which the tetragonal unit cell of martensite departs from cubic symmetry is a direct function of the carbon content of the steel. Thus, a low-carbon martensite is so little distorted by the presence of carbon that the axial ratio of its unit cell is almost unity and such a martensite closely approaches ferrite in both structure and properties[62]. As the carbon content increases, so does the axial ratio of the martensite, and this increasing structural distortion is reflected in increases in hardness, strength and brittleness. Figure 5.5. illustrates the hardness curve.

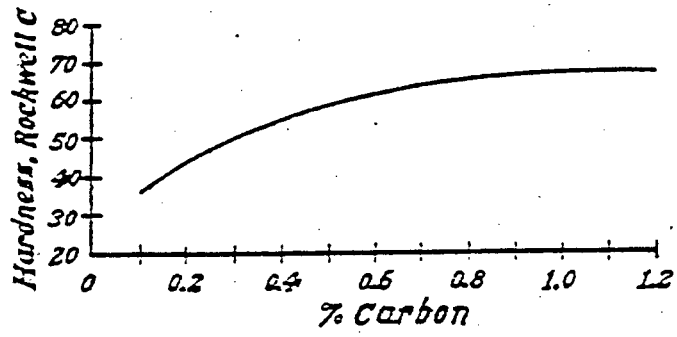

Figure 5.5. Effect of Carbon content of Martensite upon its hardness.[62]

A split transformation was observed in the dilatometry traces obtained. These have been designated x' and y', see section 4, figures 4.18 (a)-(g); where x' represents the temperature where some austenite starts to transform back to ferrite, and y' where this transformation ends. The austenite to martensite transformation is directly dependent upon the temperature and almost independent of the time during which the steel is held at temperature. Thus all specimens were held at temperature for 1 hour.

From the dilatometry results it can be seen that for the temperatures 800°C, 835°C and 870°C the austenite formed is able to transform to α-ferrite during the furnace cool. The 900°C, 950°C and 1000°C results show that some austenite transforms to α-ferrite during cooling and an Ms temperature is also observed. At 1050°C no α-ferrite forms during cooling. The results show the Ms temperatures to be decreasing as the holding temperature increases. A maximum Ms of 587°C for the specimen held at 900°C compared to and Ms of 458°C for that at 1050°C indicates this. Thus a lowering of the transformation temperature is evident. These results indicate that the austenite compositions formed during the heating must be different for the various temperatures. This is further substantiated by the fact that the hardness of the martensite increases through the temperature range. This difference in the microhardness therefore strongly suggests that the interstitial elements are actively diffusing to the austenite during the heating and holding process, and it is the concentration of these elements that is causing the observed effects.

CHAPTER 6

Conclusions

This study has led to the following conclusions:

1. The observed trend, i.e. that of increasing macrohardness in the dual phase region, was initially attributed to the effect of an increasing volume fraction of martensite. Subsequent increases were then attributed to increased interstitial concentrations, due their greater solubility at higher temperatures, which was evident in the increasing microhardness of the martensite. This was further confirmed by dilatometry. These results indicated that holding the steel at various temperatures in the dual phase region and the subsequent furnace cool, allowed for different transformations of austenite to occur. The higher the holding temperature the lower the Ms temperature on cooling. Thus implying that the stability of austenite increased due to the increased interstitial concentrations. This was further confirmed by the microhardness of the martensite itself.

2. Substitutional element partitioning occurred during the heat treatment, with the ferrite-forming elements, namely, Cr, Ti and Si partitioning to the ferrite phase, and the austenite-forming elements, Ni and Mn to the austenite phase. However, no significant changes in partitioning trends were observed despite extended holding durations. Therefore, the trends obtained by Brink[4] and Schaffer[17] and further confirmed in this study must be due to the behaviour of the interstitial elements.

3. The 3CR12 alloy used in this study did not become fully austenitic. Small ferrite grains were present at temperatures above the Af.

4. The incomplete δ-ferrite to austenite transformation resulted in retained δ-ferrite and martensite at room temperature as a banded microstructure in the hot-rolled state.

5. The diffusion controlled transformation from δ-ferrite to austenite resulted in the partitioning of ferrite-forming and austenite-forming elements to their respective phases.

6. During the solidification process, segregation occurs. The areas closest to the chill region are Cr-enriched and Ni-depleted with respect to the bulk 3CR12 composition. However, the central area of the as cast slab showed a different degree of partitioning and solidification of a bulk 3CR12 composition resulted.

7. The partitioning of substitutional elements becomes "fixed" during the rolling process. During the preheat prior to the rolling process (i.e. ≈1150°C) a greater averaging of composition across the slab occurs and during the rolling process the δ-ferrite and martensite phases become "banded" parallel to the rolling direction. The last hot roll occurs at ≈850°C and partitioning is "fixed" in this process, as no transformation to α-ferrite occurs at this temperature and residual δ-ferrite from the high temperature treatments remains in the material.

8. It has been established that partitioning occurs through the vertical section of the commercially produced slab of 3CR12.

REFERENCES

1 Honeycombe, R. W. K. (1981): Steels - Microstructure and Properties, Edward Arnold, London.

2 Ball, A., Chauhan, Y. and Schaffer, G. B. (1987): Microstructure, phase equilibria, and transformations in corrosion resistant dual phase steel designated 3CR12, Mat. Sci. and Tech., 3, pp 189-196

3 Ball, A. and Hoffmann, J. P. (1981): Microstructure and properties of a steel containing 12 % Cr, Materials Technology, 8, pp 329-338

4 Brink, A. B., (1983): The deformation characteristics of a 12 percent Chromium Steel, M.Sc Thesis, University of Cape Town.

5 Brink, A. B., (1987): Private communication.

6 Brink, A. B. and Ball, A. (1984): Proc. of Conference "Stainless Steels '84", Gotenburg, pp 69 -76

7. Chauhan, Y. (1985): A Microstructural Study of a dual phase steel, 3CR12, M. Sc. Thesis, University of Cape Town

8 Hoffman, J. P. (1984): 3CR12- An overview of mechanical and corrosion properties; Part 1 mechanical properties, Paper presented at Inaugural International 3CR12 conference, Middelburg Steel and Alloys, L1-L3.

9 Hoffman, J. P. (1984): The welding metallurgy of a Titanium stabilised 12 percent chromium ferritic-martensitic steel, ASM, 1984 international conference on new developments in stainless steel Technology, Sept 1984

10 Knutsen, R. D. (1989): A Microstructural examination of duplex ferrite-martensite corrosion resisting steels, Ph.D thesis, University of Cape Town

11 Knutsen, R. D. (1987): The use of EDS in identifying the incomplete δ-ferrite to austenite transformation, Proc. Electron Microscopy Society of South Africa, 17, pp 147 - 148.

12 Knutsen, R. D., Ball, A., Hewitt, J., Hoffman, J .P. and Hutchings, R. (1987): Review of physical metallurgy, properties and applications of dual-phase ferritic-martensitic steel designated "3CR12", Prof. Conf. Stainless Steels 1987, York, Institute of Metals, pp 512 - 520

13 Knutsen, R. D. and Hutchings, R. (1988): Occurrence of non-metallic inclusions in 3CR12 and their effect on impact toughness, Mat. Sci. and Tech., 4, pp 127- 135

14 Matthews, L. M. and DeMarsh, E. A. (1985): The response of as-rolled 3CR12 steel to heat treatment, Mintek Report No. M213,Council for Mineral Technology, Randburg, South Africa.

15 Protopappas, E. (1983): The phase equilibria and microstructure of the dual phase steel 3CR12, M.Sc. Thesis, University of Cape Town.

16 Robinson, F. P. A. (1984): 3CR12 as a member of the family of ferritic chromium steels , paper presented at Inaugural International 3CR12 conf., Middelburg Steel and Alloy, South Africa.

17 Schaffer, G. B. (1983): A constitutional study of a dual phase steel containing 12% Chromium, M.Sc. Thesis, University of Cape Town

18 Briggs, J.Z. and Parker T.D., (1965): The super - 12% Cr Steels, Climax Molybedenum Co.

19 Pickering, F. B. (1985): Physical metallurgical development of stainless steels , The Institute of Metals, London

20 Proc. Conf. on Structure and Properties of dual-phase steels,(Kot, R. A. and Morris, J.W . Eds)., 1979, Warrendale, PA., The Metallurgical Society of AIME.

21 Porter, D. A., and Easterling, K. E. (1981): Phase transformations in metals and alloys, Van Nostrand Reinhold Company, New York, USA.

22 Kaltenhauser, R. H. (1971): Improving the Engineering Properties of ferritic Stainless Steels, Met. Eng., 11, (2), pp 41-47

23 Suutala, N. (1982): Effect of Manganese and Nitrogen on the solidification mode in austenitic stainless steel welds, Met. Trans.A., 13A, pp 2121-2130.

24 Garcia, C. I. (1983): Evolution of Microstructure and microstructure-property relations in dual-phase carbon steels, PhD,. University of Pittsburgh.

25 Nehrenberg, A. E. (1950): The Growth of Austenite as related to prior structure, Transactions TMS-AIME, 188, pp 162-174

26 Wycliffe, P., Purdy, G. R. and Embury, H. D. (1981): Austenite Growth in the Intercritical Annealing of Ternary and Quaternary dual phase steels, in Fundamentals of dual-phase steels, Eds. Kot, R. A. and Bramfitt, B. L., PROC AIME. Symposium Illinois.

27 Speich, G. R, Demamest, V. A. and Millerm R. L., (1981): Formation of Austenite during Intercritical annealing of dual phase steels, Met. Trans., 12, pp 1419-1430

28 Ohmura, M. (1986): Solute partitioning and microstructural development in dual phase steel, PhD thesis., University of California, Berkeley.

29 Hultgren, A. (1947): Trans. ASM, 39, pp 915-1005

30 Jack, D. H. and Nutting, H. (1974): Phase transformations, Int. Metal Reviews., 19, pp 90-102

31 Koch, F. and Eckstein, M. J. (1978): Studies of the redistribution of chrome and nickel during the ferrite to austenite transformation in chrome-nickel steels of the 26-6 type, Steel Furnace Monthly, 13, 11, pp 441-445

32 Lenel, U. R. (1980): Reaustenitisation of some alloy steels, Ph.D thesis, University of Cambridge.

33 Koo, J. Y., Raghavan, M. and Thomas, G. (1980): Compositional Analysis of Dual Phase Steels by Transmission Electron Microscopy, Met. Trans. A. 11A, pp 351-354

34 Sarikaya, M., Thomas, G., Steeds, H. W., Barnard, S. J. and Smith, G. D. W. (1981): Solute element partitioning and austenite stabilization in steels, International Conf. on Solid-solid phase transformations, H. I. Aaronson, D. E. Laughlin, R. F. Sederda and C. M. Wayman eds., AIME, Warrendale, PA, 1981.

35 Chaturvedi, M. C. and Jena, A. K. (1987): Effect of intercritical annealing temperature on equilibrium between ferrite and austenite, Mat. Sci. and Eng., 94, L1-L3

36 Honeycombe, R. W. K. (1976): Transformation from austenite in alloy steels, Met. Trans. A, 7A, 7, pp 915-936

37 Ricks, R. A., Bee, J. V. and Howell, P. R. (1981): The decomposition of austenite in a high purity iron-chromium-nickel alloy, Met. Trans. A, 12A, pp 1587-1594

38 Irvine, K. J., Crowe, D. J and Pickering, F. B. (1960): The physical metallurgy of 12% Chromium steels, J. of the Iron and Steel Institute, 195, pp 386-405.

39 Aaronson, H. I. and Domian, H. A. (1986): Partitioning of alloying elements between austenite and proeutectoid ferrite or bainite, Trans. Met. Soc. AIME, 236, pp 768-781

40 Chilton, J. M. and Kelly, P. M. (1968): The strength of ferrous martensite, Acta. Met., 16, pp 637-656

41 Kehoe, M. and Kelly, P. M. (1970): The role of carbon in the strength of ferrous martensite, Scripta Met., 4, pp 473 - 476

42 Rashid, M. S. (1981): Dual phase steels , Ann. Rev. Mat. Sci., 11, pp 245-256

43 Gau, J. S, Koo, J. Y, Nakagawa, A, and Thomas G (1981): Microstructure and properties of dual-phase steels containing fine precipitates in "Fundamentals of dual phase steels" PROC AIME Symposium, Illinois, Eds. R. A. Kot and B. L. Bramfit, pp 47-59

44 Hayden, H. W. and Floreen, S. (1970): The influence of martensite and ferrite on the properties of two-phase stainless steels having microduplex structures , Met. Trans., 1, pp 1956-1959

45 Davies, R. G. (1978): The deformation behaviour of a vanadium strengthened dual phase steel, Met. Trans. A, 9A, pp 41-52

46 Goel, N. C., Chakravarty, J. P. and Tangri, K. (1987): The influence of starting microstructure on the retention and mechanical stability of austenite in an intercritically annealed-low alloy dual phase steel, Met. Trans. A., 18A, pp 5-9

47 Roscoe, C. V., Gradwell, K. J. and Lorimer, G. W. (1985): Structure/property relationships in a series of duplex stainless steels, Proc. Conf. Stainless Steels 1984, Gotenborg, The Institute of Metals, 1985

48 Speich, G. R. and Miller, R. L. (1979): Mechanical properties of ferrite-martensite steels, in "Structure and Properties of dual phase steels ", PROC AIME Symposium, New Orleans, Eds. J. W. Morris Jr. and R. Kot, pp 145-181

49 Thomas, G. and Koo, J. Y. (1979): Developments in strong ductile duplex ferritic-martensitic steels, in "Structure and properties of dual phase steels", PROC. AIME Symposium, New Orleans, Eds. J. W. Morris, Jr, and R. Kot, pp 183-200

50 Thorvaldsson, T., Eriksson, H., Kutka, J. and Salwen, A. (1985): Influence of microstructure on mechanical properties of a duplex stainless steel, Proc. Conf. Stainless steels, Goteborg, The Institute of Metals, 1985.

51 Tomo, T., Nishida, M., Hashiguchi, K. and Kato, T. (1979): Formation and properties of ferrite plus martensite dual-phase structures, in "Structure and Properties of dual phase steels"; Proc, AIME Symposium, New Orleans, Eds. J. W. Morris Jr, and R. Kot, pp 221-241

52 Unnikrishnan, K. and Mallik, A. K. (1987): Microstructure-strength relations in a duplex Stainless steel, Mat. Sci. and Eng., 94, pp 175-181

53 Davies, R. G. (1978): "Influence of Martensite composition and Content on the Properties of dual-phase steels", Met. Trans, 9A, pp 671-679

54 Marder, A. R. (1981): The Structure-property relationships in Chromium bearing dual phase steels, in "Fundamentals of dual phase steels, " Eds. Kot, R.A. and Bramfitt, B.L., PROC AIME Symposium, Illinois., pp 145- 160

55 Lanzillotto, C. A. N. and Pickering, F. B. (1982): Structure-property relationships in dual phase steels, Metal Science, 16, pp 371-382

56 Koo, J. Y. and Thomas, G. (1979): Design of Duplex Low Carbon Steels for Improved Strength: Weight Applications in Formable HSLA and Dual Phase Steels, A.T. Davenport ed., AIME, New York

57 Kato, T., Hashiguchi, K., Takahashi, I., Irie, T. and Ohashi, N. (1979): Development of dual phase steel sheet, in "Structure and Properties

of dual phase steels," Eds. Kot, R. A. and Morris, H. S., ASM-AIME, Warrendale

58 Hansen, S. S. and Pradhan, R. R. (1981): Structure/Property relationships and continuous yielding behaviour in dual phase steels, in "Fundamentals of dual phase steels", PROC AIME Symposium, Illinois, Eds. Kot, R. A. and Bramfitt, B. L, pp 3-47

59 Messien, P., Herman, H., Greday, T. (1981): Phase transformation and microstructure of intercritically annealed dual-phase steels, in " Fundamentals of dual phase steels, " Eds. Kot, R. A. and Bramfitt, B. L., PROC AIME Symposium, Illinois., pp 161-180

60 Physical Metallurgy, Eds. R. W. Cahn and P. Haasen, North Holland, 1983

61 Gabriel, B. L. (1985): SEM, a users' manual for Materials Science, American Society for Metals, pp 53

62 Smith, M. C. (1956): Alloy series in physical metallurgy, Constable and Company Ltd, London

63 Speich, G. R. (1981): Physical Metallurgy of dual phase steels, in "Fundamentals of dual phase steels", PROC AIME Symposium, Illinois, Eds. Kot, R. A. and Bramfitt, B. L. pp 3-47

64 Peckner, D. and Bernstein, I. M. (1977): Handbook of stainless steels, 4 ,McGraw-Hill , New York

65 Follstaedt, D. M. (1980): Microstructure of TiC Precipitates in Ti-implanted α -Fe, J. Appl. Phys, 51(2), pp 1001-1010

66 Brown, E. L., Whipple, T. A. and Krauss, G. (1985): Metallography of duplex stainless steels castings, pp 665-689

APPENDIX A

Table 1.1: Bulk hardness, microhardness and volume fraction of martensite after a 1 hour anneal and oil quench, for various temperatures. Prior state was the hot-rolled and annealed condition.

TEMPERATURE (°C)	BULK HARDNESS (HV30)	MICROHARDNESS ($KGMM^{-2}$) MARTENSITE	FERRITE	VOLUME FRACTION MARTENSITE (%)
815	145.6±2.3			19.4 ± 3.9
823		220 ± 20	218 ± 9	
835	161.5±1.2	225 ± 18		24.9 ± 5.1
843		229 ± 17	236 ± 16	
870	198.8±3.2	269 ± 9		64.3 ± 5.5
882		270 ± 10		
900	205.4±4.0	368 ± 24	257 ± 39	70.1 ± 5.6
950	221.2±3.5	408 ± 22	259 ± 28	72.0 ± 5.6
1000	237.8±3.2	418 ± 18	279 ± 40	76.4 ± 8.1
1050	251.8±2.2	410 ± 15	287 ± 28	70.0 ± 6.6

APPENDIX A

Table 1.2: Bulk hardness, microhardness and volume fraction of martensite after a 4 hour anneal and oil quench, for various temperatures. Prior state was the hot-rolled and annealed condition.

TEMPERATURE (°C)	BULK HARDNESS (HV30)	MICROHARDNESS ($KGMM^{-2}$) MARTENSITE	FERRITE	VOLUME FRACTION MARTENSITE (%)
800	140.1±1.8		193 ± 6	
815	153.4±1.23	248 ± 10	205 ± 9	38.5 ± 6.4
835	171.5±1.9	251 ± 8	195 ± 17	53.6 ± 7.3
870	196.0±2.3	264 ± 13	248 ± 17	56.1 ± 7.8
900	211.5±5.9	312 ± 20	228 ± 27	66.1 ± 5.9
950	225.9±3.5	346 ± 18	242 ± 12	77.9 ± 7.0
1000	235.5±3.9	362 ± 24	270 ± 17	76.0 ± 7.0
1050	243.5±7.1	360 ± 21	261 ± 19	70.0 ± 7.6

APPENDIX A

Table 1.3: Bulk hardness, microhardness and volume fraction of martensite after a 20 hour anneal and oil quench, for various temperatures. Prior state was the hot-rolled and annealed condition.

TEMPERATURE (°C)	BULK HARDNESS (HV30)	MICROHARDNESS ($KGMM^{-2}$) MARTENSITE	FERRITE	VOLUME FRACTION MARTENSITE (%)
815	163.0±1.9	245 ± 7		38.1 ± 4.4
835	174.1±1.3	241 ± 10	207 ± 14	47.8 ± 5.6
870	194.0±2.0	237 ± 21	214 ± 11	61.3 ± 6.4
900	203.5±2.1	365 ± 23	233 ± 32	62.5 ± 5.2
950	223.7±9.3	396 ± 18	235 ± 16	67.8 ± 5.6
1000	248.3±2.3	408 ± 10		63.7 ± 7.4
1050	257.0±6.6	412 ± 10	215 ± 22	68.1 ± 5.4

Table 1.4: **The concentration of substitutional elements for the 1, 4 and 20 hour anneal (wt%) in the austenite (now martensite) and ferrite phase for an 815°C anneal. Prior condition was the hot-rolled and annealed condition.**

Annealing time (hrs)	Cr		Ti		Si		Mn		Ni	
	Ferrite	Martensite	Ferrite	Martensite	Ferrite	Martensite	Ferrite	Martensite	Ferrite	Martensite
1	11.31±0.18	10.55±0.11	0.29±0.03	0.25±0.05	0.35±0.01	0.26±0.02	1.29±0.02	1.54±0.06	0.64±0.04	0.80±0.10
4	11.65±0.15	10.52±0.05	0.26±0.03	0.16±0.03	0.57±0.02	0.51±0.05	1.24±0.04	1.63±0.03	0.47±0.01	0.78±0.04
20	11.80±0.04	10.42±0.17	0.31±0.06	0.22±0.06	0.58±0.01	0.49±0.01	1.16±0.03	1.73±0.05	0.43±0.06	0.86±0.10

Table 1.5: **The concentration of substitutional elements for the 1, 4 and 20 hour anneal (wt%) in the austenite (now martensite) and ferrite phase for an 835°C anneal. Prior condition was the hot-rolled and annealed condition.**

Annealing time (hrs)	Cr		Ti		Si		Mn		Ni	
	Ferrite	Martensite	Ferrite	Martensite	Ferrite	Martensite	Ferrite	Martensite	Ferrite	Martensite
1	11.25±0.11	10.50±0.05	0.24±0.02	0.19±0.08	0.55±0.02	0.54±0.02	1.36±0.04	1.67±0.05	0.61±0.04	0.81±0.03
4	11.98±0.04	10.54±0.12	0.31±0.01	0.20±0.02	0.67±0.01	0.58±0.02	1.26±0.02	1.61±0.04	0.50±0.01	0.74±0.03
20	11.88±0.11	10.40±0.05	0.31±0.05	0.19±0.08	0.60±0.02	0.52±0.01	1.16±0.04	1.64±0.02	0.45±0.01	0.84±0.03

Table 1.6: **The concentration of substitutional elements for the 1, 4 and 20 hour anneal (wt%) in the austenite (now martensite) and ferrite phase for an 870°C anneal. Prior condition was the hot-rolled and annealed condition.**

Annealing time (hrs)	Cr		Ti		Si		Mn		Ni	
	Ferrite	Martensite	Ferrite	Martensite	Ferrite	Martensite	Ferrite	Martensite	Ferrite	Martensite
1	12.06±0.127	10.84±.179	0.32±.051	0.19±.052	0.57±.025	0.51±.076	1.18±.042	1.51±.076	0.45±.021	0.68±.043
4	11.43±0.13	10.49±0.06	0.27±0.03	0.16±0.01	0.57±0.03	0.50±0.02	1.37±0.06	1.72±0.05	0.54±0.05	0.75±0.04
20	12.22±0.05	10.75±0.05	0.36±0.07	0.23±0.08	0.58±0.02	0.52±0.01	1.19±0.03	1.60±0.03	0.41±0.03	0.70±0.04

Table 1.7: **The concentration of substitutional elements for the 1, 4 and 20 hour anneal (wt%) in the austenite (now martensite) and ferrite phase for an 900°C anneal. Prior condition was the hot-rolled and annealed condition.**

Annealing time (hrs)	Cr		Ti		Si		Mn		Ni	
	Ferrite	Martensite	Ferrite	Martensite	Ferrite	Martensite	Ferrite	Martensite	Ferrite	Martensite
1	12.04±0.26	10.76±0.16	0.38±0.05	0.19±0.07	0.59±0.03	0.52±0.01	1.21±0.07	1.53±0.05	0.44±0.05	0.71±0.02
4	12.06±0.14	10.68±0.07	0.35±0.06	0.17±0.01	0.56±0.02	0.49±0.01	1.22±0.03	1.58±0.02	0.31±0.02	0.69±0.09
20	12.43±0.07	10.85±0.03	0.35±0.05	0.19±0.05	0.64±0.02	0.53±0.06	1.15±0.03	1.53±0.03	0.39±0.03	0.69±0.06

Table 1.8: **The concentration of substitutional elements for the 1, 4 and 20 hour anneal (wt%) in the austenite (now martensite) and ferrite phase for an 950°C anneal. Prior condition was the hot-rolled and annealed condition.**

Annealing time (hrs)	Cr		Ti		Si		Mn		Ni	
	Ferrite	Martensite	Ferrite	Martensite	Ferrite	Martensite	Ferrite	Martensite	Ferrite	Martensite
1	12.25±0.10	10.60±0.05	0.34±0.02	0.25±0.10	0.62±0.02	0.57±0.03	1.19±0.04	1.47±0.10	0.48±0.03	0.68±0.07
4	12.28±0.06	10.74±0.02	0.36±0.01	0.27±0.07	0.61±0.02	0.54±0.02	1.20±0.04	1.46±0.04	0.41±0.05	0.65±0.04
20	12.58±0.04	10.86±0.16	0.36±0.02	0.21±0.03	0.58±0.02	0.54±0.03	1.21±0.02	1.50±0.04	0.36±0.02	0.66±0.05

Table 1.9: **The concentration of substitutional elements for the 1, 4 and 20 hour anneal (wt%) in the austenite (now martensite) and ferrite phase for an 1000°C anneal. Prior condition was the hot-rolled and annealed condition.**

Annealing time (hrs)	Cr		Ti		Si		Mn		Ni	
	Ferrite	Martensite	Ferrite	Martensite	Ferrite	Martensite	Ferrite	Martensite	Ferrite	Martensite
1	12.55±0.21	11.43±0.61	0.40±0.05	0.27±0.05	0.64±0.02	0.57±0.07	1.22±0.06	1.33±0.09	0.42±0.04	0.54±0.09
4	12.22±0.08	10.83±0.15	0.37±0.01	0.30±0.09	0.60±0.02	0.53±0.03	1.23±0.05	1.46±0.06	0.50±0.01	0.68±0.03
20	12.47±0.08	10.94±0.05	0.38±0.02	0.24±0.04	0.56±0.02	0.50±0.01	1.26±0.06	1.49±0.02	0.40±0.05	0.63±0.05

Table 1.10: **The concentration of substitutional elements for the 1, 4 and 20 hour anneal (wt%) in the austenite (now martensite) and ferrite phase for an 1050°C anneal. Prior condition was the hot-rolled and annealed condition.**

Annealing time (hrs)	Cr		Ti		Si		Mn		Ni	
	Ferrite	Martensite	Ferrite	Martensite	Ferrite	Martensite	Ferrite	Martensite	Ferrite	Martensite
1	12.19±0.06	10.63±0.36	0.20±0.02	0.12±0.01	0.37±0.03	0.38±0.03	1.10±0.04	1.37±0.07	0.34±0.03	0.56±0.04
4	11.80±0.12	10.68±0.22	0.33±0.01	0.22±0.01	0.51±0.02	0.47±0.02	1.22±0.02	1.41±0.02	0.47±0.04	0.67±0.05
20	12.37±0.04	10.90±0.07	0.40±0.02	0.23±0.01	0.58±0.02	0.54±0.03	1.27±0.04	1.48±0.03	0.42±0.04	0.65±0.03